

UNIVERSITÀ
DEGLI STUDI
DI PADOVA

Università degli Studi di Padova

DIPARTIMENTO DI INGEGNERIA INDUSTRIALE

CORSO DI DOTTORATO DI RICERCA IN INGEGNERIA INDUSTRIALE

CURRICOLO: Ingegneria dei Materiali

CICLO: XXX

HIGHLY POROUS GEOPOLYMER COMPONENTS

Coordinatore: Ch.mo Prof. Paolo Colombo

Supervisore: Ch.mo Prof. Paolo Colombo

Dottorando: *Chengying Bai*

Abstract

The geopolymers, semi-crystalline three-dimensional silico-aluminate inorganic polymers, have attracted increasing attention from a wide range of scientific interests. The topic of this study deals with the synthesis, the characterization and the potential applications of porous geopolymers (PGs) or geopolymer foams (GFs, total porosity > 70 vol%), realized through different processing routes. Firstly, the processes are divided into five categories: (i) direct foaming, (ii) replica method, (iii) sacrificial template, (iv) the 3D printing, and (v) others. The microstructure, porosity, and properties of porous geopolymers also compared and discussed. Secondly, K-based porous geopolymers were produced by direct foaming using hydrogen peroxide as chemical pore-forming agent (PFA) combined with three types of stabilizing agent (SA, egg white, Tween 80, vegetable oils), and by direct foaming plus reactive emulsion templating. Furthermore, open-celled phosphate-based porous geopolymers were obtained by a simple direct foaming method (using Triton X-100 as physical pore-forming agent). The porosity, pore morphology, high temperature performance, adsorption, mechanical, and insulating properties of PGs were investigated. High strength PGs with tailored porosity and controlled macro-porous structure were fabricated by different processes. The results suggest that the porous geopolymers are promising low-cost highly porous candidates for potential applications such as catalyst or membrane supports (high open porosity and high strength), adsorption (high removal efficiency and adsorption capacity with high open porosity) and insulating (low thermal conductivity, high porosity, and acceptable strength) materials.

Keywords: porous geopolymers; geopolymer foams; porosity; thermal conductivity; strength

Contents

1. Overview of porous geopolymers	1
1.1. Introduction.....	1
1.2. Processing routes	2
1.2.1 Direct foaming	2
1.2.2 Replica method	13
1.2.3 Sacrificial template method	13
1.2.4 The 3D printing.....	14
1.2.5 Others.....	15
1.3. Mechanical and thermal conductivity properties	17
1.4. Other properties and potential applications	20
1.5. Summary.....	21
References.....	22
2. Raw materials and equipments.....	33
2.1. Raw materials.....	33
2.2. Equipments	34
2.3. Characterization	35
2.3.1 Porosity	35
2.3.2 Compressive strength.....	36
2.3.3 Morphology and cell size distribution.....	36
2.3.4 Thermal behavior	36
2.3.5 Phase composition.....	37
2.3.6 Adsorption property	37
2.3.7 Insulating property	38
2.3.8 Electrochemical property	38
References.....	39
3. K-based porous geopolymers	41
3.1. Direct foaming using three different types of stabilizing agent.....	41
3.1.1 Introduction.....	41

3.1.2 Direct foaming using egg white as stabilizing agent.....	42
References.....	54
3.1.3 Direct foaming using Tween 80 as stabilizing agent	56
References.....	67
3.1.4 Direct foaming using vegetable oils as stabilizing agents.....	69
References.....	82
3.2. Direct foaming combined with reactive emulsion templating	84
3.2.1 Introduction.....	84
3.2.2 Metakaolin-based porous geopolymers.....	85
3.2.3 SiC-geopolymer foam composites	99
References.....	115
4. Phosphate-based porous geopolymers	118
4.1. Introduction.....	118
4.2. Experimental procedure	119
4.3. Results and discussion	121
4.4. Conclusions.....	126
References.....	127
5. Concluding remarks and future perspectives	131
Curriculum vitae.....	133
Acknowledgements	137

1. Overview of porous geopolymers

1.1. Introduction

In the 1970s, Davidovits [1-2] initially reported on geopolymers as semi-crystalline 3D aluminosilicate materials, which can be fabricated from natural/synthetic aluminosilicate minerals or industrial aluminosilicate byproducts/wastes (such as: metakaolin, fly ash, slag, red mud, glass ,perlite, sand, rice husk ash, clay, or a combination of them) mixed with an aqueous solution containing reactive ingredients (potassium/sodium hydroxide, phosphoric acid, potassium/sodium silicate, etc.) [1,3-11]. Today, porous geopolymers (PGs) or geopolymer foams (GFs, total porosity > 70 vol%) have been a focus of promising research in the field of porous materials because of their unique combination of good physical properties associated with great thermal [12] and chemical stability [13] and excellent mechanical properties [3,14-15] low CO₂ emission and low energy use [16-17]. They have been used as membrane [18] and membrane supports [19], adsorbents and filters [20-24], catalysts [25-28], and acoustic and thermal insulators [14,17, 29 - 30]. These applications cannot be achieved from their conventional dense counterparts.

There have been a series of reviews related to geopolymer [9,31-37] or geopolymer cement [38-40] or geopolymer concrete [17,41-44]. But only few of reviews focused to porous geopolymer materials [17,42-44]. Because of the large number of articles in the field and ~5-~50vol% of porosity in geopolymer materials could be formed by regulating the formula and processing [45-48], this review mainly focuses on the processing and properties of the highly porous geopolymer (porosity $\geq 50\text{vol}\%$ or bulk density $\leq 0.7\text{g/cm}^3$). Because of the widely used of porous geopolymers, this can be seen from the increase in the number of publications on this topic over the past few years. Figure 1-1 shows the results of peer-reviewed journal papers made in Web of Science for the porous geopolymer with porosity higher than 50vol% or bulk density lower than 0.7g/cm^3 , for publications since 2009.

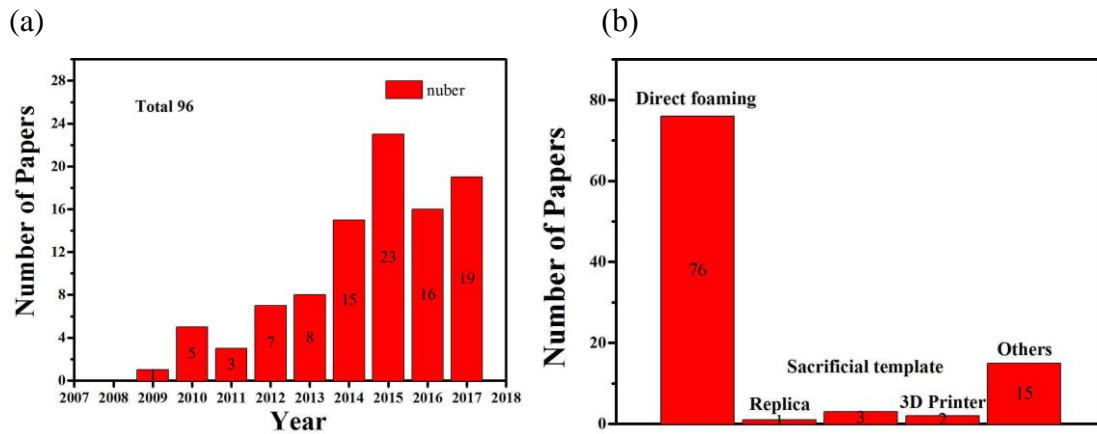


Fig. 1-1 Number of publications with the porosity larger than 50vol% or the bulk density lower than 0.7g/cm^3 over the last decade (a) and by the different route (b) correspond to bibliographic searches of the ISI Web of Science.

The processing methods used for the fabrication of porous geopolymer can be divided into five categories: (i) Direct foaming, (ii) Replica (iii) Sacrificial template, (iv) 3D printing (v) others. The processing features of each of these approaches are discussed and compared, as well as their influence on the bulk density, porosity, morphology, and mechanical and thermal conductivity properties of the porous geopolymers.

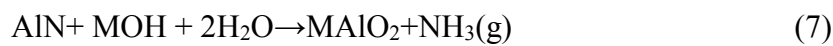
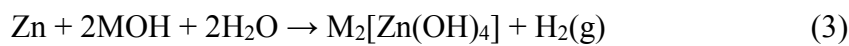
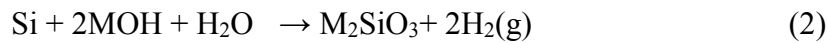
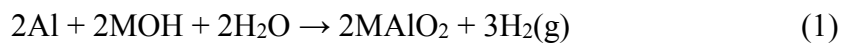
1.2. Processing routes

1.2.1 Direct foaming

The direct foaming method is the most conventional technique for producing porous geopolymers, as the preparation is a sintering-free and a suspension or liquid system process. In direct foaming method, wet foams of the geopolymers are produced by incorporating air or gas into a homogeneous liquid or a slurry medium, which is subsequently cured at certain temperature to obtain consolidated foams. However, the foaming step is a thermodynamically unstable process, as the gas bubbles in the wet foams are likely to undergo drainage, continuous Ostwald ripening, and coalescence for the sake of minimizing the overall Gibbs free energy.

Due to the instability or destabilization feature of the wet foams, there will be large pores in the final obtained porous geopolymers. In order to avoid this phenomenon, the most frequently used approach is adding the stabilizing agents (such as surfactants, particles, fibers) to the suspension or liquid media.

The generation or insertion of air or gas into the homogeneous liquid or the slurry medium is realized by the blowing agents. The blowing agents can be simply classified into physical and chemical blowing agents. Chemical blowing agents form gaseous products (such as O₂ and H₂) and other byproducts by chemical reactions and the reactions are sensitive to temperature, whereas the physical blowing agents do not refer to chemical equations and the foaming process is reversible. The usual chemical blowing agents are aluminum [46,49-50], silicon [51] powders or Si-containing agents such as silica fume (SF), SiC, FeSi alloy [50,52-54], hydrogen peroxide (H₂O₂) [8,19,21,23], Zinc powder [55], NaOCl [56], sodium perborate [57], and AlN and FeSO₃ [58-59]. The possible reactions for gas-releasing agents in alkaline solution (here, M=K or Na) are as follows:



The common chemical reactions are reactive metal powders react with water in an alkaline environment or the decomposition of peroxides, liberating bubbles of hydrogen or oxygen gas for producing porous geopolymers.

The stabilizing agents used for foam stabilization here are classified into surfactants, fibers, particles. Furthermore, the surfactants can be classified into nonionic (Triton X 100,

Tween 80), anionic (sodium dodecyl sulfate, soap), cationic, protein (vegetable or animal) types.

Numerous processing routes have been investigated to produce porous geopolymers via direct foaming technique. Table 1-1 and Table 1-2 depict the examples using chemical blowing agents and physical blowing agents reported in the literature.

As can be seen in the Table 1-1 and 1-2, several studies have been done in last decades to produce porous geopolymers by the direct foaming technique. Porous geopolymer materials can be produced by only using the blowing agents or by only using stabilizing agents or by using blowing agents in combination with stabilizing agents [19,62,70]. And the common blowing agents are H_2O_2 , Si, Al. It should be noted that the pore structure and corresponding properties are not only determined by the types of pore-forming agent. So in this work, we select three type works from previous studies, which already compared the porous geopolymers obtained by only using the blowing agents or by only using stabilizing agents or by using blowing agents in combination with stabilizing agents, to better show the effect on pore structure and corresponding properties.

Typical microstructure of porous geopolymer obtained by only using the blowing agents (pore-forming agents) or by only using stabilizing agents or by using blowing agents in combination with stabilizing agents were showed in Fig. 1-2, Fig. 1-3, Fig. 1-4, respectively. Fig. 1-2 showed and compared porous geopolymers only using H_2O_2 [19], Si [70], Al [62] as foaming agent. Cellular structures were observed but possessing a limited number of closed cells with a very inhomogeneous cell size distribution. Fig. 1-2 also showed that average pore size was about $770\mu m$, $250\mu m$, $2000\mu m$, respectively. These confirmed that the porous structure is by the corresponding chemical reactions of (5), (2), (1). Fig. 1-3 showed and compared porous geopolymers only using stabilizing agents. Compared to samples only using pore-foaming agent, the average pore size of samples using Si as pore-forming agent, showed larger than samples using vegetable protein as stabilizing agents; while the average pore size of samples using H_2O_2 or Al as pore-forming agent showed inverse results.

In addition, previous works also investigated the microstructure of specimens using

blowing agents in combination with stabilizing agents (Fig. 1-4). The synergistic effect of two different pore-foaming agents (chemical blowing agent and surfactants) are likely to lead to porous specimens with an interconnected porosity and low density. And the average cell sizes are between the samples that only using one type of pore-foaming agents.

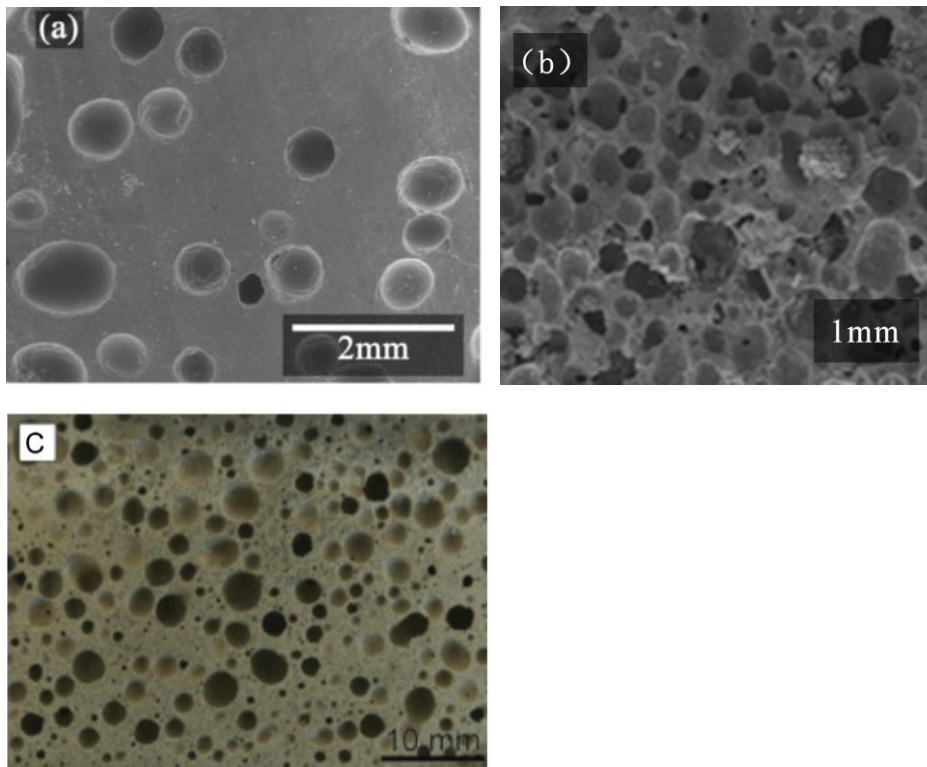
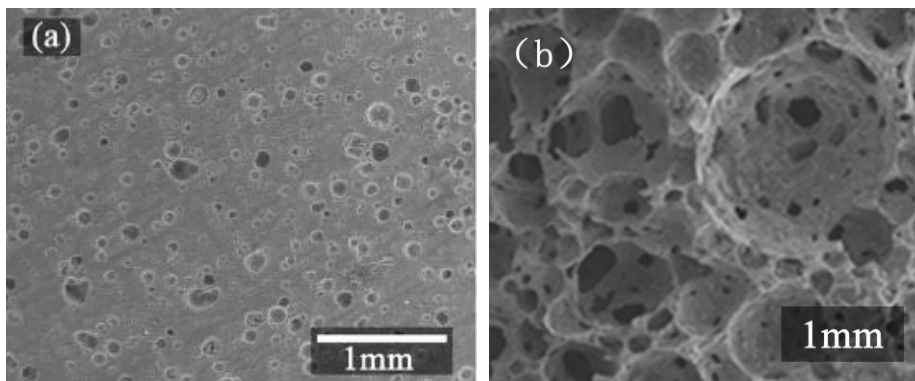


Fig 1-2 Typical microstructure of porous geopolymer only using pore-forming agent: H_2O_2 (a) [19], Si (b) [70], and Al (c) [62].



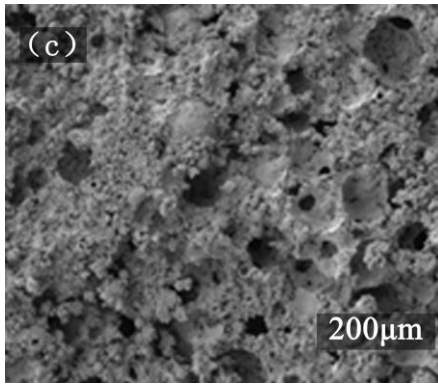


Fig 1-3 Typical microstructure of porous geopolymer only using stabilizing agents: egg white (a) [19], vegetable protein (b) [70], and Sikas Lightcrete02 (c) [62].

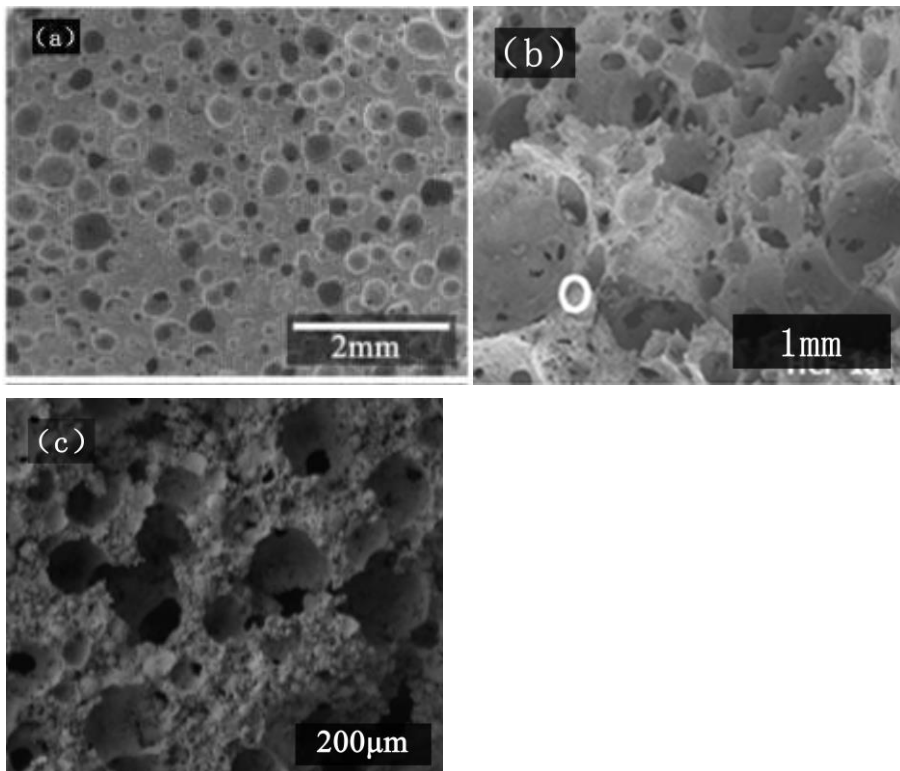


Fig. 1-4 Typical microstructure of porous geopolymer by using blowing agents in combination with stabilizing agents (H_2O_2 + egg white) (a) [19], (Si^+ vegetable protein) (b) [70], and (Al^+ Sikas Lightcrete02) (c) [62].

Table 1-1 and Table 1-2 list porous geopolymers (PGs) using different pore-forming agents with or without stabilizing agent by the direct foaming technique. Table 1-1 shows the

samples using different chemical pore-forming agents, and Table 1-2 shows the samples using different physical pore-forming agents. The main raw materials, bulk density, curing condition, and the different alkaline activators (potassium-based or sodium-based) also showed in Table 1-1 and Table 1-2. As can be seen, the widely used raw materials are fly ash and metakaolin. Various materials were selected as stabilizing agents. And the top three chemical blowing agents are H₂O₂, Al, Si. It also showed that different curing steps also carried out for different works. It showed the sealed samples put into oven at 60-80°C for 24h is one of the most suitable curing step for the porous geopolymers.

Table 1-1. Examples of direct foaming method using different chemical blowing agents reported in the literature (Room temperature=RM, sealed=S, kaolin=K, Fly ash=FA, metakaolin=MK, rice husk ash=RHA, volcanic ash=VA, D=Day, SDS=sodium dodecyl sulfate, non-metallic product =NMP, lead – silica glass =LSG)

Foaming agents	Stabilizing agents	Minerals	K/Na	Curing	Bulk density(g/cm³)	refs
Al		MK	Na	RM, (S,2weeks)		46
Al		FA	Na	RM (S,24h) 60 °C (24h) RM (24h)	0.4-1.3	49
Al,SF,Si C,FeSi	Portland cement, lime	FA	Na	80 °C (12)	0.5-1	50
Al	Alkoxysilane water-based emulsion	MK	Na	RM (7D)	0.7-1.2	55
Al	Virgin monofilament polypropylene fibers	MK	Na	70 °C (S,24)	0.8-1.1	60
Al	Virgin monofilament polypropylene fibers	FA	Na	70 °C (S,24)	0.9	61
Al		FA	Na	22 °C (2h) 80 °C (12h)	0.4-08	13
Al		K,RHA,VA	Na	-	-	62
Al		M,FA,RHA	K	50 °C (24h) RM(S) RM (7-28D)	-	63
Al		FA	Na	60 °C (S,24h)	0.6-0.9	64

Al	Sika Lightcrete 02	FA	Na	70 °C (S,24h)	0.8-1.4	65
Al		FA			0.5	66
Al	Commercial additives	FA	Na	70 °C (24h)	0.6-0.7	67
Si		MK	K	RT-80 °C (24h)	0.3-0.9	51
Si	Oligomeric dimethylsiloxane	MK,FA	Na	RM (28D) 60 °C (24h)	0.7-0.8	68
Si		MK	K	RM(24h) 80 °C (S,24h;24h)	0.6-0.9	69
Si	Na ₂ SiF ₆	MK	Na	40 °C (24h) 60 °C (72h)	1	70
Si	Na ₂ SiF ₆ +Protein	MK	Na	40 °C (24h) 60 °C (72h)	0.29	70
Si	Na ₂ SiF ₆ +Protein	MK, Diatomite	Na	40 °C (24h)	0.34-0.42	71
SF		MK	K	70 °C (S,4h) 70 °C (S,24h)	0.5	54
SF		MK, K, Illite, Montmorillonite	K	70 °C (4h)		72
SF		MK	K/Na	70 °C (4-72h)		73,74,75
SF		M, MK	K	RT-70 °C (0.5h-20D)	0.3-0.9	767778 79
SF		MK,SF	K/Na	70 °C (24h) RT (24h)	0.4-0.6	80
SiC		FA	Na	RT (30D)		52
SiC	Carbon fibers, Rice starch, Cellulose fibers	MK	K	70 °C (S,72h)	0.3-1.1	53
SiC		MK	K	RT-80 °C (24h) 80 (24h)	0.4-0.6	818283

Silicon sludge		Slag, Silicon sludge	Na	70 °C (S,24h) 3d	0.1-0.4	84
Zn	Alkoxysilane water-based emulsion	MK	Na	RM(7D)	0.5-1.2	55
NaOCl		FA	Na	30-90 °C (S,4D)	0.8	56
Sodium perborat e		FA, Sand, Calcium hydroxide	Na	RM (28D)	1.2-1.3	57
AlN+Fe SO3		NMP,LSG,MK	Na	40-100 °C (24h)	4.6-6.2	58
AlN+Fe SO3		Clay	Na	80 °C (24h)	5.4-6.7	59
H ₂ O ₂		Perlite	Na	35 °C (2h) 65 °C (24h)	0.3-0.7	8
H ₂ O ₂		MK	Na/K	35 °C (2h) 65 °C (24h)	0.3-0.6	14
H ₂ O ₂	Protein	MK	K	RM (~24h) 75 °C (S,24h)	0.4-0.8	19
H ₂ O ₂		MK,FA	Na	40 °C (S,8D) RM (21D)	0.6-1.2	15,21,85 8687
H ₂ O ₂	SDS	MK	Na	60 °C (24h)	0.8	23
H ₂ O ₂		FA,Sand, Calcium hydroxide	Na	RM (28D)	0.7-1.4	57
H ₂ O ₂	Sika® Lightcrete 02	FA	Na	70 °C (S,24h)	0.7-1.4	65
H ₂ O ₂		FA			0.2	66
H ₂ O ₂	Commercial additives	FA	Na	70 °C (24h)	0.6-1.0	67

H ₂ O ₂	KMnO ₄	MK,K,Glass	Na	30 °C (24h) RM (1-60D)	0.5-1.4	88
H ₂ O ₂	Sodium dodecyl benzene sulfonate and triethanolamine	FA	Na	70 °C (S,24h)	0.3-1.6	8990
H ₂ O ₂	Sika® Lightcrete 02, Short fiber	FA	Na	70 °C (S,24h)	0.7-0.9	91
H ₂ O ₂		FA	Na/K	RM (24h) 55-85 °C (24h)	0.2-0.4	92
H ₂ O ₂	Oleic acid	FA	Na	80 °C (10h)	0.37	93
H ₂ O ₂		Perlite waste	Na	90 °C (24h) 50 °C (72h) 35 °C (24h)	0.5-0.9	94
H ₂ O ₂		FA, Microspheres	Na	75 °C (24h) RM (28D)	0.4-0.6	95
H ₂ O ₂	SDS	FA	Na	70 °C (24h) 20 °C (3D)	0.6-1.3	96
H ₂ O ₂	Tween 80	MK	K	40 °C (~24h) 75 °C (S,24h)	0.3-0.8	97
H ₂ O ₂	Sodium dodecyl benzene sulfonate and 0.8% triethanolamine	FA	Na	70 °C (S,24h) 7d,28d	0.25-0.28	98

Table 1-2. Examples of direct foaming method using various physical blowing agents reported in the literature

Foaming agents	Stabilizing agents	Minerals	K/Na	Curing	Bulk density(g/cm ³)	refs
Diluted aqueous surface active concentrate		FA, Slag	Na	80 °C (12)	0.7-1.6	29
Diluted aqueous solution of a foaming agent		MK, Slag	Na	RM (28d)	0.4-1.0	99
A Synthetic organic foaming agent		FA, Slag	Na	40 °C (S,24h) RM (90d)		100
Tween 80		MK	K	40 °C (~24h) 75 °C (S,24h)	0.7	97
Triton x100	Polyacrylic acid	MK,FA	K	80 °C (S,1h) (4h)	0.5-0.7	101102
Tween 80	Polyacrylic acid	MK,FA	K	80 °C (S,1h) (4h)	0.6-0.9	101102
Protein	Na ₂ SiF ₆	MK	Na	40 °C (24h) 60 °C (72h)	0.45	70
Protein		MK	K	RM (~24h) 75 °C (S,24h)	0.9	19
Sika Lightcrete 02		FA	Na	70 °C (S,24h)	1-1.2	65

In the 2000s, Wagh [103] firstly suggested that inorganic polymers having [PO₄]³⁻ in place of [SiO₄]⁴⁻ should be considered as a new class of geopolymers, which was also reported by Davidovits [1]. Liu et al. [104] prepared a porous phosphorus-based geopolymers at 80 °C using MK, H₃PO₄, Alumina (Al powders as a pore forming agent). The pore size and porosity (40-83vol%) can be controlled by the content of Al powder and/or water. The porous samples

also have a high compressive strength (6-14MPa). Gualtieri et al. [105] used natural limestone as pore-forming agent to obtain phosphate-based geopolymers with irregular cell morphology. High porosity (69-76 vol%), and low effective thermal conductivity (0.07- 0.09 W/mK) of the samples were obtained. Li et al. [106-107] developed porous fly ash/phosphate geopolymer hollow spheres, the phosphate geopolymer acted as a bonder. The porous fly ash/phosphate geopolymer composites with a total porosity of 75%, open porosity as high as 48%, and possessing a compressive strength of 5.8 MPa were produced by pre-bonding and curing technology. Open cell phosphate-based porous geopolymers with a homogeneous microstructure were fabricated by frothing using TritonX-100 as pore-forming agent [7]. The frothing route enabled the production of geopolymer foams with a total porosity of 78.3vol% (open porosity 76.8vol%), average cell size about 280 μ m, and possessing a compressive strength of 0.64MPa.

1.2.2 Replica method

The replica method, dating back to the early 1960s, is based on the copy of original cellular materials regard to its pore shape and structure. However, only few of reports about porous geopolymers obtained by replica method. Kovářík et al. [108] used polyurethane sponge as a template. In the study, pores of cube-shaped polyurethane foam with average porosity of ~10 pores-per inch and bulk density of ~0.02 g/cm³ were filled with aqueous potassium-based geopolymer slurry. A solid substrate the geopolymer/polyurethane sponge was obtained after drying step. The porous geopolymer matrix with high porosity (open) ranging from ~79 to ~88 vol% high compressive strength ranging from ~0.15~0.85MPa were produced after sintering at 1100-1300 °C for 4h.

1.2.3 Sacrificial template method

The sacrificial template method, leading to cellular materials showing a negative replica

of the original template, is opposed to the positive porous structure obtained by the replica method. The porosity is generated by extracting from a biphasic composite, comprising geopolymer slurry and a dispersed sacrificial phase. The way that the sacrificial material is extracted from the consolidated composite depends primarily on the type of pore former used. A wide variety of sacrificial materials could be employed as templates. Papa and coworkers [109] processed porous geopolymer by an ice-templating (freeze-casting) method. The final products with hierarchical pore structure had 53-83% total porosity depending on the water content. Franchin et al. [110] developed a new processing method that based on 3D printer technique for fabricating macroporous geopolymers with controlled and designed porosity. In the process, PLA (polylactic acid) sacrificial templates (molds) with different patterns were firstly produced by a 3D printer, homogeneous geopolymer slurry was poured into molds under vacuum (~0.1Pa) conditions for 15min. After curing step (48-72h at room temperature), the PLA/geopolymer composites were immersed in 15M KOH solution (72°C for 24h) in order to destroy the polymer chain links, and then washed with hot water to extract the PLA, finally heat-treated at 330°C for 24h. The template was removed by this combined chemical and thermal treatment, resulting in porous geopolymer with porosity ranging from ~66 to 71vol%.

1.2.4 The 3D printing

Recently, additive manufacturing (AM) or 3D printing technologies have successfully applied to fabricate porous materials (such as scaffolds, filters, lightweight materials), as the fact that, AM technologies can produce complex-shaped porous structures with precise dimension, shape, and amount of pores and fine filigree structures from micro down to the nano-size scale, which can not be achieved by traditional technologies[111]. Franchin et al. [112] used Direct Ink Writing (DIW) technique which is also known as Robocasting to fabricate porous geopolymer scaffolds. The scaffolds with high porosity ranging from 50 to 71vol% and high compressive strength (2-12MPa) were obtained.

1.2.5 Others

Unlike the traditional porous ceramics, the fabrication processing of geopolymer materials is a sintering-free and a suspension or liquid system. Actually, the microstructure of a fully reacted geopolymeric matrix is intrinsically meso-porous (~10nm) [69,113]. And since the porosity can be up to 60vol% only by adjusting the process parameters such as SiO₂/Al₂O₃ or H₂O/MO₂ molar ratio [18]. There are some methods cannot be simply classified to the above-mentioned method. Ge et al. [18] used a designed molar ratio (SiO₂/Al₂O₃=2.96, Na₂O/Al₂O₃=0.8 and H₂O/Na₂O = 19) to prepare porous geopolymer. The porous specimens with pore sizes mainly ranging from 10 to 1000nm and with porosity about 63vol% were obtained. Medpelli and coworkers[114] developed a reactive emulsion templating method to produce porous geopolymer with hierarchically porous structure. The alkaline geopolymer slurry first mixed with the triglyceride oils to form a homogeneous viscous emulsion, the wet foam was cured at 60°C. The saponification reaction between the oil and alkaline emulsion will be complete during the curing step. The reaction products (soap and glyceride) are water-soluble and can be extracted by hot water from the hard monolithic materials to finally yield porous geopolymers. Based on this work, a novel saponification/peroxide combined route was proposed by Cilla et al. [115-116]. In their work, geopolymer foams with a total porosity of ~85vol%, open porosity as high as ~70 vol%, average cell size (D50) of 318µm were obtained by the saponification/peroxide combined route. In addition, the properties of porous geopolymer produced by only saponification or peroxide route were also compared, the vegetable oils worked as an in situ formation of surfactant molecules and emulsion templates. And the addition of oils enabled to create more cell windows, increasing the permeability, in comparison to a simple peroxide route. Larger open cells and higher porosity were obtained than the samples that only addition of oil or hydrogen peroxide. Glad and Kriven [117] developed an emulsion templating method for producing porous geopolymers with tailored porosity (≥70vol%) and pore size(0.2-10µm). A hydrophobic film firstly formed on pore interiors using alkylalkoxysilanes, and the porosity and pore size were tuned by manipulating

initial water content, quantity of hydrophobic phase, drying humidity, and emulsion stability. Ehsan et al.[118] used well mixed of bottom ash, sodium silicate and NaOH by microwave foaming technique for processing high porosity (72%), high compressive strength of 3.55 MPa, and low thermal conductivity (0.075 W/m·K) porous geopolymers. In the microwave method, sodium silicate acted as a foaming agent. An impervious skin of slurry firstly formed by the microwave heating, as the silicate groups will react and crosslink. The cellular scaffold was obtained due to the expansion, as the steam generated above 100 °C will inflate the impervious skin. And the expansion step will continue until the gelling of silicate group and dehydration will form a rigid brittle network. It is possible to modulate the porosity, physical, and insulating properties of the samples by varying the bottom ash to sodium silicate ratio.

1.3. Mechanical and thermal conductivity properties

Table 1-3. The porosity, thermal conductivity and mechanical properties of porous geopolymers using different routes.

Foaming agents	Stabilizing agents	Pore size(μm)	Porosity(vol%)	Thermal Conductivity($\text{W m}^{-1} \text{K}^{-1}$)	Compression strength(MPa)	refs
Al		0.01-150	30-70	0.15-0.6		46
Al				-	0.9-4.4	49
Al,SF,SiC,FeSi	Portland cement, Lime	100		0.1-0.25	2-8	50
Al	Virgin monofilament polypropylene fibers	-	>10-55	0.3-0.65	4.4-9.5	60
Al	Virgin monofilament polypropylene	<3000		0.3	5.5-10.9	61
Al		<4000	>50-70	0.15	6	13
Al		0.005-2690	60-90	0.1-0.25		62
Al	Fibers		>10-70		1-15	63
Al		<3500	56-66		0.4-1.6	64
Al	Sika Lightcrete 02	<8000			1.7-2.4	65
Al				0.08	1.5	66
Al	Commercial additives	<6000	48-58		3.3-4.3	67
Si		<8000	60-80			51
Si	Na_2SiF_6	70-350			4.6	70
Si	Na_2SiF_6 +Protein	200-700			0.5	70
Si	Na_2SiF_6 +Protein		82-85		0.6-1.5	71
SF		20-600	-	0.22-0.24	-	54
SF		100-1600	65-85	0.12-0.35		77,78,79

SF		0.01-2100	75-85	0.12-0.17		80
SF		<300	32-52	0.42-0.67	1.2-4.1	52
SiC	Carbon fibres, Rice starch, Cellulose fibers	<6800		0.075-0.12		53
SF		<600	78-83		0.9-1.7	8182
silicon sludge					0.4-4.2	84
NaOCl		<100	35-62		3.1-3.3	56
sodium perborate				0.05-0.2	3-5	57
AlN+FeSO3			80-83	0.14-0.15	1.1-2.3	58
AlN+FeSO3			72-79		1.4-3.8	59
H ₂ O ₂		<3000	74-89	0.03-0.06	0.2-0.8	8
H ₂ O ₂			>44-62	0.15-0.17	1.8-5.2	14
H ₂ O ₂	Protein	<1000	62-81	-	1.1-10.0	19
H ₂ O ₂		<2000	42-73	0.1-0.4	1.2-7.0	15
H ₂ O ₂		<3000	48-81	0.08-0.2	0.3-21	85
H ₂ O ₂		<3000	54-80	0.09-0.26	0.2-5	86
H ₂ O ₂		<3000	41-78		0.2-9	87
H ₂ O ₂				0.1-0.2	0.2-5	57
H ₂ O ₂	Sika Lightcrete 02	<8000			1.3-4.7	65
H ₂ O ₂				0.07	<0.5	66
H ₂ O ₂	KMnO ₄		28-82	0.88-0.42	3.1-68.7	88
H ₂ O ₂	Sodium dodecyl benzene sulfonate and triethanolamine	100-600	11->63		0.4-8	89
H ₂ O ₂			74-81	0.07-0.09	0.4-1.4	92
H ₂ O ₂	Oleic acid	<1500			0.6	93
H ₂ O ₂			59-71	0.08-0.1		94
H ₂ O ₂				0.08-0.13	1.9-3.4	95

H ₂ O ₂	SDS	<2000	19-55		2.6-12.2	96
H ₂ O ₂	Tween 80	<800	68-87	0.09-0.29	0.3-9.4	97
H ₂ O ₂	Sodium dodecyl benzene	200-1000		-	0.45-0.86	98
Diluted aqueous surface active concentrate				0.15-0.48	3-48	29
Diluted aqueous solution of a foaming agent		100-1000			0.5-20	99
A Synthetic organic foaming agent		<100	44-65		3.4-16.2	100
Tween 80	Polyacrylic acid	<150	68		11.0	101
Triton x100	Polyacrylic acid	<1000	52-82		0.5-2.7	10110 2
Tween 80	Polyacrylic acid	<1000	53-82		0.5-3.3	10110 2
Protein	Na ₂ SiF ₆	70-700			1.4	70
Protein	Na ₂ SiF ₆	50-150	58	-	21.4	19
Sika Lightcrete 02		<150			3.6-7.2	65

As porous geopolymers were mainly oriented for insulating materials [37], the porosity, thermal conductivity and mechanical properties of porous geopolymers are listed in Table 1-3. Table 1-3 shows that the total porosity of directly foamed geopolymers is proportional to the amount of gas incorporated into the suspension or liquid medium during the foaming process. Furthermore, the increasing of the porosity will reduce the both the strength and the thermal conductivity. More investigations should be carried out to compare and discuss about the factors that affect the porosity, mechanical and thermal conductivity properties.

1.4. Other properties and potential applications

Besides insulating applications, porous geopolymers were also produced with or without pore-forming agents, for potential application such as adsorbents materials. The effect of Ni²⁺ removal using a low cost self-supporting metakaolin-geopolymer membrane was studied by Ge et al. [18]. The geopolymer-based inorganic membrane with a total porosity of 62% was produced without pore-forming agent added. The CO₂ adsorption capacity also investigated by Minelli et al. [20]. Fumed silica was used as the pore-forming agent to produce the adsorbent samples. It showed that the adsorption capacity of porous geopolymers about 0.6mmol/g at atmospheric pressure. Furthermore, the CO₂/N₂ (~200) and CO₂/CH₄ (~100) capacity selectivity was excellent. The sound adsorbing property also investigated by Hung et al. [99]. With higher than 7.5wt% Ca loading in the porous geopolymer, porous geopolymer-based catalysts were produced by Sharma et al. [25]. It indicated that almost 100% conversion (biodiesels) has been achieved in one hour under refluxing conditions with methanol solvent using this new geopolymer-based catalyst. The solidification/stabilization of liquid oil waste in metakaolin-based geopolymer was also studied by Cantarel et al. [119]. It showed that oil waste can be immobilized in the alkali-based geopolymer, simultaneously, a porous structure can be formed.

1.5. Summary

Tremendous efforts have been devoted to novel processing of porous geopolymers and investigation of properties and their potential application in various fields during the recent decades, driven by the huge need of low-cost eco-friendly engineering components. Different processing routes for porous geopolymer materials have been developed. Direct foaming is the simplest and easiest way to produce porous geopolymers. And the frequently-used pore-forming agents are H_2O_2 , Al, Si. Since porous geopolymers were mainly oriented for insulating materials, the porosity, mechanical and thermal conductivity properties of porous geopolymer also compared.

References

- 1 Davidovits J. Geopolymer chemistry & applications. (Institut Géopolymère, Saint-Quentin, 2011), p. XI, 612 p.
- 2 Davidovits J. Geopolymers and geopolymeric materials[J]. *Journal of Thermal Analysis and Calorimetry*, 1989, 35(2): 429-441.
- 3 Lecomte I, Liégeois M, Rulmont A, et al. Synthesis and characterization of new inorganic polymeric composites based on kaolin or white clay and on ground-granulated blast furnace slag[J]. *Journal of materials research*, 2003, 18(11): 2571-2579.
- 4 He J, Jie Y, Zhang J, et al. Synthesis and characterization of red mud and rice husk ash-based geopolymer composites[J]. *Cement and Concrete Composites*, 2013, 37: 108-118.
- 5 Shiu H S, Lin K L, Chao S J, et al. Effects of foam agent on characteristics of thin-film transistor liquid crystal display waste glass-metakaolin-based cellular geopolymer[J]. *Environmental Progress & Sustainable Energy*, 2014, 33(2): 538-550.
- 6 Davidovits J. Geopolymers: inorganic polymeric new materials[J]. *Journal of Thermal Analysis and calorimetry*, 1991, 37(8): 1633-1656.
- 7 Bai C, Conte A, Colombo P. Open-cell phosphate-based geopolymer foams by frothing[J]. *Materials Letters*, 2017, 188: 379-382.
- 8 Vaou V, Papias D. Thermal insulating foamy geopolymers from perlite[J]. *Minerals Engineering*, 2010, 23(14): 1146-1151.
- 9 Khale D, Chaudhary R. Mechanism of geopolymerization and factors influencing its development: a review[J]. *Journal of Materials Science*, 2007, 42(3): 729-746.
- 10 Panagiotopoulou C, Kontori E, Perraki T, et al. Dissolution of aluminosilicate minerals and by-products in alkaline media[J]. *Journal of Materials Science*, 2007, 42(9): 2967-2973.
- 11 Badanoiu A I, Al Saadi T H A, Stoleriu S, et al. Preparation and characterization of foamed geopolymers from waste glass and red mud[J]. *Construction and Building Materials*, 2015, 84: 284-293.
- 12 Hemra K, Aungkavattana P. Effect of cordierite addition on compressive strength and thermal stability of metakaolin based geopolymer[J]. *Advanced Powder Technology*, 2016, 27(3): 1021-1026.
- 13 Hlaváček P, Šmilauer V, Škvára F, et al. Inorganic foams made from alkali-activated fly ash: Mechanical, chemical and physical properties[J]. *Journal of the European Ceramic*

-
- Society, 2015, 35(2): 703-709.
- 14 Palmero P, Formia A, Antonaci P, et al. Geopolymer technology for application-oriented dense and lightened materials. Elaboration and characterization[J]. *Ceramics International*, 2015, 41(10): 12967-12979.
 - 15 Novais R M, Buruberri L H, Ascensão G, et al. Porous biomass fly ash-based geopolymers with tailored thermal conductivity[J]. *Journal of Cleaner Production*, 2016, 119: 99-107.
 - 16 Al-Majidi M H, Lampropoulos A, Cundy A, et al. Development of geopolymer mortar under ambient temperature for in situ applications[J]. *Construction and Building Materials*, 2016, 120: 198-211.
 - 17 Zhang Z, Provis J L, Reid A, et al. Geopolymer foam concrete: An emerging material for sustainable construction[J]. *Construction and Building Materials*, 2014, 56: 113-127.
 - 18 Ge Y, Yuan Y, Wang K, et al. Preparation of geopolymer-based inorganic membrane for removing Ni²⁺ from wastewater[J]. *Journal of hazardous materials*, 2015, 299: 711-718.
 - 19 Bai C, Colombo P. High-porosity geopolymer membrane supports by peroxide route with the addition of egg white as surfactant[J]. *Ceramics International*, 2017, 43(2): 2267-2273.
 - 20 Minelli M, Medri V, Papa E, et al. Geopolymers as solid adsorbent for CO₂ capture[J]. *Chemical Engineering Science*, 2016, 148: 267-274.
 - 21 Novais R M, Buruberri L H, Seabra M P, et al. Novel porous fly-ash containing geopolymer monoliths for lead adsorption from wastewaters[J]. *Journal of hazardous materials*, 2016, 318: 631-640.
 - 22 López F J, Sugita S, Kobayashi T. Cesium-adsorbent geopolymer foams based on silica from rice husk and metakaolin[J]. *Chemistry Letters*, 2013, 43(1): 128-130.
 - 23 Ge Y, Cui X, Kong Y, et al. Porous geopolymeric spheres for removal of Cu (II) from aqueous solution: synthesis and evaluation[J]. *Journal of hazardous materials*, 2015, 283: 244-251.
 - 24 Medpelli D, Sandoval R, Sherrill L, et al. Iron oxide-modified nanoporous geopolymers for arsenic removal from ground water[J]. *Resource-Efficient Technologies*, 2015, 1(1): 19-27.
 - 25 Sharma S, Medpelli D, Chen S, et al. Calcium-modified hierarchically porous aluminosilicate geopolymer as a highly efficient regenerable catalyst for biodiesel production[J]. *RSC Advances*, 2015, 5(80): 65454-65461.

-
- 26 Zhang Y J, Liu L C, Xu Y, et al. A new alkali-activated steel slag-based cementitious material for photocatalytic degradation of organic pollutant from waste water[J]. *Journal of hazardous materials*, 2012, 209: 146-150.
 - 27 Sazama P, Bortnovsky O, Dědeček J, et al. Geopolymer based catalysts—new group of catalytic materials[J]. *Catalysis today*, 2011, 164(1): 92-99.
 - 28 Alzeer M I M, MacKenzie K J D, Keyzers R A. Porous aluminosilicate inorganic polymers (geopolymers): a new class of environmentally benign heterogeneous solid acid catalysts[J]. *Applied Catalysis A: General*, 2016, 524: 173-181.
 - 29 Zhang Z, Provis J L, Reid A, et al. Mechanical, thermal insulation, thermal resistance and acoustic absorption properties of geopolymer foam concrete[J]. *Cement and Concrete Composites*, 2015, 62: 97-105.
 - 30 Papa E, Medri V, Kpogbemabou D, et al. Porosity and insulating properties of silica-fume based foams[J]. *Energy and Buildings*, 2016, 131: 223-232.
 - 31 Provis J L, Lukey G C, van Deventer J S J. Do geopolymers actually contain nanocrystalline zeolites? A reexamination of existing results[J]. *Chemistry of materials*, 2005, 17(12): 3075-3085.
 - 32 Duxson P, Fernández-Jiménez A, Provis J L, et al. Geopolymer technology: the current state of the art[J]. *Journal of Materials Science*, 2007, 42(9): 2917-2933.
 - 33 Komnitsas K, Zaharaki D. Geopolymerisation: A review and prospects for the minerals industry[J]. *Minerals engineering*, 2007, 20(14): 1261-1277.
 - 34 Pacheco-Torgal F, Castro-Gomes J, Jalali S. Alkali-activated binders: A review: Part 1. Historical background, terminology, reaction mechanisms and hydration products[J]. *Construction and Building Materials*, 2008, 22(7): 1305-1314.
 - 35 Pacheco-Torgal F, Castro-Gomes J, Jalali S. Alkali-activated binders: a review. Part 2. About materials and binders manufacture[J]. *Construction and Building Materials*, 2008, 22(7): 1315-1322.
 - 36 Provis J L, Bernal S A. Geopolymers and related alkali-activated materials[J]. *Annual Review of Materials Research*, 2014, 44: 299-327.
 - 37 Lemougna P N, Wang K, Tang Q, et al. Recent developments on inorganic polymers synthesis and applications[J]. *Ceramics International*, 2016, 42(14): 15142-15159.

-
- 38 Davidovits J. Geopolymer cement[J]. A review. Geopolymer Institute, Technical papers, 2013, 21: 1-11.
 - 39 Abdullah M M A, Hussin K, Bnhussain M, et al. Mechanism and chemical reaction of fly ash geopolymer cement-a review[J]. Int. J. Pure Appl. Sci. Technol, 2011, 6(1): 35-44.
 - 40 Liew Y M, Heah C Y, Kamarudin H. Structure and properties of clay-based geopolymer cements: A review[J]. Progress in Materials Science, 2016, 83: 595-629.
 - 41 Saravanan G, Jeyasehar C A, Kandasamy S. Flyash Based Geopolymer Concrete—A State of the Art Review[J]. Journal of Engineering Science and Technology Review, 2013, 6(1): 25-32.
 - 42 Singh B, Ishwarya G, Gupta M, et al. Geopolymer concrete: A review of some recent developments[J]. Construction and building materials, 2015, 85: 78-90.
 - 43 Amran Y H M, Farzadnia N, Ali A A A. Properties and applications of foamed concrete; a review[J]. Construction and Building Materials, 2015, 101: 990-1005.
 - 44 Dhamanage M P M, Salunkhe M R S, Patil M S S. Light-Weight Geopolymer Concrete-A Review[J]. International Journal of Research in Advent Technology,2016,49-51.
 - 45 Jämstorp E, Forsgren J, Bredenberg S, et al. Mechanically strong geopolymers offer new possibilities in treatment of chronic pain[J]. Journal of Controlled Release, 2010, 146(3): 370-377.
 - 46 Kamseu E, Nait-Ali B, Bignozzi M C, et al. Bulk composition and microstructure dependence of effective thermal conductivity of porous inorganic polymer cements[J]. Journal of the European Ceramic Society, 2012, 32(8): 1593-1603.
 - 47 Ma Y, Hu J, Ye G. The pore structure and permeability of alkali activated fly ash[J]. Fuel, 2013, 104: 771-780.
 - 48 Lee S, Jou H T, Van Riessen A, et al. Three-dimensional quantification of pore structure in coal ash-based geopolymer using conventional electron tomography[J]. Construction and Building Materials, 2014, 52: 221-226.
 - 49 Sanjayan J G, Nazari A, Chen L, et al. Physical and mechanical properties of lightweight aerated geopolymer[J]. Construction and Building Materials, 2015, 79: 236-244.
 - 50 František Š, Rostislav Š, Zdeněk T, et al. Preparation and properties of fly ash-based geopolymer foams[J]. Ceramics-Silikaty, 2014, 58(3): 188-197.

-
- 51 Medri V, Papa E, Dedecek J, et al. Effect of metallic Si addition on polymerization degree of in situ foamed alkali-aluminosilicates[J]. *Ceramics International*, 2013, 39(7): 7657-7668.
- 52 Gualtieri M L, Cavallini A, Romagnoli M. Interactive powder mixture concept for the preparation of geopolymers with fine porosity[J]. *Journal of the European Ceramic Society*, 2016, 36(10): 2641-2646.
- 53 Prud'homme E, Joussein E, Rossignol S. Use of silicon carbide sludge to form porous alkali-activated materials for insulating application[J]. *The European Physical Journal Special Topics*, 2015, 224(9): 1725-1735.
- 54 Prud'homme E, Michaud P, Joussein E, et al. Silica fume as porogent agent in geo-materials at low temperature[J]. *Journal of the European Ceramic Society*, 2010, 30(7): 1641-1648.
- 55 Yang T Y, Chien C C. A Study on Chemical Foaming Geopolymer Building Materials[C]//Advanced Materials Research. Trans Tech Publications, 2014, 853: 202-206.
- 56 Böke N, Birch G D, Nyale S M, et al. New synthesis method for the production of coal fly ash-based foamed geopolymers[J]. *Construction and Building Materials*, 2015, 75: 189-199.
- 57 Abdollahnejad Z, Pacheco-Torgal F, Félix T, et al. Mix design, properties and cost analysis of fly ash-based geopolymer foam[J]. *Construction and Building Materials*, 2015, 80: 18-30.
- 58 Bajare D, Bumanis G, Korjakins A. New porous material made from industrial and municipal waste for building application[J]. *Materials Science*, 2014, 20(3): 333-338.
- 59 Bumanis G, Vitola L, Bajare D, et al. Impact of reactive $\text{SiO}_2/\text{Al}_2\text{O}_3$ ratio in precursor on durability of porous alkali activated materials[J]. *Ceramics International*, 2017, 43(7): 5471-5477.
- 60 Rickard W D A, Vickers L, Van Riessen A. Performance of fibre reinforced, low density metakaolin geopolymers under simulated fire conditions[J]. *Applied Clay Science*, 2013, 73: 71-77.
- 61 Rickard W D A, Van Riessen A. Performance of solid and cellular structured fly ash geopolymers exposed to a simulated fire[J]. *Cement and Concrete Composites*, 2014, 48: 75-82.
- 62 Kamseu E, NGouloure Z N M, Ali B N, et al. Cumulative pore volume, pore size distribution and phases percolation in porous inorganic polymer composites: relation microstructure and effective thermal conductivity[J]. *Energy and buildings*, 2015, 88: 45-56.

-
- 63 Ziegler D, Formia A, Tulliani J M, et al. Environmentally-Friendly Dense and Porous Geopolymers Using Fly Ash and Rice Husk Ash as Raw Materials[J]. *Materials*, 2016, 9(6): 466.
- 64 Hajimohammadi A, Ngo T, Mendis P, et al. Regulating the chemical foaming reaction to control the porosity of geopolymer foams[J]. *Materials & Design*, 2017, 120: 255-265.
- 65 Masi G, Rickard W D A, Vickers L, et al. A comparison between different foaming methods for the synthesis of light weight geopolymers[J]. *Ceramics International*, 2014, 40(9): 13891-13902.
- 66 Zhao Y, Jow J, Cai X, et al. Fly ash-based geopolymer foam technology for thermal insulation and fire protection applications[J]. *Proceedings of the 2015 World of Coal Ash (WOCA), Nashville, TN, USA, 2015: 5-7.*
- 67 Ducman V, Korat L. Characterization of geopolymer fly-ash based foams obtained with the addition of Al powder or H₂O₂ as foaming agents[J]. *Materials Characterization*, 2016, 113: 207-213.
- 68 Strini A, Roviello G, Ricciotti L, et al. TiO₂-based photocatalytic geopolymers for nitric oxide degradation[J]. *Materials*, 2016, 9(7): 513.
- 69 Landi E, Medri V, Papa E, et al. Alkali-bonded ceramics with hierarchical tailored porosity[J]. *Applied Clay Science*, 2013, 73: 56-64.
- 70 Verdolotti L, Liguori B, Capasso I, et al. Synergistic effect of vegetable protein and silicon addition on geopolymeric foams properties[J]. *Journal of materials science*, 2015, 50(6): 2459-2466.
- 71 Liguori B, Capasso I, Romeo V, et al. Hybrid geopolymeric foams with diatomite addition: Effect on chemico-physical properties[J]. *Journal of Cellular Plastics*, 2017: 53(5):525-536.
- 72 Prud'Homme E, Michaud P, Joussein E, et al. In situ inorganic foams prepared from various clays at low temperature[J]. *Applied Clay Science*, 2011, 51(1): 15-22.
- 73 Prud'Homme E, Michaud P, Joussein E, et al. Role of alkaline cations and water content on geomaterial foams: monitoring during formation[J]. *Journal of Non-Crystalline Solids*, 2011, 357(4): 1270-1278.
- 74 Prud'Homme E, Michaud P, Joussein E, et al. Structural characterization of geomaterial foams-Thermal behavior[J]. *Journal of Non-Crystalline Solids*, 2011, 357(21): 3637-3647.

-
- 75 Delair S, Prud'homme É, Peyratout C, et al. Durability of inorganic foam in solution: The role of alkali elements in the geopolymer network[J]. *Corrosion Science*, 2012, 59: 213-221.
- 76 Henon J, Alzina A, Absi J, et al. Porosity control of cold consolidated geomaterial foam: temperature effect[J]. *Ceramics International*, 2012, 38(1): 77-84.
- 77 Henon J, Alzina A, Absi J, et al. Potassium geopolymer foams made with silica fume pore forming agent for thermal insulation[J]. *Journal of Porous Materials*, 2013, 20(1): 37-46.
- 78 Henon J, Pennec F, Alzina A, et al. Analytical and numerical identification of the skeleton thermal conductivity of a geopolymer foam using a multi-scale analysis[J]. *Computational Materials Science*, 2014, 82: 264-273.
- 79 Henon J, Alzina A, Absi J, et al. Analytical estimation of skeleton thermal conductivity of a geopolymer foam from thermal conductivity measurements[J]. *The European Physical Journal Special Topics*, 2015, 224(9): 1715-1723.
- 80 Papa E, Medri V, Kpogbemabou D, et al. Porosity and insulating properties of silica-fume based foams[J]. *Energy and Buildings*, 2016, 131: 223-232.
- 81 Medri V, Ruffini A. Alkali-bonded SiC based foams[J]. *Journal of the European Ceramic Society*, 2012, 32(9): 1907-1913.
- 82 Medri V, Ruffini A. The influence of process parameters on in situ inorganic foaming of alkali-bonded SiC based foams[J]. *Ceramics International*, 2012, 38(4): 3351-3359.
- 83 Medri V, Papa E, Landi E. Behavior of alkali bonded silicon carbide foams in modified synthetic body fluid[J]. *Materials Letters*, 2013, 106: 377-380.
- 84 Kim Y, Kim S, Jang C. Fabrication of porous geopolymer using fused slag with silicon sludge[J]. *Journal of Ceramic Processing Research*, 2016, 17(11): 1202-1207.
- 85 Novais R M, Ascensão G, Buruberri L H, et al. Influence of blowing agent on the fresh-and hardened-state properties of lightweight geopolymers[J]. *Materials & Design*, 2016, 108: 551-559.
- 86 Novais R M, Buruberri L H, Ascensao G, et al. Low thermal conductivity geopolymers produced from fly ash based industrial residues[J]. *3rd International Symposium on Enhanced Landfill Mining*, 2016, 342-357.
- 87 Novais R M, Buruberri L H, Seabra M P, et al. Novel porous fly ash-containing geopolymers for pH buffering applications[J]. *Journal of Cleaner Production*, 2016, 124: 395-404.

-
- 88 Shiu H S, Lin K L, Chao S J, et al. Effects of foam agent on characteristics of thin - film transistor liquid crystal display waste glass - metakaolin - based cellular geopolymer[J]. *Environmental Progress & Sustainable Energy*, 2014, 33(2): 538-550.
- 89 Liu Z, Shao N, Wang D, et al. Fabrication and properties of foam geopolymer using circulating fluidized bed combustion fly ash[J]. *International Journal of Minerals, Metallurgy, and Materials*, 2014, 21(1): 89-94.
- 90 Liu Z, Shao N, Huang T, et al. Effect of SiO₂/Na₂O mole ratio on the properties of foam geopolymers fabricated from circulating fluidized bed fly ash[J]. *International Journal of Minerals, Metallurgy, and Materials*, 2014, 21(6): 620-626.
- 91 Masi G, Rickard W D A, Bignozzi M C, et al. The influence of short fibres and foaming agents on the physical and thermal behaviour of geopolymer composites[J]. *Advances in Science and Technology*, 2014, 92: 56.
- 92 Feng J, Zhang R, Gong L, et al. Development of porous fly ash-based geopolymer with low thermal conductivity[J]. *Materials & Design (1980-2015)*, 2015, 65: 529-533.
- 93 Liu Y, Yan C, Zhang Z, et al. A facile method for preparation of floatable and permeable fly ash-based geopolymer block[J]. *Materials Letters*, 2016, 185: 370-373.
- 94 Tsaousi G M, Douni I, Taxiarchou M, et al. Development of foamed Inorganic Polymeric Materials based on Perlite[C]//*IOP Conference Series: Materials Science and Engineering*. IOP Publishing, 2016, 123(1): 012062.
- 95 Łach M, Korniejeko K, Mikula J. Thermal insulation and thermally resistant materials made of geopolymer foams[J]. *Procedia Engineering*, 2016, 151: 410-416.
- 96 Korat L, Ducman V. The influence of the stabilizing agent SDS on porosity development in alkali-activated fly-ash based foams[J]. *Cement and Concrete Composites*, 2017, 80: 168-174.
- 97 Bai C, Franchin G, Elsayed H, et al. High-porosity geopolymer foams with tailored porosity for thermal insulation and wastewater treatment[J]. *Journal of Materials Research*, 2017, 32(17), 3251-3259.
- 98 Liu Z, Shao N, Qin J, et al. Strength and thermal behavior of low weight foam geopolymer using circulating fluidized bed combustion fly ash[J]. *Journal of Central South University*, 2015, 22(9): 3633-3640.

-
- 99 Hung T C, Huang J S, Wang Y W, et al. Inorganic polymeric foam as a sound absorbing and insulating material[J]. *Construction and Building Materials*, 2014, 50: 328-334.
- 100 Zhang Z, Provis J L, Reid A, et al. Fly ash-based geopolymers: the relationship between composition, pore structure and efflorescence[J]. *Cement and Concrete Research*, 2014, 64: 30-41.
- 101 Cilla M S, Colombo P, Morelli M R. Geopolymer foams by gelcasting[J]. *Ceramics International*, 2014, 40(4): 5723-5730.
- 102 Cilla M S, Morelli M R, Colombo P. Effect of process parameters on the physical properties of porous geopolymers obtained by gelcasting[J]. *Ceramics International*, 2014, 40(8): 13585-13590.
- 103 Wagh A S. Chemically Bonded Phosphate Ceramics-A Novel Class of Geopolymers[J]. *Advances in Ceramic Matrix Composites X, Volume 165*, 2006: 107-116.
- 104 Le-Ping L, Xue-Min C, Shu-Heng Q, et al. Preparation of phosphoric acid-based porous geopolymers[J]. *Applied Clay Science*, 2010, 50(4): 600-603.
- 105 Gualtieri M L, Romagnoli M, Gualtieri A F. Preparation of phosphoric acid-based geopolymer foams using limestone as pore forming agent—Thermal properties by in situ XRPD and Rietveld refinements[J]. *Journal of the European Ceramic Society*, 2015, 35(11): 3167-3178.
- 106 Li R, Wu G, Jiang L, et al. Characterization of multi-scale porous structure of fly ash/phosphate geopolymer hollow sphere structures: From submillimeter to nano-scale[J]. *Micron*, 2015, 68: 54-58.
- 107 Li R, Wu G, Jiang L, et al. Interface microstructure and compressive behavior of fly ash/phosphate geopolymer hollow sphere structures[J]. *Materials & Design*, 2015, 65: 585-590.
- 108 Kovářik T, Křenek T, Rieger D, et al. Synthesis of open-cell ceramic foam derived from geopolymer precursor via replica technique[J]. *Materials Letters*, 2017.209,497-500.
- 109 Papa E, Medri V, Benito P, et al. Synthesis of porous hierarchical geopolymer monoliths by ice-templating[J]. *Microporous and Mesoporous Materials*, 2015, 215: 206-214.
- 110 Franchin G, Colombo P. Porous geopolymer components through inverse replica of 3D printed sacrificial templates[J]. *Journal of Ceramic Science and Technology*, 2015, 6(2): 105-111.

-
- 111 Zocca A, Colombo P, Gomes C M, et al. Additive manufacturing of ceramics: issues, potentialities, and opportunities[J]. *Journal of the American Ceramic Society*, 2015, 98(7): 1983-2001.
- 112 Franchin G, Scanferla P, Zeffiro L, et al. Direct ink writing of geopolymeric inks[J]. *Journal of the European Ceramic Society*, 2017, 37(6): 2481-2489.
- 113 Kriven W M, Bell J L, Gordon M. Microstructure and microchemistry of fully-reacted geopolymers and geopolymer matrix composites[J]. *Ceramic Transactions*, 2003, 153(1994).
- 114 Medpelli D, Seo J M, Seo D K. Geopolymer with hierarchically meso - /macroporous structures from reactive emulsion templating[J]. *Journal of the American Ceramic Society*, 2014, 97(1): 70-73.
- 115 Cilla M S, Morelli M R, Colombo P. Open cell geopolymer foams by a novel saponification/peroxide/gelcasting combined route[J]. *Journal of the European Ceramic Society*, 2014, 34(12): 3133-3137.
- 116 Cilla M S, Mello Innocentini M D, Morelli M R, et al. Geopolymer foams obtained by the saponification/peroxide/gelcasting combined route using different soap foam precursors[J]. *Journal of the American Ceramic Society*, 2017, 100(8): 3440-3450.
- 117 Glad B E, Kriven W M. Highly porous geopolymers through templating and surface interactions[J]. *Journal of the American Ceramic Society*, 2015, 98(7): 2052-2059.
- 118 Haq E U, Padmanabhan S K, Licciulli A. Microwave synthesis of thermal insulating foams from coal derived bottom ash[J]. *Fuel Processing Technology*, 2015, 130: 263-267.
- 119 Cantarel V, Nouaille F, Rooses A, et al. Solidification/stabilisation of liquid oil waste in metakaolin-based geopolymer[J]. *Journal of Nuclear Materials*, 2015, 464: 16-19.

2. Raw materials and equipments

2.1. Raw materials

The main raw materials (RMs) of this study were listed in Table 2-1. Previous studies[1] showed that diluted hydrogen peroxide was expected to provide less anisotropic pores, so 3wt% of H₂O₂ solution obtained from 30wt% H₂O₂ was used as pore-forming agent.

Table 2-1 Raw materials

RMs	Specification	Addition information
Metakaolin	Argical 1200s, AGS Mineraux, France	
SiC	F1000, ESK-SiC-GmbH	~6.5 μ m
Potassium hydroxide pellets	Sigma-Aldrich	
Potassium silicate	KSIL 0465, Crosfield Italia, Italy	
H ₂ O ₂	Sigma-Aldrich	30wt%
Egg white	Panreac AppliChem, Germany	~80%
Canola oils	Great Value, Wal-Mart, Canada	
Olive oils	Fragrante, Bertolli, Italy	
Sunflower oils	Panorama, Pam, Italy	
Tween 80	VWR BDH Prolabo	
Triton X-100	Sigma-Aldrich	
Phosphoric acid	Sigma-Aldrich	~85wt%

Copper sulfate pentahydrate	Hetalab Chemical Corp., USA	
Ammonium dihydrogen phosphate	Carlo Erba s.p.a., Italy	

2.2. Equipments

The main equipments of this study were listed in Table 2-2.

Table 2-2 Main instruments and equipments

Names	Abbreviation	Specification	Place of production	Addition information
Mixer		OST Basic, IKA-Werke Gmbh & Co. KG	Staufen, Germany	
Differential thermal analysis /Thermogravimetry analysis	DTA/TG	STA409, Netzsch GmbH	Selb, Germany	3°C/min up to 1100 °C in air
Dilatometer	DIL	402C, Netzsch GmbH	Selb, Germany	10°C/min up to 1100 °C in air
X-ray diffractometer	XRD	AXS-D8 advance, Bruker	Germany	40 kV, 40 mA, Cu K step width 0.05°(5–55°)
Automatic true density analyzer		Accupyc1330, Micromeritics	USA	

Universal material testing machine		Instron 1121 Canton,	Massachusetts,U SA	cross-head speed of 1 mm/min
Optical microscope		AxioCam ERc 5s, Carl Zeiss,	Germany	
Scanning Electron Microscope	SEM	FEI Quanta 200	Netherlands	
UV-visible spectrophotometer		FP12 Macherey Nagel	Dueren, Germany	
Hot-disc thermal analyzer		DRE-III	Xiangtan, China	
Viscometer		DV-II + Pro EXTRA, Brookfield	USA	Spindle R4, rpm 12,
Electrochemical impedance spectroscopy	EIS	Autolab PGSTAT 204M	Netherlands	FRA module

2.3. Characterization

After curing and polishing, the dimensions of the resulting samples were $\sim 20\text{mm} \times 50\text{mm} \times 50\text{mm}$. Prior to the characterization of bulk density, porosity, pore morphology, pore size distribution, and mechanical properties, the selected specimens were cut into small parallelepipeds ($\sim 11\text{mm} \times \sim 15\text{mm} \times \sim 15\text{mm}$). After that, the porous geopolymers (PGs) were dried at 40°C for about one week.

2.3.1 Porosity

The relative (bulk) density (ρ_b) of the geopolymer foams (GFs) or porous geopolymers (PGs) was obtained as the ratio between the mass of parallelepiped-foam samples and the geometrical volume (as measured with a digital caliper). The true (skeleton) density (ρ_0) was measured with an automatic true density analyzer at room temperature. The total porosity (TP) was calculated based on the relation: $TP=100\% (1-\rho_b/\rho_0)$ [2-3], and the corresponding open porosity (OP) was determined by the Archimedes method using distilled water as the immersion medium.

2.3.2 Compressive strength

Compressive strength (σ) was measured using an universal material testing machine, and at least four specimens were tested to obtain the average strength value and standard deviation. Samples were tested parallel to the foaming directions (axial direction), but in comparison purpose also perpendicularly to it (radial direction).

2.3.3 Morphology and cell size distribution

The morphology of porous specimens was observed using optical microscope and Scanning Electron Microscope. Cut surfaces of the samples were used to better observe the microstructure. The average cell size (ACS) and cell size distribution of PGs were characterized based on digital images (at least 100 cell sizes were measured per image) using a Nano Measurer 1.2 program (Fudan University, China) [4,5]. Values computed by the analysis of SEM images were converted to three-dimensional values using the stereological equation: $D_{\text{sphere}}= D_{\text{circle}}/0.785$ according to ASTM D3576-98 [2,6].

2.3.4 Thermal behavior

The thermal behavior or high temperature performance of the samples was characterized by thermogravimetry analysis (TG) and differential thermal analysis (DTA)

(3 °C/min up to 1100 °C in air) and by dilatometer (10 °C/min up to 1100 °C in air).

2.3.5 Phase composition

The crystalline phase assemblage was identified on ground samples using a XRD instrument. Semi-automatic phase identification was performed via the Match! software package (Crystal Impact GbR, Bonn, Germany) supported by PDF-2 Powder Diffraction File from ICDD (International Centre for Diffraction Data, Newtown Square, PA, USA).

2.3.6 Adsorption property

Stock solutions used for adsorption tests were prepared by dissolving copper sulfate pentahydrate and ammonium dihydrogen phosphate respectively in distilled water. The current World Health Organization (WHO, 2008) guideline value for copper concentrations in drinking water is set at 2 ppm. There is no guideline value for ammonia at this time from WHO, instead, WHO does recognize odor and taste effects at 1.5 ppm and 35 ppm, respectively. In this work, both copper (Cu^{2+}) and ammonium (NH_4^+) concentrations in the stock solution were fixed at 3 ppm (mg/L), which simulated real wastewater. Batch experiments were performed in order to test the adsorption properties for specific contaminants (copper and ammonium ions) in water of porous geopolymers, and compare them to the performance of geopolymer powder obtained from the crushing of foams, sieved through a 125micron screen.

A fixed amount of geopolymer was brought in contact with a specific amount of test solution with magnetic stirring, and the concentration of the contaminant was monitored as a function of time in order to characterize removal efficiency (R) and adsorption capacity (q) of the adsorbent, which were calculated according to the following formulas:

$$R(\%) = (C_0 - C_t) / C_0 \quad (1)$$

$$q(\%) = ((C_0 - C_t) \times V) / M \quad (2)$$

where C_0 is the starting concentration of the test solution and C_t is the concentration at time t . V is the volume of solution (L) and M the weight of adsorbent (g).

Quantitative analysis of copper and ammonium ions was performed using an UV-visible spectrophotometer [7]. The presence of copper ions was determined by spectrophotometric quantification of a chromogenic blue complex with cuprizone in weakly basic conditions. The presence of ammonium ions was detected by observing the products of the chromogenic reaction with sodium hypochlorite and sodium salicylate in presence of sodium nitroprusside as catalyst.

2.3.7 Insulating property

To ensure a limited humidity and moisture content for the thermal conductivity (λ) measurement, the selected porous geopolymer (PG) specimens were measured shortly after drying (40°C, 3 weeks), as humidity in the same batch of specimens has a significant influence on the λ values[8,9]. The λ data was obtained via a hot-disc thermal analyzer at ambient environment (transient plane source technique). Each selected sample was measured at least three times to obtain a relatively precise average value.

2.3.8 Electrochemical property

The electrochemical impedance spectroscopy (EIS) data of the porous samples were obtained in an O₂ saturated Na₂SO₄ (Aldrich) solution (0.1 M) at open circle potential with exposed volume of 5x5x2 mm³. Pt (805/SPG/12R, AMEL S.r.l., Italy) and saturated mercury sulfate electrode (Hg/Hg₂SO₄) (383/SHG/12J, AMEL S.r.l., Italy) were used as counter electrode and reference electrode respectively. The frequency range of spectra was from 10⁵ Hz to 100 mHz, with 10 mV amplitude [10].

References

- ¹ Feng J, Zhang R, Gong L, et al. Development of porous fly ash-based geopolymer with low thermal conductivity[J]. *Materials & Design (1980-2015)*, 2015, 65: 529-533.
- ² Cilla M S, Morelli M R, Colombo P. Open cell geopolymer foams by a novel saponification/peroxide/gelcasting combined route[J]. *Journal of the European Ceramic Society*, 2014, 34(12): 3133-3137.
- ³ Jämstorp E, Strømme M, Frenning G. Modeling structure–function relationships for diffusive drug transport in inert porous geopolymer matrices[J]. *Journal of pharmaceutical sciences*, 2011, 100(10): 4338-4348.
- ⁴ Nie T, Xue L, Ge M, et al. Fabrication of poly (L-lactic acid) tissue engineering scaffolds with precisely controlled gradient structure[J]. *Materials Letters*, 2016, 176: 25-28.
- ⁵ Chen C, Pang H, Liu Z, et al. Enhanced foamability of isotactic polypropylene composites by polypropylene-graft-carbon nanotube[J]. *Journal of Applied Polymer Science*, 2013, 130(2): 961-968.
- ⁶ Zhang Y, Rodrigue D, Ait - Kadi A. High-density polyethylene foams. I. Polymer and foam characterization[J]. *Journal of applied polymer Science*, 2003, 90(8): 2111-2119.
- ⁷ Hagenkamp-Korth F, Haeussermann A, Hartung E. Effect of urease inhibitor application on urease activity in three different cubicle housing systems under practical conditions[J]. *Agriculture, Ecosystems & Environment*, 2015, 202: 168-177.
- ⁸ Liu M Y J, Alengaram U J, Jumaat M Z, et al. Evaluation of thermal conductivity, mechanical and transport properties of lightweight aggregate foamed geopolymer concrete[J]. *Energy and Buildings*, 2014, 72: 238-245.
- ⁹ Zhang Z, Provis J L, Reid A, et al. Geopolymer foam concrete: An emerging material for sustainable construction[J]. *Construction and Building Materials*, 2014, 56: 113-127.
- ¹⁰ Bard A J, Faulkner L R, Leddy J, Zoski C-G. *Electrochemical methods: fundamentals and applications*. 1980 New York: Wiley.

3. K-based porous geopolymers

3.1. Direct foaming using three different types of stabilizing agent

3.1.1 Introduction

As mentioned above, porous geopolymers (PGs) can be produced by five different routes (direct foaming, replica method, sacrificial template method, the 3D printing, and others), and the direct foaming route showed a series of advantageous features such as easy-handling, low-cost, without complex or expensive equipment, high-efficiency. In this part of the thesis, a series of potassium-based porous geopolymers were fabricated and characterized by a combined of pore-forming agent (PFA, H₂O₂) and stabilizing agent (SA, egg white, Tween 80, vegetable oils).

(1) High-porosity porous geopolymers were fabricated by direct foaming technique using hydrogen peroxide as pore-forming agent and egg white as stabilizing agent, and the high temperature performance of the specimens was investigated;

(2) High-porosity porous geopolymers were produced with tailored porosity by direct foaming technique using hydrogen peroxide as pore-forming agent and Tween 80 as stabilizing agent, and the adsorption properties of the specimens were discussed;

(3) High-porosity porous geopolymers were produced with tailored porosity by direct foaming technique using hydrogen peroxide as pore-forming agent and vegetable oils as stabilizing agents, and the insulating properties of the specimens were discussed.

3.1.2 Direct foaming using egg white as stabilizing agent

3.1.2.1 Experimental procedure

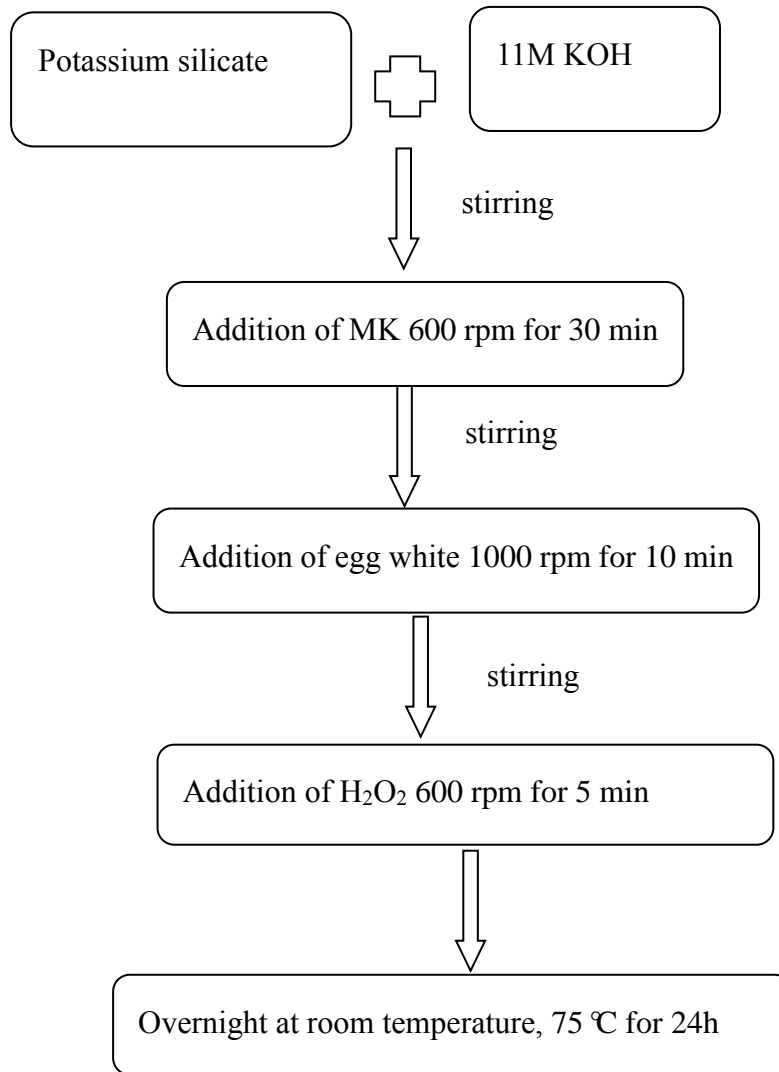


Fig. 3-1 Synthesis protocol of the porous geopolymers using egg white as stabilizing agent.

The synthesis protocol of the porous geopolymers (PGs) was showed in Fig. 3-1. Metakaolin (MK) was used as aluminosilicate source. 11M KOH solution (prepared by dissolving potassium hydroxide pellets) and potassium silicate solution were mixed for at least 24h as reactive ingredients. 3wt% of H₂O₂ solution, was used as chemical pore-forming agent

(PFA). Albumin crude protein from chicken egg white was acted as stabilizing agent (SA) or surfactant. The original suspension (OS), with a theoretical oxide molar ratios: $\text{SiO}_2/\text{Al}_2\text{O}_3=3.53$, $\text{K}_2\text{O}/\text{SiO}_2=0.29$ and $\text{H}_2\text{O}/\text{K}_2\text{O}= 15.1$, was prepared by mechanical mixing of MK and the alkali medium solution. The egg white and H_2O_2 were then successively added to the suspension, respectively. We define the weight fraction of protein in OS as x , and the weight fraction of H_2O_2 in OS as y .

The wet porous geopolymers were obtained by casting the slurry into a sealed plastic mold. Finally, the PGs were cured in a laboratory oven in two steps: (1) overnight at room temperature, to prevent cracking due to an abrupt loss of water; (2) at $75\text{ }^\circ\text{C}$ for 24h in an oven, to consolidate. And one step curing procedure (directly to $75\text{ }^\circ\text{C}$ for 24h) was also conducted for comparison (sample labelled SAO).

Measurements were conducted on samples cured at $75\text{ }^\circ\text{C}$ and after firing for 2h at $600\text{ }^\circ\text{C}$, $800\text{ }^\circ\text{C}$, and $1000\text{ }^\circ\text{C}$ in a muffle furnace and static air atmosphere with $3\text{ }^\circ\text{C}/\text{min}$ heating rate. The high temperature performance and phase transformation characteristics of the samples were evaluated, respectively, by TG/DTA and by dilatometer. The crystalline phase assemblage was identified on ground samples using an X-ray diffractometer. The porosity (open and total), mechanical properties, macrostructure, cell size distribution were investigated.

3.1.2.2 Results and discussion

3.1.2.2.1. Effect of curing process

Since the strength and porosity are two important factors for membrane supports [1], a preliminary study was carried out to investigate the influence of the curing process. The compressive strength (σ , measured on as-cured samples, without any further heat treatment) and the porosity of the PGs with different curing procedures (one-step and two-step curing) are reported in Table 3-1. For comparison, sample SAO was subjected to one-step curing; all the other ones were subjected to two-step curing.

Microstructure analysis (Fig. 3-2) was performed to provide a comparison of the

morphology of the samples according to the two types of curing procedure (samples SAO and SAT), and between the axial (along the foaming direction) and the radial (perpendicular to the foaming direction) cross-sections (sample SAT). To better observe the morphology, the PGs samples were cut into slices. Simultaneously, the homogeneous and isotropic of the microstructure were also investigated. Obviously, a cellular structure, with a large amount of “closed” integrated cells (surrounded by relatively thick struts) having a cell size distribution ranging from $\sim 100\mu\text{m}$ to $\sim 600\mu\text{m}$, was observed in Fig. 3-2. All of the pores among cells and struts, and cell wall widows growing here had typical teardrop-shape morphology. However, the samples cured by the one-step method (Fig. 3-2a) showed that most of cell-like structure could not maintain the integrity. The curing process was found to have a significant effect on both the strength and the pore structure. The probably explain of the phenomenon is that the relatively high temperature treatment can accelerate the decomposition of H_2O_2 , i.e., the sudden relatively high temperature curing treatment leading to either underdeveloped or to a not stabilized cell structure.

Although the samples (SAO) obtained by one-step curing showed higher on both open porosity ($\sim 74.4\%$) and total porosity ($\sim 78.8\%$) than two-step samples (SAT) on both open porosity ($\sim 65.3\%$) and total porosity ($\sim 74.3\%$), the compressive strength (1.2MPa) is far lower than two-step specimens (4.5MPa), and in particular lower than expected according to the value of the TP (the expected value was $\sim 2.0\text{MPa}$, see Fig. 3-5 later). Previous works [2-4] showed that the pre-heat treatment can improve the physical strength and the degree of geopolymerization; specifically, longer curing leads to better mechanical properties. Therefore, the two-step curing process is to be preferred.

The average cell size of the foams computed by image analysis for each sample are as follows: $160.7\pm 70.1\mu\text{m}$ (SAO), $238.6\pm 83.9\mu\text{m}$ (SAT; axial cross-section), and $213.7\pm 90.1\mu\text{m}$ (SAT; radial cross-section). The different cross-sections show a similar cell size distribution, microstructure, and mechanical properties, i.e., the sample appears to possess a very good homogeneity, and therefore it could be used without taking into account the foaming direction. Furthermore, some smaller pores, having a size distribution ranging from ~ 10 to $\sim 70\mu\text{m}$, exist in the cell walls and the struts of all samples. Their presence increase the permeability of the

structure. Simultaneously, the thick struts are beneficial to achieve excellent mechanical strength.

Table 3-1. Data of the relative density (ρ_b), average cell size (ACS), open porosity (OP), total porosity (TP), and compressive strength (σ) depending on the amounts of protein (x) and H₂O₂ (y).

Sample label	x	y	ρ_b (g/cm ³)	ACS (μm)	OP (vol%)	TP (vol%)	σ (MPa)
SA0	0.000	0.1	0.80±0.01	779.4±205.5	61.6±0.7	65.8±1.4	10.0±3.6
SA1	0.025	0.1	0.48±0.01	328.9±119.9	74.3±0.5	77.1±1.2	2.1±0.4
SA0	0.050	0.1	0.46±0.01	160.7±70.1	74.4±0.3	78.8±1.8	1.2±0.3
SAT	0.050	0.1	0.54±0.01	238.6±83.9	65.3±0.8	74.3±1.0	4.5±1.0
SAT radial	0.050	0.1	0.54±0.01	213.7±90.1	65.3±0.8	74.3±1.0	3.8±0.8
SA3	0.075	0.1	0.61±0.01	198.5±70.4	57.2±0.9	71.2±0.5	5.5±0.5
SA4	0.100	0.1	0.67±0.01	140.9±54.1	n.d.*	68.1±0.5	7.0±1.5
SH0	0.05	0	0.89±0.02	112.0±38.9	52.1±0.3	58.4±0.9	21.4±4.5
SH2	0.05	0.05	0.80±0.01	147.3±59.6	n.d.*	61.9±0.6	11.2±3.0
SH3	0.05	0.075	0.65±0.02	156.0±58.8	53.3±0.8	69.6±0.8	5.7±1.1
SH4	0.05	0.1	0.54±0.01	261.4±89.6	65.3±0.8	74.3±1.0	4.5±1.0
SH5	0.05	0.125	0.47±0.01	284.7±104.8	73.6±0.9	78.0±0.6	2.3±0.4
SH6	0.05	0.15	0.40±0.02	336.8±156.2	78.7±1.0	81.3±1.1	1.1±0.3

(*: not determined, the samples break when immersed in boiling water)

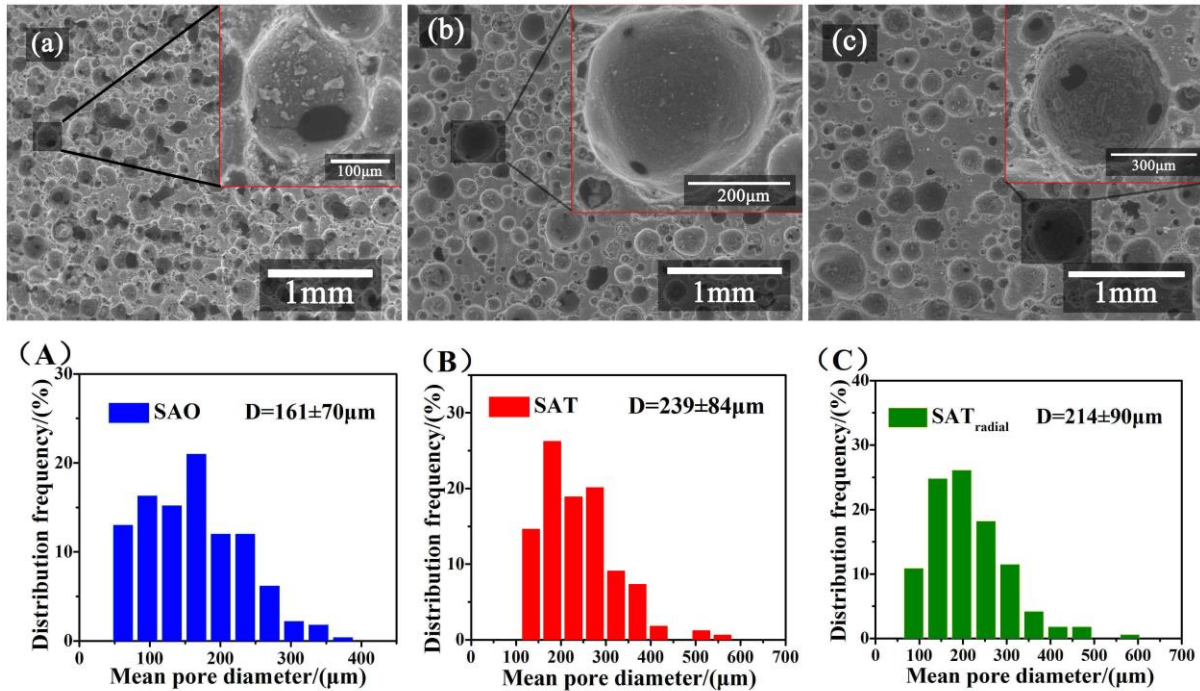


Fig. 3-2. SEM images of PGs specimens: (a) axial direction and one-step curing; (b) axial direction and two-step curing; (c) radial direction and two-step curing. The insets of (a)-(c) are a magnified view of a cell and surrounding struts. (A-C) are the respective cell size analysis.

3.1.2.2.2 Effect of stabilizing agent content

Figs. 3-3(a-d) show the morphological properties of PGs obtained with various stabilizing agent (SA, protein) loadings, and Table 3-1 reports the values of the porosity (total and open), relative density (ρ_b), average cell size (ACS), and compressive strength (σ) depending on amounts of SA. It shows that different contents of albumen had a significant effect on the pore structure. When the protein content increased from 2.5 to 10wt%, the total porosity fell slightly from ~ 77.1 to ~ 68.1 vol%; this could be explained by the observed increase in viscosity of the slurry with increasing amount of protein. The corresponding σ increased from ~ 2.1 to ~ 7.0 MPa. The average cell size for samples with different content of protein was compared with fixed (10wt%) hydrogen peroxide added, the results showed that the average cell size ($328.9 \pm 119.9 \mu\text{m}$ SA1, $238.6 \pm 83.9 \mu\text{m}$ SAT, $213.7 \pm 90.1 \mu\text{m}$ SA3, and $140.9 \pm 54.1 \mu\text{m}$ SA4, respectively) demonstrate a gradually descending trend with increasing

amount of stabilizing agent. This is in accordance with the fact that the SA stabilizes the liquid-gas interface, and the more stabilizing agent is present the larger amount of surface per unit volume can be stabilized.

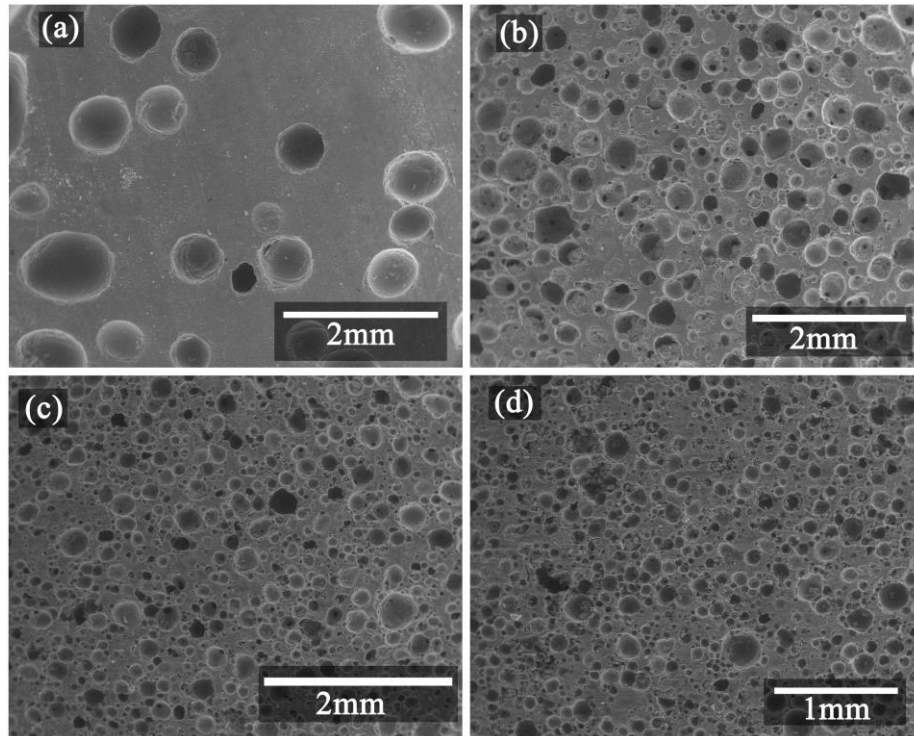


Fig. 3-3. Morphology of PGs produced with various amounts of SA: (a) without protein; (b) $x=0.025$; (c) $x=0.075$; (d) $x=0.1$.

For comparison purposes, a sample (SH0, without protein added) was produced only using PFA (H_2O_2). As can be seen in Fig. 3-3a, a limited amount of closed cells and a very inhomogeneous cell size distribution of the sample SH0 can be observed. This confirms that the porous structure is formed by the decomposition reaction of H_2O_2 , and that the stabilizing agent is necessary to obtain a homogeneous cell size distribution as well as interconnected porosity. And previous studies [5] showed that presence of a stabilizing agent stabilizes the foaming procedure, reducing the pore collapse and coalescence when the foam is still in the liquid state. The high amount of open porosity ($\sim 61.6\text{vol}\%$) for the porous geopolymer produced without SA could be explained by the presence of intrinsic interconnected meso/macro-pores in the geopolymer matrix [6], which can be infiltrated by the boiling water during the measurement (Archimedes principle).

3.1.2.2.3 Effect of hydrogen peroxide content

The SEM images of PGs produced with different H₂O₂ loadings (SAT, SH(0-6)) and fixed amount of protein ($x=0.05$) are compared in Fig. 3-4, and the data concerning TP, OP, ρ_b , ACS, and σ are listed in Table 1 (see above). As can be seen, the porosity of the foams was controlled by changing the pore-forming agent (PFA, H₂O₂) content, the increase in the H₂O₂ amount reduced the ρ_b (from ~ 0.9 to $\sim 0.4\text{g/cm}^3$) and σ (from ~ 21.4 to $\sim 1.1\text{MPa}$) at same content of stabilizing agent. The corresponding axial ACS and TP rise from ~ 112.0 to $\sim 336.8\mu\text{m}$ and from ~ 58.4 to $\sim 81.3\text{vol}\%$, respectively. Simultaneously, the average pore size obtained by the cut surface (SAT; $238.6\pm 83.9\mu\text{m}$) and fracture surface of same sample (SH4; $261.4\pm 89.6\mu\text{m}$) are similar.

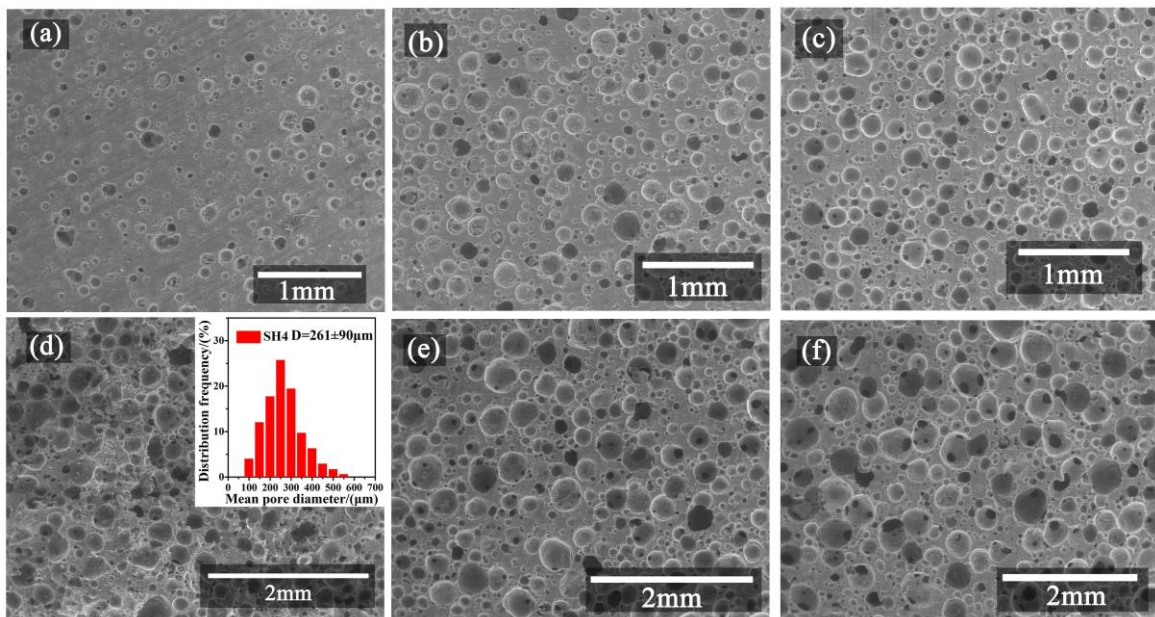


Fig. 3-4 SEM images (axial direction) of PGs produced using various amounts of hydrogen peroxide with fixed stabilizing agent (protein) content: (a) $y=0.0$; (b) $y=0.05$; (c) $y=0.075$; (d) $y=0.1$, fracture surface; (e) $y=0.125$; (d) $y=0.15$). The inset of (d) is the pore size analysis.

The behavior of total porosity (TP) and the corresponding compression strength (σ) was also investigated. As can be seen in Fig. 3-5, the average σ of the PGs samples are plotted as a

function of the TP. The data show that the strength significantly decreases with the porosity, and the relationship can be well described, as proposed by Rice [7,8], by equation $\sigma = \sigma_0 \exp(-bp)$ where σ is the strength at total porosity p , σ_0 is the strength at zero porosity ($p=0$) and b is an empirical constant, and value of b is a parameter depending on the pore structure and material composition. The parameter b represents the dependency level of strength on porosity, i.e., the higher of b value, the more susceptibility of strength on porosity [9].

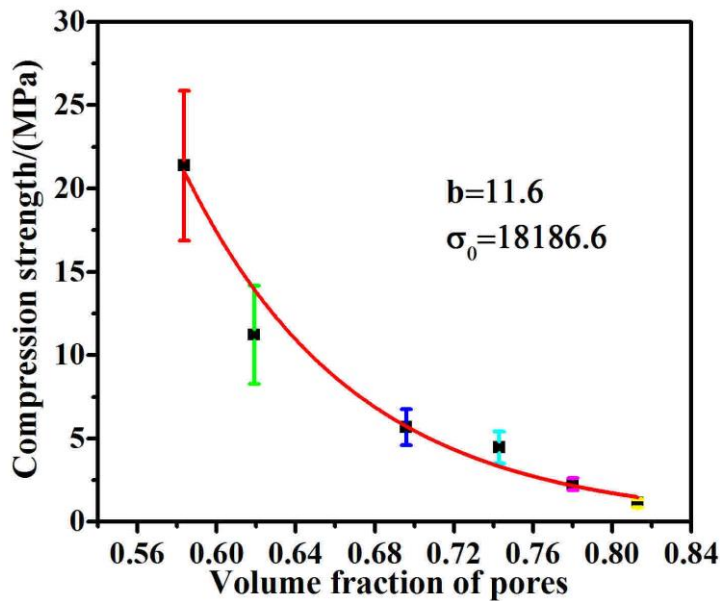


Fig. 3-5. Plot of compressive strength vs. total porosity for PGs with various content of H₂O₂ and fixed amount of stabilizing agent (protein).

A value of $\sigma_0 = 18186.6$ MPa and $b = 11.6$, with a correlation factor $R^2 = 0.96$ were derived from the fitting of compressive strength–porosity data. The reasonably good fitting demonstrates that that the compression strength can be well approximated by equation at least in the total porosity (p) range from ~58 to ~82 vol%, i.e., the relationship of compressive strength and total porosity can be elaborated by the minimum solid area (MSA) model. And The value of parameter $b=11.6$ calculated from equation showed that a high porosity-dependent compressive strength of porous geopolymers. And more investigations should be done to discuss the behavior of strength and porosity.

3.1.2.2.4 Effect of high temperature heat treatment

The high temperature performance of the porous geopolymer samples is reported in Figs. 3-6(a-b), showing an endothermic peak at ~ 113 °C and an exothermic peak at ~ 257 °C, with a corresponding marked weight loss (~ 16.0 wt% at 500 °C), and no further mass change was observable when the temperature greater than 500 °C. The results were similar with geopolymer materials reported in the literature [10]. The weight loss below ~ 150 °C was due to evaporation of free water and condensation/polymerization of hydroxyl [11], while the further one can be explained by the burning out of egg white [12,13]. Another exothermic peak at ~ 935 °C was observed in Fig. 3-6(b). Combined with the XRD analysis (see Fig. 3-6(d)), the exothermic peak was due to potassium aluminum silicate crystallization.

Associated with the weight loss, a concurrent shrinkage occurred (Fig. 3-6(c)). As others' works [14,15] showed that the linear shrinkage curve of alkali-based geopolymers can be divided into four stages as a function of the occurring phenomena. And in our study, the dilatometric analysis also can be broken down into four fields:

- (I) < 130 °C: evaporation of free water from large pores and surface;
- (II) $130\text{--}300$ °C: desorption of water trapped in the pores by capillary strain/dehydration;
- (III) $300\text{--}800$ °C: physical contraction during condensation/polymerization of the Si/Al–OH group;
- (IV) ≥ 800 °C: sintering by viscous flow and crystallization, fusion of the samples.

Fig. 3-6(d) reports the X-ray diffractograms of the samples after heat treatment at different temperatures. A typical amorphous peak characteristic of geopolymer samples (before and after exposure less than or equal to 800 °C in air) centered at around $27^\circ\text{--}29^\circ 2\theta$ was displayed, with some peaks attributable to quartz (SiO_2) and anatase (TiO_2) crystalline impurities in the MK[15-16]. However, after exposure to a higher temperature of 1000 °C, while the impurities remained in the material, there are traces of the formation of new crystalline (KAlSiO_4), which is supported by the exothermic peak at ~ 935 °C in Fig. 3-6(b). The final phase compositions of the PGs significantly depend on the sintering temperature, i.e.,

heat-treating the sample for longer periods significantly increased the amount of crystalline phase in the sample.

With the increasing of heat-treatment temperature, the PGs maintained the open porous structure up to 800 °C (Fig. 3-7), and the mechanical properties displayed a slight increase (Table 3-1). Although the ACS showed a decreasing trend, in accordance with the observed linear shrinkage, the total porosity increased due to the complete elimination of water from the meso-pores in the structure. When $T \geq 800$ °C, a part of the cells was filled by viscous flow, and both the OP (~23.6 vol%) and TP (~51.8 vol%) decreased sharply (see Fig. 3-6(c)), with concurrent significant increase of the σ (from 6.3 to 20.4MPa) and pb (from 0.56 to 1.18 g/cm³).

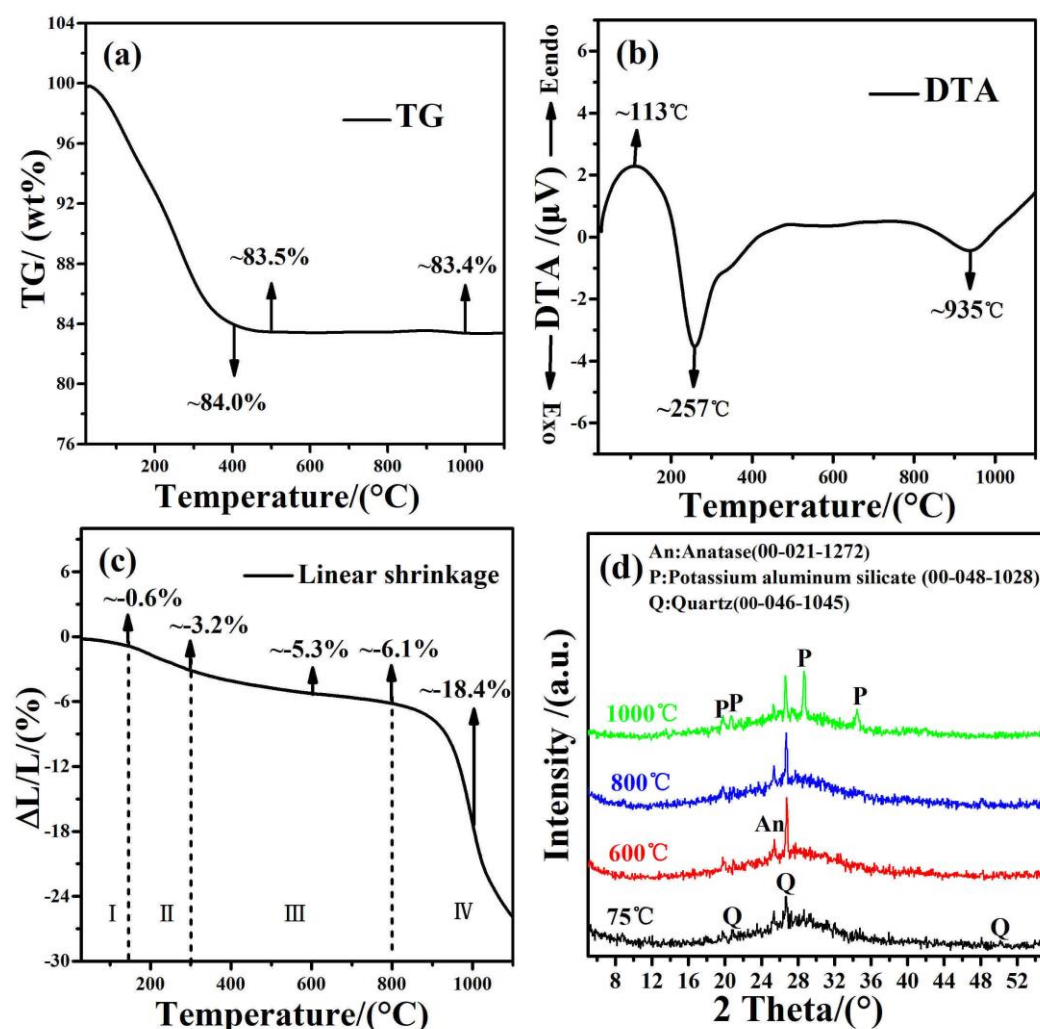


Fig. 3-6. Thermal behavior of PGs sample SAT: (a) TG analysis; (b) DT analysis; (c) linear shrinkage; (d) XRD patterns for samples heat-treated at different temperatures.

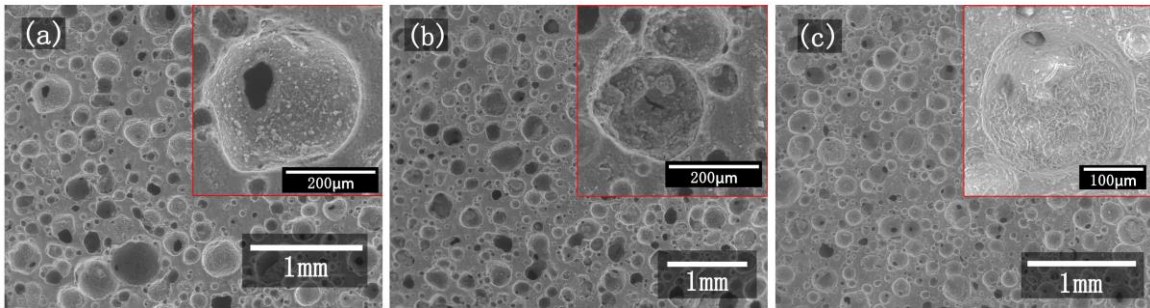


Fig. 3-7. SEM images of PGs (axial direction) heat treated at different temperature: (a) 600°C, (b) 800°C, (c) 1000°C; The insets of (a)~(c) are a magnified view of a cell and surrounding struts.

Table 3-2. The data of ρ_b , ACS, TP, OP, and σ depending on different heat treatment temperature.

Heat treatment temperature (°C)	ρ_b (g/cm ³)	ACS (μm)	OP (vol%)	TP (vol%)	σ (MPa)
RT	0.54±0.01	238.6±83.9	65.3±0.8	74.3±1.0	4.5±1.0
600	0.55±0.01	210.0±83.2	73.6±0.9	76.6±0.4	5.6±1.5
800	0.56±0.02	197.4±83.9	72.6±1.0	76.5±0.9	6.3±2.1
1000	1.18±0.02	171.8±65.5	23.6±1.9	51.8±0.8	20.4±5.3

The porous geopolymers, with hierarchical pore architectures, with good thermal resistance up to 800 °C, with controlled mechanical properties and porosity, and with monomodal pore size distribution (with respect to the cell size), are promising candidates to be employed as membrane support or for other applications where a large volume of interconnected porosity and high chemical and thermal stability is required.

3.1.2.3. Conclusions

High strength PGs with controlled macroporous structure and porosity were produced by direct foaming technique using H₂O₂ as pore-forming agent plus albumen as stabilizing agent. The synergistic effect of hydrogen peroxide and egg white led to high interconnected porosity, good mechanical properties and low bulk density of the cellular geopolymers. The porosity, mechanical properties, bulk density, average cell size can be tuned by the different addition of H₂O₂ and/or protein and the high temperature treatment. The compressive strength increased with the hydrogen peroxide content, as the minimum solid cross-sectional areas were obvious reduced.

These results (morphology, porosity and mechanical properties, and high temperature resistance) for the metakaolin-based porous geopolymer show that they could be used as promising eco-friendly substitutes for highly porous materials in applications such as catalysis and membrane supports, high temperature separation and filtration and refractory components.

This work is published in Ceramics International

Bai C, Colombo P. High-porosity geopolymer membrane supports by peroxide route with the addition of egg white as surfactant[J]. Ceramics International, 2017, 43(2): 2267-2273.

References

- 1 C. Bai, Y. Li, Z. Liu, P. Liu, X. Deng, J. Li, J. Yang, Fabrication and properties of mullite-bonded porous SiC membrane supports using bauxite as aluminum source, *Ceram. Int.* 41 (2015) 4391-4400
- 2 M. Muñoz-Villarreal, A. Manzano-Ramírez, S. Sampieri-Bulbarela, J.R. Gasca-Tirado, J.L. Reyes-Araiza, J.C. Rubio-Ávalos, J. Pérez-Bueno, L. Apatiga, A. Zaldivar-Cadena, V. Amigó-Borrás, The effect of temperature on the geopolymerization process of a metakaolin-based geopolymer, *Mater Lett.* 65 (2011) 995-998
- 3 E. Papa, V. Medri, P. Benito, A. Vaccari, S. Bugani, J. Jaroszewicz, et al. Synthesis of porous hierarchical geopolymer monoliths by ice-templating. *Microporous and Mesoporous Materials*, 215 (2015) 206-214.
- 4 J. Feng, R. Zhang, L. Gong, Y. Li, W. Cao, and X. Cheng. Development of porous fly ash-based geopolymer with low thermal conductivity. *Mater Des*, 65 (2015) 529-533.
- 5 G Masi, W.D.A. Rickard, L. Vickers, et al. A comparison between different foaming methods for the synthesis of light weight geopolymers. *Ceram. Int.*, 40(2014) 13891-13902.
- 6 R.R. Lloyd, J.L. Provis, K.J. Smeaton, J.S.J. van Deventer, Spatial distribution of pores in fly ash-based inorganic polymer gels visualised by Wood's metal intrusion, *Microporous and Mesoporous Materials*. 126 (2009) 32-39
- 7 R. Rice, Comparison of physical property-porosity behaviour with minimum solid area models, *J. Mater. Sci.* 31 (1996) 1509-1528
- 8 R. Rice, Comparison of stress concentration versus minimum solid area based mechanical property-porosity relations, *J. Mater. Sci.* 28 (1993) 2187-2190
- 9 S, Li, C. A. Wang, J. Zhou. Effect of starch addition on microstructure and properties of highly porous alumina ceramics. *Ceram. Int.*, 39 (2013) 8833-8839.
- 10 M.S. Cilla, M.R. Morelli, P. Colombo, Effect of process parameters on the physical properties of porous geopolymers obtained by gelcasting, *Ceram. Int.* 40 (2014) 13585-13590
- 11 P. He, D. Jia, M. Wang, Y. Zhou, Thermal evolution and crystallization kinetics of potassium-based geopolymer, *Ceram. Int.* 37 (2011) 59-63
- 12 S. Dhara, Synthesis of nanocrystalline alumina using egg white, *J Am Ceram Soc.* 88 (2005) 2003-2004

-
- 13 C. Masingboon, S. Maensiri, T. Yamwong, P. Anderson, S. Seraphin, Nanocrystalline $\text{CaCu}_3\text{Ti}_4\text{O}_{12}$ powders prepared by egg white solution route: synthesis, characterization and its giant dielectric properties, *Applied Physics A*. 91 (2008) 87-95
- 14 C. Kuenzel, L.J. Vandeperre, S. Donatello, A.R. Boccaccini, C. Cheeseman, Ambient Temperature Drying Shrinkage and Cracking in Metakaolin-Based Geopolymers, *J Am Ceram Soc.* 95 (2012) 3270-3277
- 15 J.L. Bell, P.E. Driemeyer, W.M. Kriven, Formation of Ceramics from Metakaolin - Based Geopolymers. Part II: K-Based Geopolymer, *J Am Ceram Soc.* 92 (2009) 607-615
- 16 E. Prud'homme, P. Michaud, E. Joussein, C. Peyratout, A. Smith, S. Arrii-Clacens, J. Clacens, S. Rossignol, Silica fume as porogent agent in geo-materials at low temperature, *J. Eur. Ceram. Soc.* 30 (2010) 1641–1648.

3.1.3 Direct foaming using Tween 80 as stabilizing agent

3.1.3.1 Experimental procedure

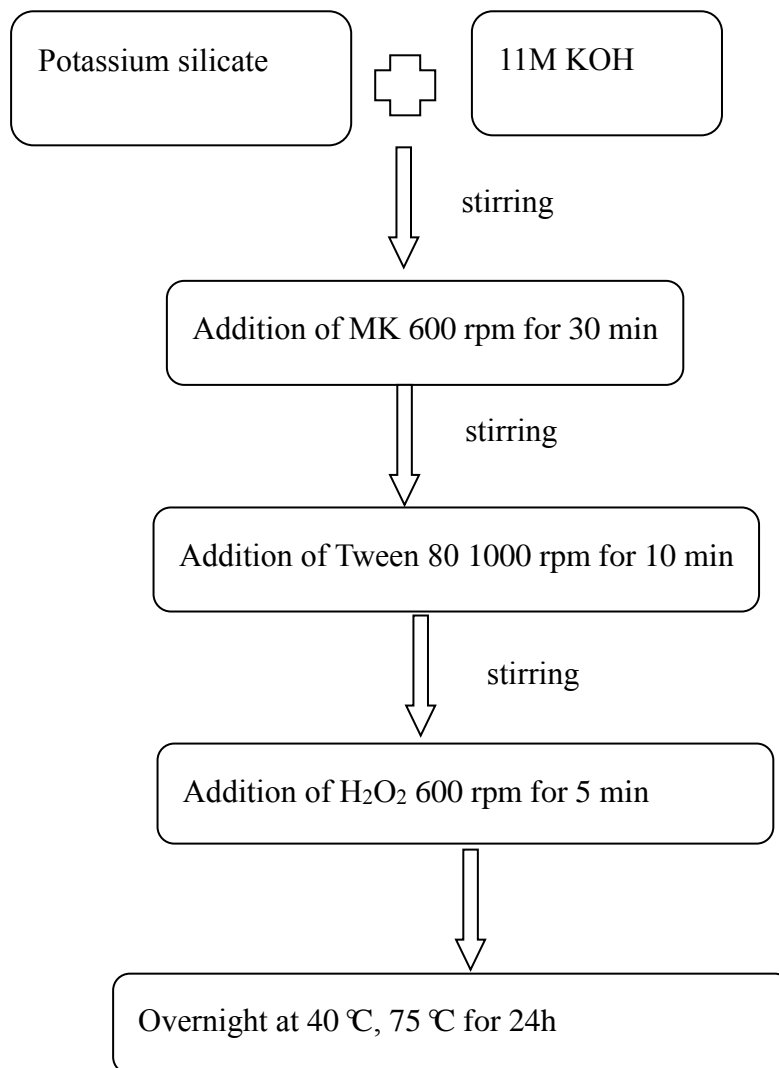


Fig. 3-8 Synthesis protocol of the porous geopolymers using Tween 80 as stabilizing agent.

As showed by Fig. 3-8, homogeneous geopolymer slurries (GSs) were prepared by well mixing metakaolin (MK) and the alkali medium solution (obtained from a solution of 11M KOH and liquid potassium silicate). 3wt% of hydrogen peroxide solution was selected as pore-forming agent (PFA) [1]. Tween 80 was added as stabilizing agent (SA) or surfactant. Afterwards, wet foams were obtained by successively adding the SA and PFA into the pastes. The weight fraction of SA (Tween 80) in GPs was defined as $X \times 100\%$, and the weight fraction of PFA (H_2O_2) in GPs as $Y \times 100\%$. Based on these above-mentioned materials, the slurry resulted in the following theoretical oxide molar ratios: $SiO_2/Al_2O_3=3.53$, $K_2O/SiO_2=0.29$ and $H_2O/K_2O=15.1$.

Immediately after mixing, the wet foams were poured into plastic molds, sealed, and cured in a laboratory oven in two steps: (1) overnight at 40 °C (2) at 75 °C for 24 h. The porosity, phase composition, cellular morphology, mechanical properties, and adsorption properties were investigated.

3.1.3.2 Results and discussion

3.1.3.2.1 Effect of the stabilizing agent content

Table 3-3 lists the data for the relative density (ρ_b), average cell size (ACS), open porosity (OP), total porosity (TP), compression strength (σ), of the porous geopolymers (PGs). Figs. 3-9(a-d) show the morphological characteristics and the cell size distribution of the porous samples produced with different addition of SA. The SEM images of the cut surface (Figs. 3-9(b-d)) show the typical porous microstructure of foams obtained by direct foaming method [2]. A sample (ST0) was produced without the Tween 80 to highlight the role of the stabilizing agent. And a limited amount of closed cells and a very inhomogeneous cell size distribution of the sample SH0 can be observed. Its strength, total porosity and average cell size and cell size distribution values are in accordance with our previous work [3].

A porous structure, comprised of a large amount of spheroidal cells surrounded by relatively thick struts, having a size distribution ranging from $\sim 100\mu m$ to $\sim 600\mu m$, was observed. As can be seen in Figs. 3-9(b-d), and confirmed by the data reported in Table 3-3,

different contents of Tween 80 led to samples possessing similar pore features, porosity (from 83 to 82vol%), and compression strength (about 1 MPa). When the SA content increased from 1.25 to 6.25wt%, the variation trends of ACS (from 270 μ m to 220 μ m) were decreased. The most likely reason of the trends is that: the viscosity of the slurry will increase and the foamability will decrease with increasing amount of stabilizing agent [4-5].

Table 3-3. Values of the ρ_b , ACS, OP, TP, and σ of porous samples produced with different amounts of SA (X%) and PFA (Y%).

Sample label	X(%)	Y(%)	ρ_b (g/cm ³)	ACS (μ m)	OP (vol%)	TP (vol%)	σ (MPa)
ST0	0	10	0.75 \pm 0.01	416.1 \pm 181.9	63.8 \pm 0.6	67.9 \pm 0.4	9.4 \pm 2.9
ST1	1.25	10	0.37 \pm 0.01	264.6 \pm 166.3	82.2 \pm 0.4	83.3 \pm 0.4	1.0 \pm 0.2
ST2	3.75	10	0.39 \pm 0.02	230.0 \pm 144.8	80.3 \pm 0.7	82.4 \pm 0.9	1.3 \pm 0.3
ST3	6.25	10	0.40 \pm 0.01	223.3 \pm 150.1	79.2 \pm 0.9	82.0 \pm 0.5	1.1 \pm 0.1
SH0	3.75	0	0.72 \pm 0.01	96.2 \pm 35.9	-	67.6 \pm 0.6	11.0 \pm 2.1
SH2	3.75	5	0.58 \pm 0.01	185.0 \pm 62.6	72.5 \pm 0.2	73.9 \pm 0.4	4.4 \pm 0.4
SH3	3.75	7.5	0.43 \pm 0.01	211.4 \pm 123.7	78.6 \pm 0.8	80.6 \pm 0.3	1.7 \pm 0.2
SH4	3.75	10	0.39 \pm 0.02	258.1 \pm 156.9	80.3 \pm 0.7	82.4 \pm 0.9	1.1 \pm 0.2
SH5	3.75	12.5	0.33 \pm 0.01	261.0 \pm 191.6	82.4 \pm 0.9	85.1 \pm 0.4	0.6 \pm 0.1
SH6	3.75	15	0.30 \pm 0.02	318.3 \pm 156.2	84.4 \pm 0.3	86.5 \pm 0.9	0.3 \pm 0.1

And when compared with our previous work [3], as curing temperature increased from room temperature to 40 °C, the ratio of OP to TP and ACS increased due to the more effective decomposition of the H₂O₂ (pore-forming agent). The pore collapse and coalescence would increase with the increase of curing temperature for wet foams, but it also benefit for the increase of the permeability of the samples, and this property was confirmed by previous work [3]. Furthermore, most of spheroidal cells surrounded by relatively thick struts showed the presence of interconnecting pores created by gas release at high pressure. To better observe the struts and smaller pores. A higher magnification images were also performed, as can be seen in Figs.3-9(e-f), its show cell windows and smaller pores in the cell wall (< 100 μm), which were also reported in previous works [3,6], and would also improve the permeability of the porous component.

The inset in Fig. 3-9b reports the phase composition of only one of the produced samples (ST1) for brevity as they had the almost same XRD patterns. A typical amorphous peak characteristic of geopolymer samples centered at around 27 °–29° 2θ [3,7] can be detected, with some peaks attributable to quartz (SiO₂), anatase (TiO₂), and muscovite impurities in the MK [3]. After the geopolymer solidification, the center of the scattering diffraction of the diffuse halo shifted from ~22 to ~28 °2θ, confirming the occurrence of the geopolymerization reaction.

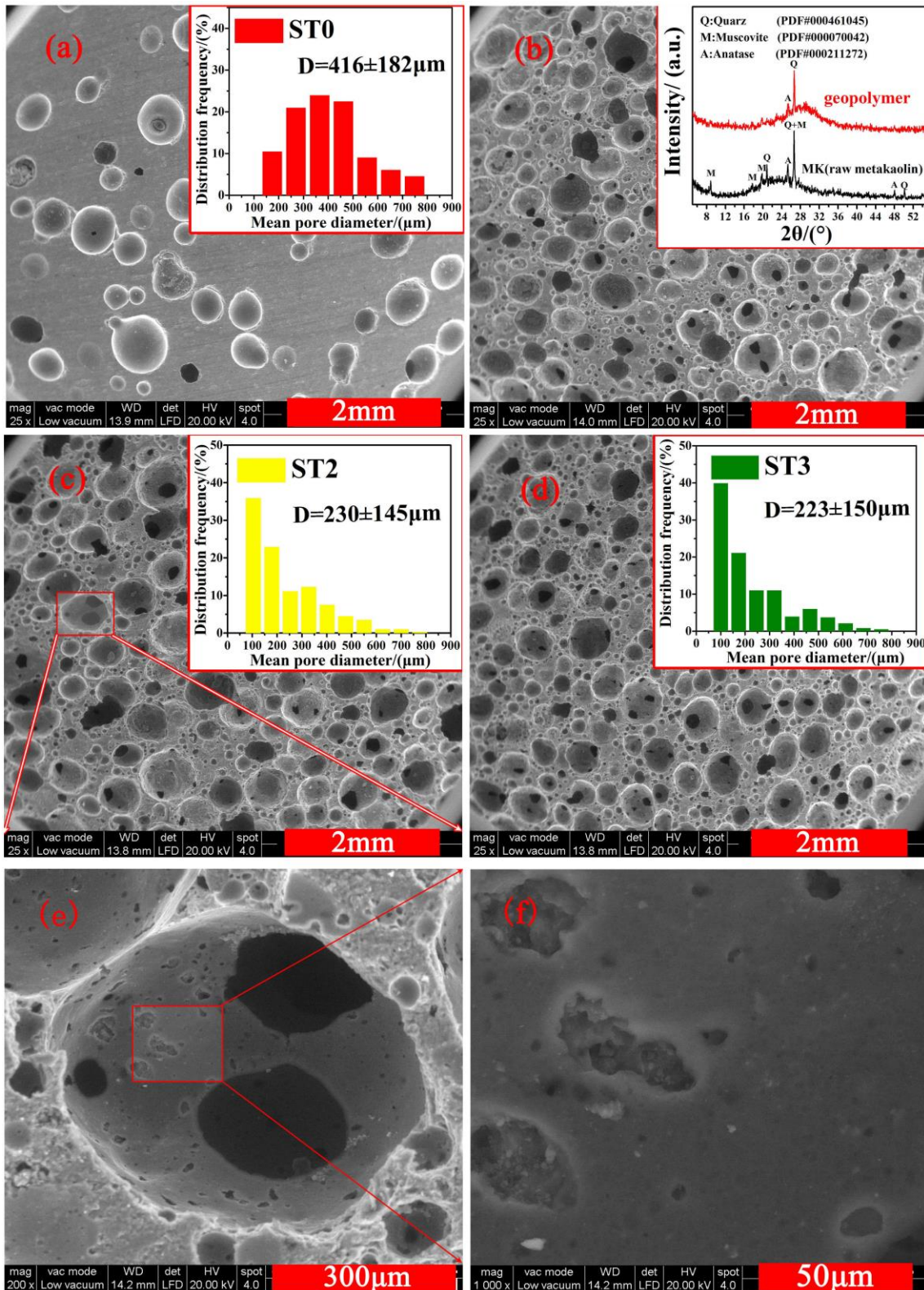


Fig. 3-9. Morphology of PGs produced with various amounts of stabilizing agent (X%): (a) without Tween 80; (b) X=1.25; (c) X=3.75; (d) X=6.25. The insets are the cell size distributions (a, c, d), the XRD patterns (b). (e)-(f) are a magnified views of a cell and of the cell wall.

3.1.3.2.2 Effect of the hydrogen peroxide content

The SEM analysis of porous samples obtained by different content of H₂O₂ (SH(0-6)) and fixed content of Tween 80 (X=3.75) are compared in Fig. 3-4, and the data concerning TP, OP, ρ_b , ACS, and σ are listed in Table 3-3 (see above). As can be seen, The significant morphology differences for porous samples with various content of pore-forming agent can be observed from the SEM images, and it is also evident that the number of cell windows increased with increasing amount of PFA, leading to larger amounts of open porosity, which can be also confirmed in Table 3-3 [3,8].

To investigate the anisotropy of the cellular samples, a radial (perpendicular to the foaming direction) cross section (cut surface) of samples (X=3.75, Y=10, SH4, Fig. 3-10(c)) were also observed. The results (Fig. 3-9(c), Fig. 3-10(c) and Table 3-3) indicate that similar values for the ACS, morphology, and mechanical properties were achieved for the sample produced using 3.75 wt% of SA and 10 wt% of H₂O₂ and measured along the axial (sample ST2) and radial (sample SH4) direction, respectively, suggesting that the porosity in the foams was homogeneously distributed throughout the volume. Sample ST0 (without stabilizing agent) and SH0 (without pore-forming agent) were produced in order to highlight the synergistic effect of two different additives: pore-forming agent (PFA) and stabilizing agent (SA). Sample ST0 and SH0 possessed similar TP (67.9vol% and 67.6vol%) and strength (9.4MPa and 11MPa), but significantly different ACS (~416 μ m and ~96 μ m). The relatively high amount of open porosity (~63.8 vol%) for Sample ST0, whose cells SEM investigations show do not possess a large amount of interconnecting cell windows, can be explained by the presence of intrinsic meso/macro-pores in the geopolymer matrix [9].

The synergistic effect of SA and PFA led to the generation of a good interconnected homogeneous cell structure and low relative density. The porosity of the foams was controlled by changing the pore-forming agent (PFA, H₂O₂) content, the increase in the hydrogen peroxide content from 5 to 15wt% with same amount of SA reduced the relative density from ~0.58 to ~0.30g/cm³ and compressive strength from ~4.4 to ~0.3MPa, respectively. The corresponding axial ACS and TP increased from ~185.0 to ~318.3 μ m and from ~73.9 to ~86.5

vol%, respectively.

The relationship between total porosity and the corresponding compressive strength was also explored. The average compressive strength of the FGs samples are plotted as a function of the total porosity. The data indicate, as expected, that the strength significantly decreases with porosity, and the relationship can be described by the minimum solid area (MSA) model proposed by Rice [10,11], when the total porosity ranges between ~74 to ~ 87 vol%. As the strength of a cellular component is related to its total porosity by the following equation: $\sigma = \sigma_0 \exp(-bp)$ where σ is the strength at relative total porosity p , σ_0 is the strength of the dense solid ($p=0$) and b is an empirical constant. The parameter b represents the dependency level of strength on porosity, i.e., the higher of b value, the more susceptibility of strength on porosity [3]. Based on the results (SH2-6) of the σ and TP data, values of $\sigma_0 = 1384846.7$ MPa and $b = 17.1$, with a correlation factor $R^2 = 0.96$ were obtained fitting the experimental data with equation. The reasonably good fitting demonstrate that the dependence of compression strength on total porosity can be described by the minimum solid area (MSA) model, when p value ranges between ~0.74 to ~ 0.87.

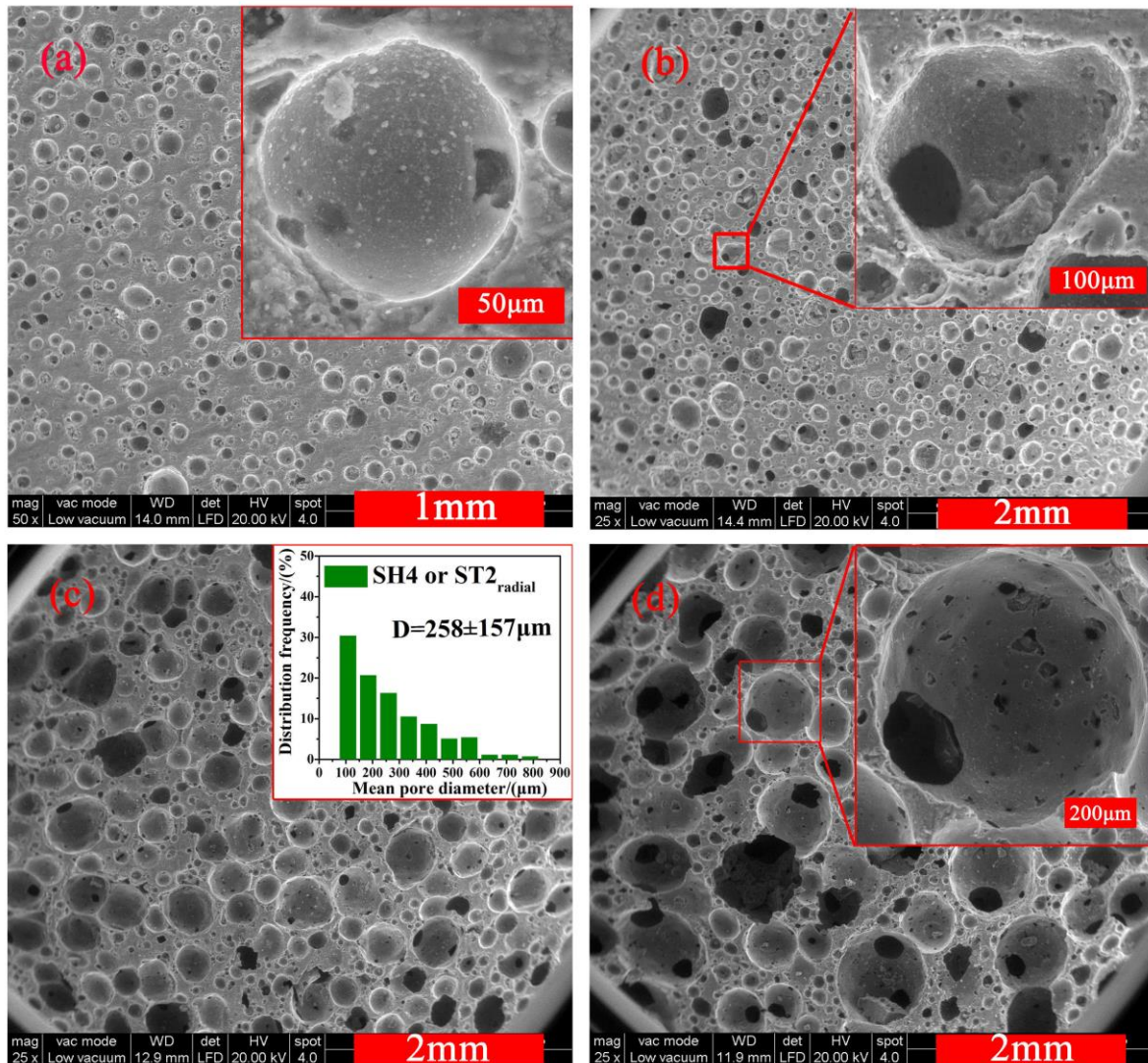


Fig. 3-10. SEM images of PGs produced using different amounts of hydrogen peroxide with fixed stabilizing agent (Tween 80) content: (a) Y=0.0; (b) Y=5; (c) Y=10; radial direction (d) Y=15). The insets of (a, b, d) are the magnified view of a cell and surrounding struts and the inset of (c) is the cell size distribution for sample SH4 (radial direction).

3.1.3.2.3 Copper and ammonium ion removal test

The amount of copper (Cu^{2+}) and ammonium (NH_4^+) ions removed for different contact time and various foamed geopolymer samples are presented in Table. 3-4. It can be seen that the amount of Cu^{2+} adsorbed was found to be dependent on contact time [12]. Furthermore, the Cu^{2+} ions removal efficiency increased with the porosity of PGs, as the active contact sites increased with porosity [13]. This result suggests that the higher adsorption can be achieved by

the higher porosity geopolymers foams with longer contact time. Besides a series of rectangular parallelepiped samples were immersed in Cu^{2+} and NH_4^+ ion solution to measure the adsorption tests. For comparison, the adsorption tests of the grinded powder of PGs were also performed. It showed that the foamed geopolymer samples (SH4) can also obtained high removal efficiency (86.7%) as geopolymer powders (90.0%).

The maximum Cu^{2+} (0.54 mg/g) and NH_4^+ (0.57 mg/g) uptake listed here are significantly smaller than those reported for metakaolin-based geopolymer powders (21.07 mg/g for ammonium) [14]. The reason can be explained by: (1) the adsorbent dose is high (50g/L), (2) initial content of Cu^{2+} and NH_4^+ is low (3ppm). But the data show in any case that most of the ions are removed from the solutions. The above-mentioned results (Table 3-4), therefore, indicate the potential that these foams have as adsorbent materials for copper and ammonium removal with high uptake efficiency. As far as ammonium adsorption data is concerned, it would have been more effective to compare powder vs. foamed sample at the same time. More investigations should be carried out to the ammonium adsorption.

Considering the advantages of monolithic porous geopolymers: (1) easy of shaping, (2) lower pressure drop, higher mixing (high convection inside the cells, with enhanced mass and heat transfer) and optimizable contact time [15-16], (3) easier to collect and recycle in comparison with powdered adsorbents, (4) cheaper and more durable in comparison with traditional inorganic membranes. We can thus propose the use of these eco-friendly adsorbing materials as monolithic filters, components for packed beds or self-supported inorganic membranes.

Table 3-4. Removal efficiency and adsorption capacity of copper and ammonium ions for different samples as a function of contact time.

Sample label	Time (h)	Cu²⁺/C_t (ppm)	Cu²⁺/R(%)	Cu²⁺/q (mg/g)	NH₄⁺/C_t (ppm)	NH₄⁺/R(%)	NH₄⁺/q (mg/g)
SH4	0,5	2.6	13.3	0.08			
SH4	1.5	2.2	30.0	0.18			
SH4	6	2.1	26.7	0.16			
SH4	24	1.1	63.3	0.38	0.14	95.3	0.57
SH4	60	0.4	86.7	0.52			
SH2	24	1.6	46.7	0.28			
SH6	24	0.5	83.3	0.5			
SH4-Powder	6	0.3	90.0	0.54	0.23	92.3	0.55

3.1.3.3. Conclusions

High strength PGs with tailored porosity and macro-porous structure were produced by direct foaming method using H₂O₂ as pore-forming agent plus Tween 80 as stabilizing agent. The synergistic effect of hydrogen peroxide and Tween 80 led to high interconnected porosity, good mechanical properties, low bulk density of porous geopolymers. Different porosity (~74-~87vol%), average pore size (185-318µm), and compressive strength (0.3-4.4MPa) were obtained by changing the content of H₂O₂ and Tween 80. The relationship between the porosity and strength could be explained by the MSA model.

High removal efficiency for copper ions (~87%) and ammonium ions (~95%) for a system simulating real drinking wastewater (with low concentration (3 ppm) of pollutants) was achieved using employing monolithic foamed components. The results obtained for the foamed geopolymers (porosity, pore morphology, mechanical properties, adsorption efficiency and capacity) display that they could be employed as promising eco-friendly substitutes for highly porous materials in potential applications in wastewater treatment.

This work is published in Journal of Materials Research

Bai C, Franchin G, Elsayed H, et al. High-porosity geopolymer foams with tailored porosity for thermal insulation and wastewater treatment[J]. Journal of Materials Research, 2017:32(17), 3251-32597.

References

- 1 J. Feng, R. Zhang, L. Gong, Y. Li, W. Cao, and X. Cheng: Development of porous fly ash-based geopolymer with low thermal conductivity. *Mater. Des.* **65**, 529 (2015)
- 2 L. Verdolotti, B. Liguori, I. Capasso, A. Errico, D. Caputo, M. Lavorgna, and S. Iannace: Synergistic effect of vegetable protein and silicon addition on geopolymeric foams properties. *J. Mater. Sci.* **50**, 2459 (2015).
- 3 C. Bai and P. Colombo: High-porosity geopolymer membrane supports by peroxide route with the addition of egg white as surfactant. *Ceram. Int.* **43**(2), 2267 (2017).
- 4 L. Yin, H. X. Peng, S. Dhara, L. Yang, and B. Su: Natural additives in protein coagulation casting process for improved microstructural controllability of cellular ceramics. *Compos. Part B Eng.* **40**(7), 638 (2009).
- 5 L. yan Yin, X. gui Zhou, J. shan Yu, H. lei Wang, S. Zhao, Z. Luo, and B. Yang: New consolidation process inspired from making steamed bread to prepare Si₃N₄ foams by protein foaming method. *J. Eur. Ceram. Soc.* **33**(7), 1387 (2013).
- 6 Z. Liu, N. N. Shao, D. M. Wang, J. F. Qin, T. Y. Huang, W. Song, M. X. Lin, J. S. Yuan, and Z. Wang: Fabrication and properties of foam geopolymer using circulating fluidized bed combustion fly ash. *Int. J. Miner. Metall. Mater.* **21**(1), 89 (2014)
- 7 I. Lecomte, M. Liégeois, A. Rulmont, R. Cloots, and F. Maseri: Synthesis and characterization of new inorganic polymeric composites based on kaolin or white clay and on ground-granulated blast furnace slag. *J. Mater. Res.* **18**, 2571 (2003).
- 8 Z. Liu, N. N. Shao, D. M. Wang, J. F. Qin, T. Y. Huang, W. Song, M. X. Lin, J. S. Yuan, and Z. Wang: Fabrication and properties of foam geopolymer using circulating fluidized bed combustion fly ash. *Int. J. Miner. Metall. Mater.* **21**(1), 89 (2014)
- 9 R.R. Lloyd, J.L. Provis, K.J. Smeaton, J.S.J. van Deventer: Spatial distribution of pores in fly ash-based inorganic polymer gels visualised by Wood's metal intrusion. *Micropor. Mesopor. Mat.* **126**, 32 (2009)
- 10 R. Rice: Comparison of physical property-porosity behaviour with minimum solid area models. *J. Mater. Sci.* **31**, 1509 (1996)

-
- 11 R. Rice: Comparison of stress concentration versus minimum solid area based mechanical property-porosity relations. *J. Mater. Sci.* **28**, 2187 (1993)
 - 12 Y. Ge, X. Cui, Y. Kong, Z. Li, Y. He, and Q. Zhou: Porous geopolymeric spheres for removal of Cu(II) from aqueous solution: Synthesis and evaluation. *J. Hazard. Mater.* **283**, 244 (2015).
 - 13 R. M. Novais, L. H. Buruberry, M. P. Seabra, and J. A. Labrincha: Novel porous fly-ash containing geopolymer monoliths for lead adsorption from wastewaters. *J. Hazard. Mater.* **318**, 631 (2016).
 - 14 T. Luukkonen, M. Sarkkinen, K. Kemppainen, J. Rämö, and U. Lassi: Metakaolin geopolymer characterization and application for ammonium removal from model solutions and landfill leachate. *Appl. Clay Sci.* 119, Part 2, 266 (2016).
 - 15 M. V. Twigg and J. T. Richardson: Fundamentals and applications of structured ceramic foam catalysts. *Ind. Eng. Chem. Res.* **46**(12), 4166 (2007).
 - 16 F. Lucci, A. Della Torre, G. Montenegro, and P. Dimopoulos Eggenschwiler: On the catalytic performance of open cell structures versus honeycombs. *Chem. Eng. J.* **264**, 514 (2015).

3.1.4 Direct foaming using vegetable oils as stabilizing agents

3.1.4.1 Experimental procedure

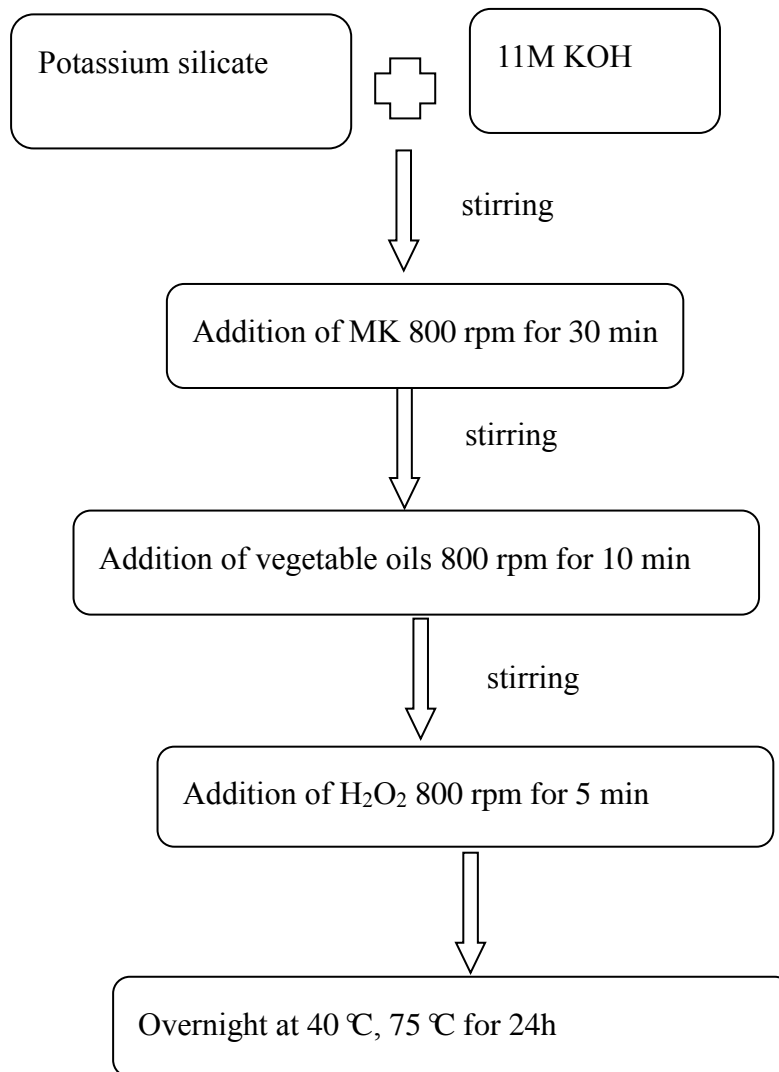


Fig. 3-11 Synthesis protocol of the porous geopolymers using vegetable oils as stabilizing agents.

Fig. 3-11 showed the synthesis protocol of the porous geopolymers (PGs) using vegetable oils as stabilizing agent. Commercially available metakaolin (MK) was used as raw material to prepare the geopolymer. Alkali activator solution was prepared by mixing a solution of 11M KOH and liquid potassium silicate. 3 wt% hydrogen peroxide (H₂O₂) solution was used as the pore-forming agent (PFA). Three easily available vegetable oils (sunflower oil, canola oil, olive oil) were selected as stabilizing agents (SAs), or surfactants.

Geopolymer slurries (GSs) were obtained by mechanically mixing MK with the liquid alkali solution as showed in Fig. 3-11. The GSs with a 36.5 wt% MK content had the following theoretical oxide molar ratios: K₂O/SiO₂=0.29, SiO₂/Al₂O₃=3.53, and H₂O/K₂O=15.1.

Afterwards, homogenous wet foams (WFs) were obtained by successively adding the SA and PFA. The mass ratio of stabilizing agents in GSs was defined as X×100%, and the weight ratio of pore-forming agent (H₂O₂) in GSs as Y×100%. It should be noted that KOH will be consumed by the addition of oil (saponification reaction) giving additional surfactant (soap molecules) and glycerol, and the corresponding true K₂O/SiO₂ values as a function of oil content (X) therefore were 0.28 (X=1.25), 0.27 (X=2.5), 0.26 (X=5), 0.22 (X=10), 0.19 (X=15).

Immediately after mixing, the sealed plastic molds containing the specimens were cured in two steps: (1) overnight at 40 °C in an oven; (2) at 75 °C for 24 h. The dimensions of the resulting samples were ~13×~50×~50 mm³ after polishing. After drying (40°C, 3 weeks), the thermal conductivity (λ) of selected porous geopolymers (PGs) specimens were measured using a hot-disc thermal analyzer. Prior to the characterization of bulk density, porosity, pore morphology, pore size distribution, and mechanical properties, the selected specimens were cut into parallelepipeds (~15×~15×~11 mm³). Afterwards, an extraction step for the removal of glycerol and (potential) residual oil, was carried out. The obtained geopolymer specimens were put in a beaker and submerged with distilled water (in an oven at ~80°C), and the water was renewed every 40~80 min until it remained clear (it took about 1~2d). Afterwards, the PGs were dried at 40°C in an oven for two weeks.

3.1.4.2 Results and discussion

3.1.4.2.1 Effect of different types of oil

The data for the relative density (ρ_b), average cell size (ACS), total porosity (p), compression strength (σ), and thermal conductivity (λ) of the porous geopolymers (PGs) using three different type of edible oils (SS, sunflower oil; SC, canola oil; SO, olive oil) as stabilizing agents are listed in Table 3-5. Both the optical (Figs.3-12(a-c)) and SEM (Figs. 3-12(d-f)) images of the cellular specimens obtained by the different kinds of oil (SA, Stabilizing agent, X=5) with same H_2O_2 (PFA, Pore-forming agent, Y=10) content were showed and compared. The PGs, produced by the synergistic effect of SA (oil) and PFA (H_2O_2), led to the generation of a well interconnected, homogeneous cell structure and low relative density. A homogeneous distribution of macro-pores, ranging from 150 to 400 μ m, was observed (Figs. 3-12(a-f)). The cell size distribution (based on the Figs.3-12(a-f)) is reported in Fig. 3-12(g-i). Both the microstructure and cell size distribution results are in agreement with previous works using direct foaming methods [1-3].

Clearly, different types of the three vegetable oil led to similar bulk density ($\sim 0.5\text{g/cm}^3$), pore structure, thermal conductivity ($\sim 0.14\text{W/mK}$), and porosity ($\sim 75\text{vol}\%$) (Figs. 3-12(a-i) and Table 3-5). However, the PGs obtained using sunflower and canola oil as stabilization agent presented similar porosity but lower mechanical strength ($\sim 2.5\text{MPa}$) than foamed via olive oil ($\sim 3.5\text{MPa}$). This could be interpretation considering the different average cell size (ACS) and cell size distribution [4]. The ACS of the PGs computed by image analysis for each sample are as follows: $281\pm 76\mu\text{m}$ (sunflower oil, Fig. 3-12g), $285\pm 78\mu\text{m}$ (canola oil, Fig. 3-12h), and $258\pm 75\mu\text{m}$ (olive oil, Fig. 3-12i). Previous work showed that the compression strength of porous ceramics linearly increased with the decreasing of the macro-pore size for a given total porosity [5]. The different ACS is likely due to the features of lathers produced by the different oils, i.e., different oils with different composition of aliphatic chains produce different types of soap molecules [4].

Table 3-5. Values of relative density (ρ_b), average cell size (ACS), total porosity (TP), compression strength (σ) and thermal conductivity (λ) for PGs obtained using different amounts of stabilizing agent (X%) and pore-forming agent (Y%).

Sample label	X (wt%)	Y (wt%)	ρ_b (g/cm ³)	ACS (μ m)	TP (vol%)	σ (MPa)	λ (W/mK)
SS	5	10	0.54±0.01	281±76	75.0±0.4	2.4±0.5	0.1462
SC	5	10	0.52±0.02	285±78	75.6±0.7	2.5±0.7	0.1452
SO	5	10	0.55±0.01	258±75	74.8±0.5	3.5±0.6	0.1373
SO1	1.25	10	0.57±0.01	263±75	75.1±0.4	3.1±0.8	-
SO2	2.5	10	0.56±0.01	264±66	75.0±0.4	2.7±0.9	-
SO4	10	10	0.51±0.01	221±63	75.6±0.4	3.2±0.5	
SO5	15	10	0.55±0.01	204±63	72.3±0.5	2.3±0.4	
[6]	0	10	0.75±0.01	420±180	67.9±0.4	9.4±2.9	0.2893
SH0	5	0	0.87±0.02	-	60.2±0.7	30.7±4.2	-
SH1	5	5	0.74±0.01	124±57	66.1±0.3	11.6±1.5	0.1732
SH2	5	10	0.55±0.01	250±73	74.8±0.4	3.5±0.6	0.1373
SH3	5	15	0.42±0.01	555±147	80.8±0.4	0.5±0.1	0.1131
SH4	5	20	0.37±0.01	579±149	83.1±0.3	0.3±0.1	0.1065

Based on the above-mentioned results, olive oil gave a better strength (3.5 MPa) and similar thermal conductivity (0.14 W/mK) and porosity (75vol%) with same content of stabilization agent, and thus olive oil was used as stabilizing agent in the following investigation concerning the effect of the amount of oil and hydrogen peroxide on the porosity, bulk density, average cell size, thermal conductivity, and strength.

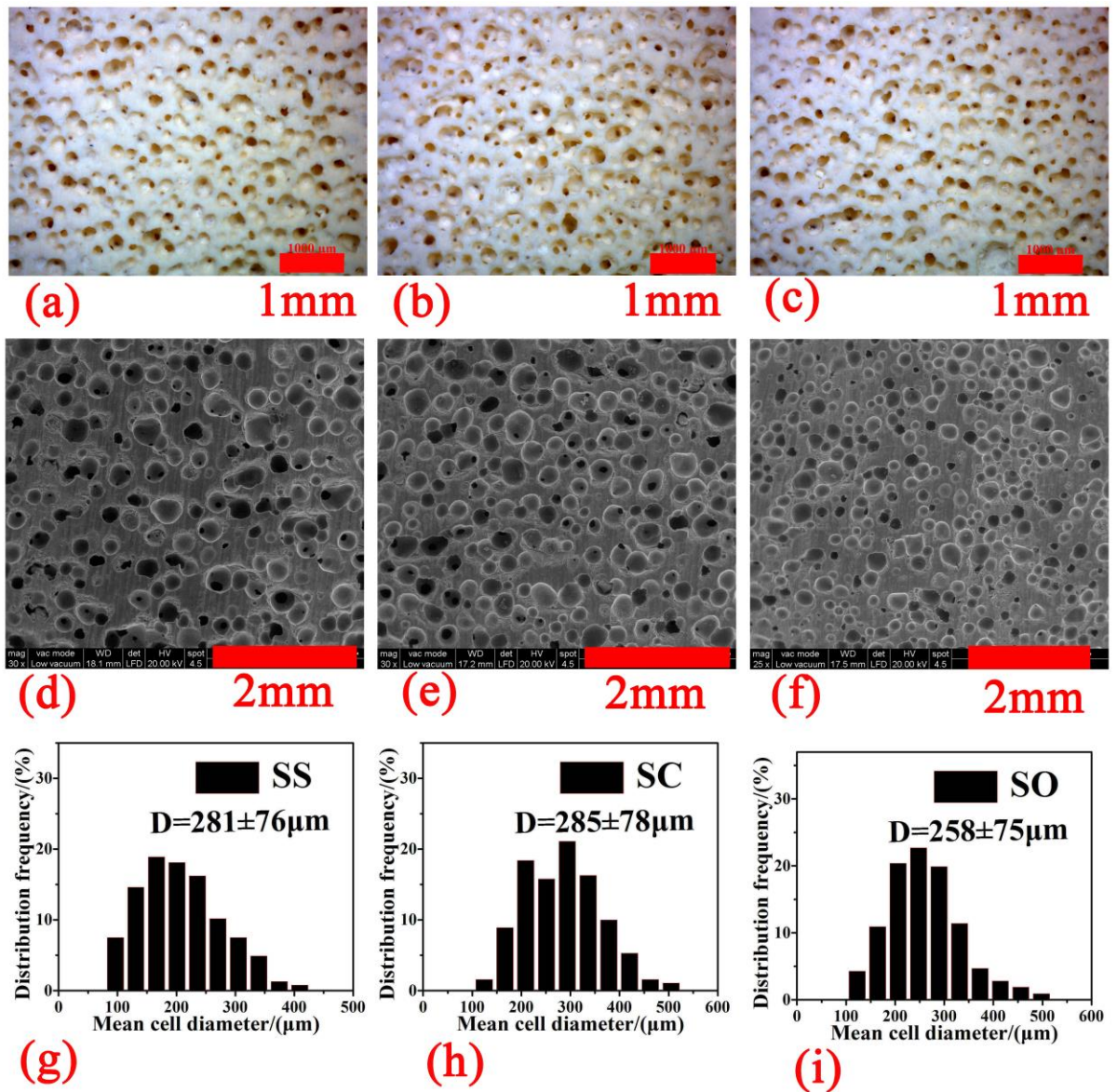


Fig. 3-12. Optical (a-c) and SEM (d-f) images and cell size distributions (g-i) of PGs produced with three different types of oil (X%): (a,d,g) sunflower oil; (b,e,h) canola oil; (c,f,i) olive oil.

3.1.4.2.2 Effect of different amounts of olive oil and of hydrogen peroxide

Different olive oil contents ($X=1.25-15$) and fixed content of H_2O_2 ($Y=10$) in the production of PGs samples were trialed. The data concerning the relative density (ρ_b), average cell size (ACS), total porosity (TP), and compression strength (σ) are also reported in Table 3-

5. The microstructural features of the cellular geopolymers produced using different amounts of stabilizing agent (SA) are showed in Fig. 3-12 (f) and Fig. 3-13 (a-d).

As it can be observed in the SEM results, and confirmed in Table 3-5, when $x < 15$, various contents of SA (olive oil) led to samples possessing similar pore morphology, porosity. The measured ρ_b decreased slightly from 0.57 g/cm^3 to 0.51 g/cm^3 as the mass fraction of stabilizing agent to geopolymer slurry increased from 1.25% to 10%, the compression strength (about 3MPa) and total porosity ($\sim 75\text{vol}\%$) are no obvious variation. However, after that the ρ_b was increased to 0.55 g/cm^3 and the both the TP and the σ dropped by adding more olive oil contents ($X=15$). Excess oil cannot enhance the p and σ , and the reason for this is related to the complex interplay between all the processing variables. In this case when a higher amount of oil ($X > 5$) was added, it cannot neglect the influence by the saponification reaction, as KOH will be consumed and the value of the $\text{K}_2\text{O}/\text{SiO}_2$ ratio in the geopolymer dropped from $0.29(X=0)$ to $0.19(X=15)$ with increasing amount of oil. Furthermore, a decrease trend of the ACS from $\sim 263\mu\text{m}$ to $\sim 204\mu\text{m}$ with increasing oil content was presented. It was likely due to that the larger amount of liquid-gas interface can be stabilized with the increase of SA addition [1] and/or to the rise in viscosity in the slurry [6]. Sample only with PFA ($Y=10$) and without SA were discussed in previous study [6], which can be applied to highlight the role of SA and the synergistic effect of SA (oil) and PFA (H_2O_2).

Also, PGs with a homogeneous spheroidal pore structure as well as high porosity and mechanical strength could be achieved by the synergistic effect of stabilizing agent (oil) and pore-forming agent (H_2O_2) (Figs. 3-(12-14)). Furthermore, the optic and SEM micrographs of PGs with different of PFAs were also compared in Figs. 3-12(c, f) and Fig. 3-14. From the optic and SEM images and table 3-5, the significant morphology differences (pore size, pore volume fraction) for PGs with the increase of the PFA can be clearly observed, and it also showed that the relatively homogeneous cells structure are interconnected (see insets of Figs 3-14(d-f)) and some smaller pores in the cell walls and the struts. The smaller pores (see insets of Figs. 3-14(d-f)) due to oil droplets which can be removed by the hot water extraction step. When the proportion of the added pore-forming agent ($Y=5-20$, $X=5$) was increased, the ρ_b and σ sharply dropped from ~ 0.74 to $\sim 0.37 \text{ g/cm}^3$ and from ~ 11.3 to $\sim 0.3 \text{ MPa}$, respectively.

The corresponding ACS and p increased from ~ 190 to $\sim 320\mu\text{m}$ and from ~ 661.9 to $\sim 83.1\text{vol}\%$, respectively. Additionally, with the rise of H_2O_2 proportion, the λ dropped from 0.17 to 0.11 W/mK due to the increasing of pore volume fraction [7].

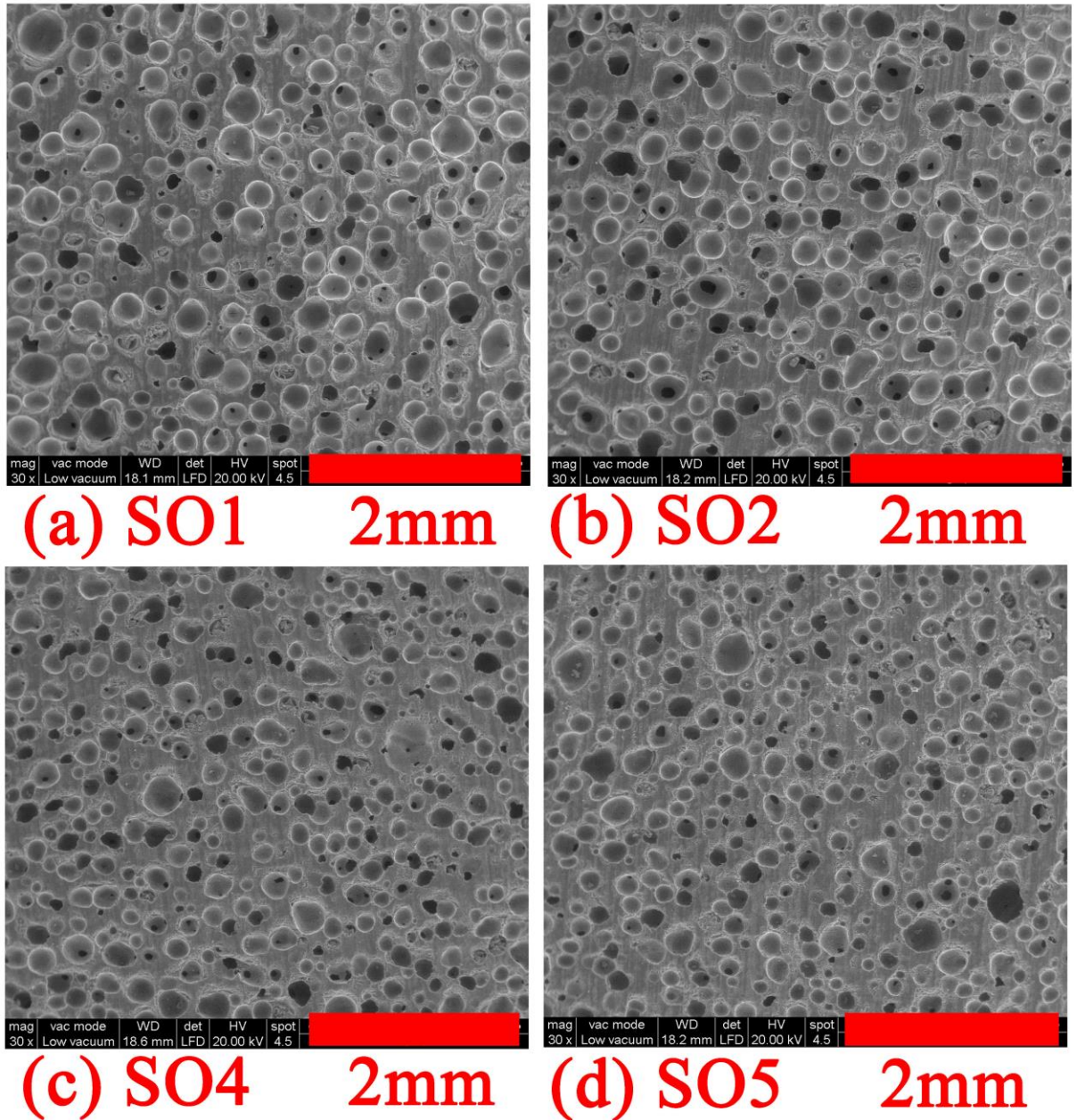


Fig. 3-13. SEM images of PGs produced using different amounts of stabilizing agent (olive oil) with fixed pore-forming agent content.

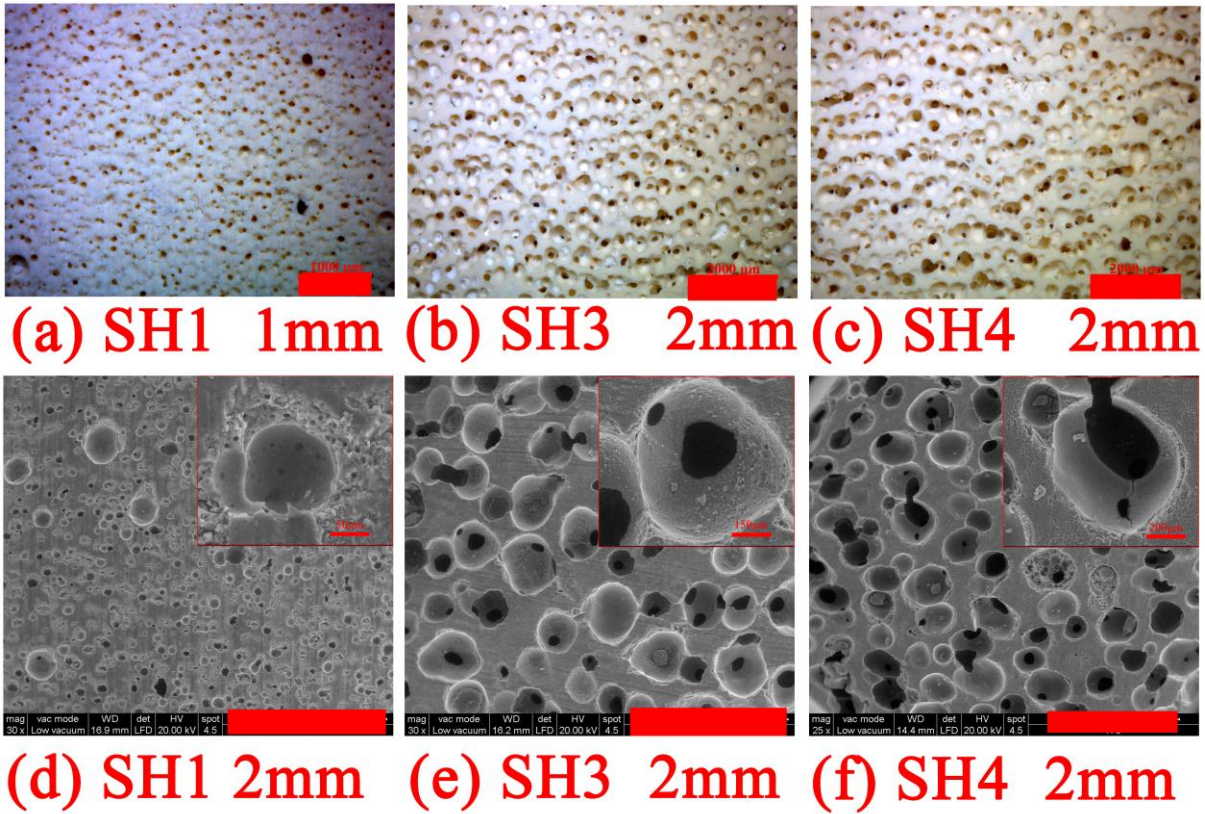


Fig. 3-14. Optical (a-c) and SEM (d-f) images of PGs produced using different amounts of pore-forming agent with fixed stabilizing agent (olive oil) content. The insets of (d, e, f) are the magnified view of a cell and surrounding struts.

Table 3-6. Values of the main thermo-physical characteristics of porous geopolymers, from this work and literature (RM= raw materials; PFA=pore-forming agent; MK=metakaolin; FA=fly ash)

RM	Reference	PFA	ρ_b (g/cm ³)	ACS (μ m)	TP (vol%)	σ (MPa)	λ (W/mK)
MK	This work	H ₂ O ₂	0.37-0.74	124-579	66-83	0.3-11.6	0.11-0.17
FA,slag	8	SAC	0.6-1.2	-	-	2-30	0.1-0.5
FA	9	Al	0.89-0.93	-	-	5.5-10.9	0.25-0.39
FA	10	H ₂ O ₂	0.6-1.2	-	42-73	1.2-7.0	0.1-0.4
MK	11	H ₂ O ₂	0.42-0.57	-	-	0.2-0.8	0.16-0.19
Perlite	12	H ₂ O ₂	0.28-0.66	530-2100	79-90	0.25-0.82	0.03-0.06
FA	13	H ₂ O ₂	0.2-0.4	-	74-81	0.4-1.4	0.07-0.09
FA	14	H ₂ O ₂	0.4-0.6	-	-	1.9-3.4	0.08-0.13
FA	15	Al	0.55-0.97	-	-	2-8	0.1-0.25
MK	16	H ₂ O ₂	0.3-0.6	-	-	1.8-5.2	0.15-0.17
MK,FA	17	H ₂ O ₂	0.44-0.84	-	60-81	0.3-6	0.08-0.17
MK, glass	18	H ₂ O ₂	0.5-1.4	-	36-82	3.1-24	0.42-0.75

Values of relative density (ρ_b), average cell size(ACS), total porosity(TP), compression strength(σ) and thermal conductivity (λ) of related porous geopolymers were listed in Table 3-6 using different RMs (raw materials) and PFAs (Pore-forming agents). Comparing the σ and λ of present work with other porous geopolymers, it can be seen that this material showed better σ with similar λ [8,10-11,15-17].

Simultaneously, considering its non inflammability in high temperature, simple and low resource and energy requirements, and low CO₂ emissions, the PGs produced in this work shows potential for fireproof thermal insulation application. It also confirmed that PGs with the lower bulk density (higher porosity) exhibited lower thermal conductivities and compression strengths, as lower density foamed geopolymer samples contain more porosity (air bubbles) which has a very low thermal conductivity [13]. Furthermore, Geopolymer samples synthesized only with pore-forming agent (without stabilizing agent) showed larger average cell size.

3.1.4.2.3 Porosity, thermal conductivity, and compression strength

Reports show that both the thermal conductivity and compression strength of porous ceramics is associated with the porosity (relative density), pore morphology and pore size, chemical composition, etc., [8-12,17]. According to the minimum solid area (MSA) models by Rice [19], the compression strength (σ) of a porous component is related to its total porosity (p) by the following equation: $\sigma = \sigma_0 \exp(-bp)$, where σ_0 is the compression strength when $p=0$ (dense solid), and b is an empirical constant.

The relationship of the σ to the p in Table 3-5 were well fitted by equation, as clearly shown in Fig. 3-15. Theoretical values of $\sigma_0 = 8040485$ MPa and $b = 20.2$, with a correlation factor $R^2 = 0.93$ were calculated by fitting the experimental data (Table 3-5) with equation. The relative high values of R^2 demonstrate that the compressive strength can be described by the MSA model when the porosity ranges from ~66 to ~ 83 vol%. Hence, the MSA model is an effective way to estimate the relation between porosity and mechanical strength for PGs at fixed composition, which is also reported by previous work [19].

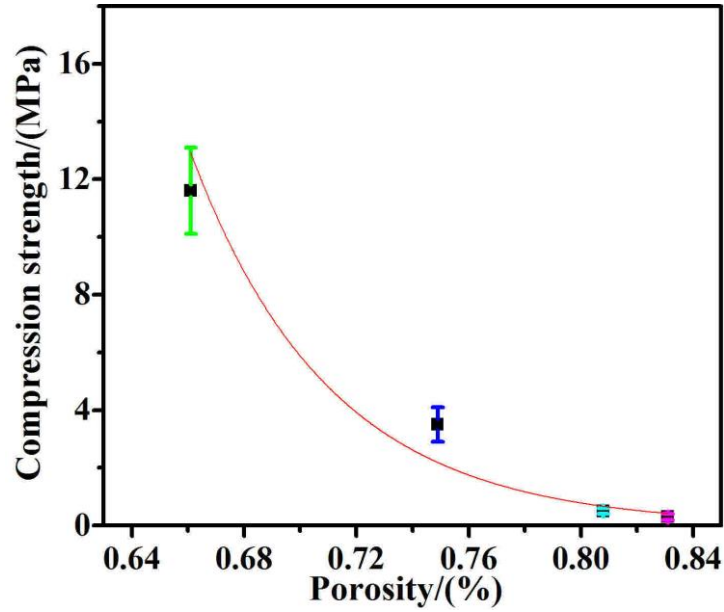


Fig. 3-15. Compression strength vs. total porosity for PGs produced with various content of H₂O₂ and fixed amount of stabilizing agent (olive oil).

The thermal conductivity (λ) of PGs with various content of pore-forming agent was presented in Table 3-5. The results demonstrate that the λ can be tailored by changing pore-forming agent content. Five fundamental effective thermal conductivity models (Parallel, Series, Maxwell-Eucken-1, Maxwell-Eucken-2, and Effective medium theory (EMT models)) for two-component or two-phase materials were put forward to show the behavior of thermal conductivity and porosity. And previous works showed that the five models depending on various pore properties can be integrated into an universal or unifying model (Eq. (UM)) [20-21]. In this study, the relationship between the thermal conductivity data and porosity were investigated via comparing the experimental data to the six theoretical models (see Fig. 3-16). Fig. 3-16 shows that the correlation trend of the experimental data between total porosity and effective thermal conductivity cannot be explained by the five basic models but can be fitted very well with the universal model (Eq. (UM)).

$$\lambda = \frac{\sum_{i=1}^m \lambda_i V_i ((d_i k') / (d_i - 1) k' + \lambda_i)}{\sum_{i=1}^m V_i ((d_i k') / (d_i - 1) k' + \lambda_i)}$$

where λ is the thermal conductivity of the sample, m is the number of components, λ_i and V_i are the thermal conductivity and porosity of each component present in the sample, respectively.

In this study, the samples contained two components ($m=2$), dense geopolymer ($\lambda_1=1$ W/Mk, component 1, V_1) [22] and air ($\lambda_2=0.026$ W/Mk; component 2, V_2 ; V_2 is the porosity of PGs), respectively, [23,24], with $V_1+V_2=1$. Here $k'=0.3$ (without straightforward physical meaning), and $d_i=3$ (associated with the pore shape factor and sphericity) [21,24], were selected as the parameter.

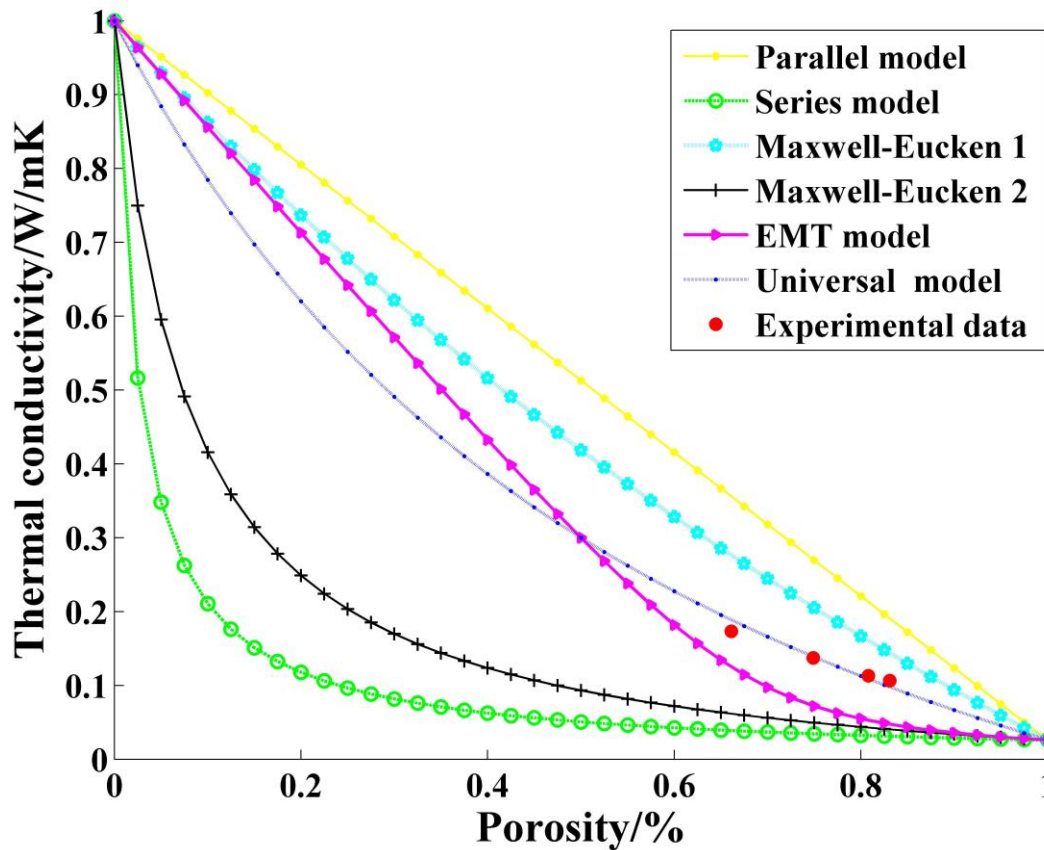


Fig. 3-16 Comparison of experimental thermal conductivity data and calculated values from different effective thermal conductivity models (five basic models and the universal model) at various amounts of total porosity.

As it can be observed in Fig. 3-16, the results suggested a good agreement between the experimentally obtained λ values and data simulated from the universal model. Hence, the universal model also could be used as an effective route to illustrate the relationship between porosity (V_2 or TP) and thermal conductivity (λ) for PGs with multiple pore sizes and structures [21,24].

3.1.4.3. Conclusions

Porous geopolymers (PGs) with tailored porosity, strength, and thermal conductivity were produced by direct foaming using hydrogen peroxide as pore-foaming agent plus vegetable oils as the stabilizing agents. The effect of the amount and the type of the vegetable oil, as well as that of the amount of the hydrogen peroxide, were evaluated. Results showed that it was possible to obtain a homogeneous porous structure by the addition of cheap available stabilizing agent. When the composition is fixed, the relationship between the porosity and strength could be described by the Minimum Solid Area model, and the thermal conductivity of PGs could be estimated relatively well by an universal model derived from the five basic effective thermal conductivity models. The results suggest that the foamed geopolymers are promising candidates as thermally insulating components for the building industry.

This work is published in Journal of the European Ceramic Society

Bai C, Ni T, Wang Q, et al. Porosity, mechanical and insulating properties of geopolymer foams using vegetable oil as the stabilizing agent [J]. Journal of the European Ceramic Society, 2018, 38(2): 799-805.

References

- 1 C. Bai, P. Colombo, High-porosity geopolymer membrane supports by peroxide route with the addition of egg white as surfactant, *Ceram. Int.* 43 (2017) 2267–2273.
- 2 L. Korat, V. Ducman, The influence of the stabilizing agent SDS on porosity development in alkali-activated fly-ash based foams, *Cem. Concr. Compos.* 80 (2017) 168–174.
- 3 G. Masi, W.D.A. Rickard, L. Vickers, M.C. Bignozzi, A. Van Riessen, A comparison between different foaming methods for the synthesis of light weight geopolymers, *Ceram. Int.* 40 (2014) 13891–13902.
- 4 M.S. Cilla, M.D. Mello Innocentini, M.R. Morelli, P. Colombo, Geopolymer foams obtained by the saponification/peroxide/gelcasting combined route using different soap foam precursors, *J Am Ceram Soc.* (2017) 1–11.
- 5 D. M. Liu: Influence of Porosity and Pore Size on the Compressive Strength of Porous Hydroxyapatite Ceramic, *Ceram. Int.* 8842 (1997) 135–139.
- 6 C. Bai, G. Franchin, H. Elsayed, A. Zaggia, L. Conte, H. Li, P. Colombo, High-porosity geopolymer foams with tailored porosity for thermal insulation and wastewater treatment, *J. Mater. Res.* 32 (17) (2017) 3251–3259.
- 7 J. Feng, R. Zhang, L. Gong, Y. Li, W. Cao, X. Cheng, Development of porous fly ash based geopolymer with low thermal conductivity, *Mater. Des.* 65 (2015) 529–533.
- 8 Z. Zhang, J.L. Provis, A. Reid, H. Wang, Mechanical thermal insulation, thermal resistance and acoustic absorption properties of geopolymer foam concrete, *Cem. Concr. Compos.* 62 (2015) 97–105.
- 9 W.D.A. Rickard, A. Van Riessen, Performance of solid and cellular structured fly ash geopolymers exposed to a simulated fire, *Cem. Concr. Compos.* 48 (2014) 75–82.
- 10 R.M. Novais, L.H. Buruberry, G. Ascensão, M.P. Seabra, J.A. Labrincha, Porous biomass fly ash-based geopolymers with tailored thermal conductivity, *J. Clean. Prod.* 119 (2016) 99–107.
- 11 A. Hajimohammadi, T. Ngo, P. Mendis, T. Nguyen, A. Kashani, J.S.J. Deventer, Pore characteristics in one-part mix geopolymers foamed by H₂O₂: The impact of mix design, *Mater. Des.* 130 (2017) 381–391.
- 12 V. Vaou, D. Papias, Thermal insulating foamy geopolymers from perlite, *Miner. Eng.* 23 (2010) 1146–1151.

-
- 13 J. Feng, R. Zhang, L. Gong, Y. Li, W. Cao, X. Cheng, Development of porous fly ash based geopolymer with low thermal conductivity, *Mater. Des.* 65 (2015) 529–533.
 - 14 M. Lach, K. Korniejenko, J. Miku, Thermal insulation and thermally resistant materials made of geopolymer foams, *Procedia Engineering* 151 (2016) 410–416.
 - 15 S. Frantisek, S. Rostislav, T. Zdenek, S. Petre, S. Vit, Z.C. Zuzana: Preparation and properties of fly ash-based geopolymer foams, *Ceram-Silikaty* 58 (2014) 188–197.
 - 16 P. Palmero, A. Formia, P. Antonaci, S. Brini, J.M. Tulliani, Geopolymer technology for application-oriented dense and lightened materials. Elaboration and characterization, *Ceram. Int.* 41 (2015) 12967–12979.
 - 17 R. M. Novais, G. Ascensão, L.H. Buruberry, L. Senff, J.A. Labrincha: Influence of blowing agent on the fresh- and hardened-state properties of lightweight geopolymers. *Mater. Des.* 108 (2016) 551–559.
 - 18 H. Shiu, K. Lin, S. Chao, C. Hwang, T. Cheng, Effects of Foam Agent on Characteristics of Thin-Film Transistor Liquid Crystal Display Waste Glass-Metakaolin-based Cellular Geopolymer, *Environ. Prog.*, 33(2014) 168–170.
 - 19 R. Rice, Comparison of stress concentration versus minimum solid area based mechanical property-porosity relations, *J. Mater. Sci* 28 (1993) 2187–2190.
 - 20 J. Wang, J.K. Carson, M.F. North, D.J. Cleland, A new approach to modelling the effective thermal conductivity of heterogeneous materials, *Int J Heat Mass Tran* 49 (2006) 3075–3083.
 - 21 C. Li, Y. Han, L. Wu, K. Chen, L. An, Fabrication and properties of porous anorthite ceramics with modelling pore structure, *Mater. Lett.* 190 (2017) 95–98.
 - 22 P. Duxson, G.C. Lukey, J.S.J. Van Deventer, Thermal Conductivity of Metakaolin Geopolymers Used as a First Approximation for Determining Gel Interconnectivity, *Mater Struct.* (2006) 7781–7788.
 - 23 T. Shimizu, K. Matsuura, H. Furue, K. Matsuzak, Thermal conductivity of high porosity alumina refractory bricks made by a slurry gelation and foaming method, *J. Eur. Ceram. Soc.* 33 (2013) 3429–3435.
 - 24 Z. Wu, L. Sun, J. Wang, Synthesis and characterization of porous Y_2SiO_5 with low linear shrinkage, high porosity and high strength, *Ceram. Int.* 42 (2016) 14894–14902.

3.2. Direct foaming combined with reactive emulsion templating

3.2.1 Introduction

Porous geopolymers (PGs) or Geopolymer foams (GFs, total porosity > 70 vol%) have been the focus of attention in the field of eco-friendly porous materials because of their favorable mechanical and chemical stability, low shrinkage after forming, high temperature resistance, etc. [1-4]. They have been employed in photocatalytic degradation applications or used as membrane supports, catalyst supports, heavy metals adsorbents and so on [4-9]. Aluminum and silicon and H₂O₂ have been used as pore foaming agents for the fabrication of PGs [1,10-11], but the pores generated by this foaming technique are typically closed, thereby limiting the range of applications for the components.

Recently, alternative processing routes for the fabrication of porous geopolymers have been proposed. An oil-based reactive emulsion templating route was put forward, which enables to obtain hierarchically porous geopolymers suitable for catalyst applications [9,12]. Other experiments related to the addition of oil to geopolymers, showed that waste oil can be trapped inside the geopolymeric matrix [13]. Geopolymers with a mesoporous matrix and unidirectional lamellar macro-porosity were also produced by the freeze-casting technique [14], and a saponification/peroxide/gelcasting combined method was proposed by Cilla et al. [15]. Although geopolymer foams with an open porosity of ~70 vol% and a total porosity as high as ~85 vol% were successfully produced by the combined technique, the compression strength of the foam was only ~0.45 MPa, which limited the range of applications for the components.

Despite an increasing number of papers dealing with the fabrication of porous geopolymers using different approaches, more investigation is still required to improve the process, especially in reference to the amount of open porosity and mechanical strength of the components. In particular, components possessing high strength and a high amount of open porosity, with controlled pore size and distribution, are of interest for several applications.

In this study, high mechanical strength metakaolin-based porous geopolymers (MPGs) and SiC-geopolymer composite foams with open porosity were fabricated using the direct foaming combined with reactive emulsion templating route. Their porosity, cell and cell

window size and mechanical properties were controlled by adding different oils and different contents of hydrogen peroxide.

3.2.2 Metakaolin-based porous geopolymers

3.2.2.1 Experimental procedure

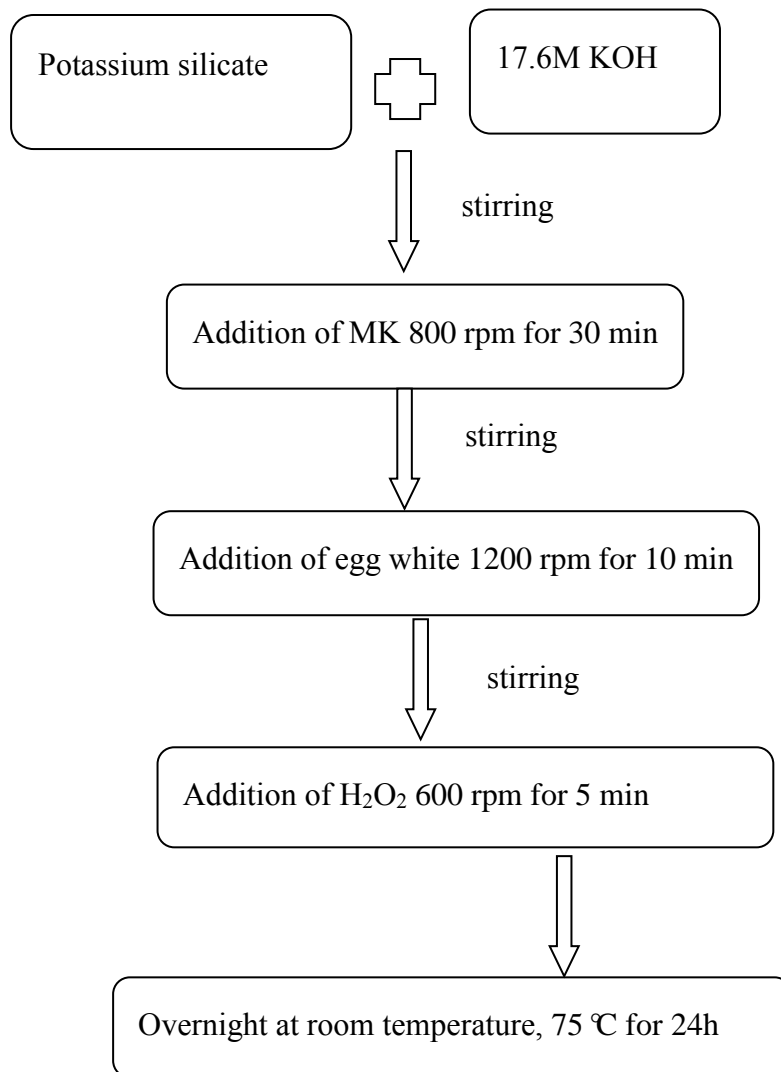


Fig. 3-17 Synthesis protocol of the metakaolin-based porous geopolymers

Artificial pozzolana (MK, Metakaolin) was used to fabricate the MPGs. Both the potassium silicate solution and KOH solution were mixed as alkali activator. 17.6M KOH solution were prepared by dissolving potassium hydroxide pellets. The alkali activator solution was allowed to dissolve at least 24h at room temperature [1, 15]. Three vegetable oils (canola oil, sunflower oil; olive oil) and H₂O₂ solution (with 3%w/w diluted through 30%w/w) were used as chemical foaming agents. Rasouli [8] reported that the molar ratio of SiO₂/Al₂O₃≈4 showed better mechanical properties, the original suspension (OS), with a theoretical oxide molar ratios: SiO₂/Al₂O₃=3.53, K₂O/SiO₂=0.36 and H₂O/K₂O=11.1, was prepared by the mechanical mixing of MK and the alkali activator solution.

The oil and H₂O₂ then added successively at room temperature to the suspensions. Fig 3-17 showed synthesis protocol of the metakaolin-based porous geopolymers (MPGs). We defined the weight fraction of oil in OS as x and the weight fraction of H₂O₂ in OS as y. Thereby; the porous geopolymers were prepared by casting the slurry into a sealed plastic mold and curing for 24 h at room temperature and another 24 h at 75 °C in an oven. Previous works [1,14] showed that the pre-heat treatment can contribute to improve the physical strength and the rate of geopolymerization.

To obtain the MPGs, an extraction step should be carried out by saturating the samples with hot water (renewed every 20 minutes until it remained clear), to completely evacuate water-soluble soap and glycerol molecules generated by the saponification. Additionally, when the hardened geopolymer is put for boiling water at 20 minutes, non-fully condensed geopolymer would be disaggregated (undergo dehydroxylation and expansion), i.e., partial condensed geopolymer are very sensitive to boiling water, so the extraction processing (boiling water test) can be used as a fast testing technique to verify the degree of the geopolymerization reaction. [4, 15].

Prior to the characterization, the MPGs were dried at 40 °C for one week. The porosity, phase composition, cellular morphology, and mechanical properties were investigated. A Brookfield viscometer was used for evaluating the viscosity of slurry at room temperature as a criterion of gel strength.

3.2.2.2 Results and discussion

3.2.2.2.1 Effect of different kinds of oil

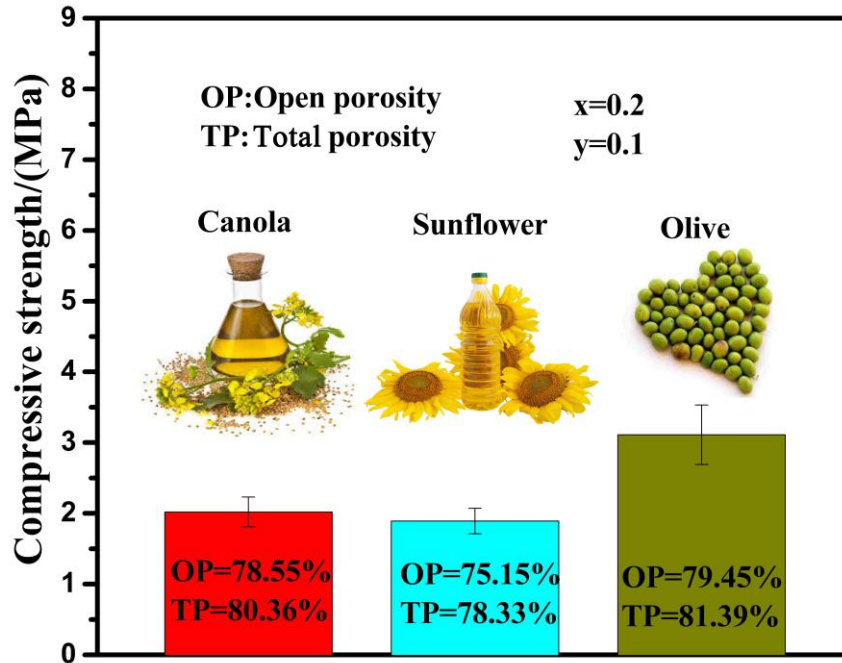


Fig. 3-18 Porosity and compressive strength of MPGs with different type of oils.

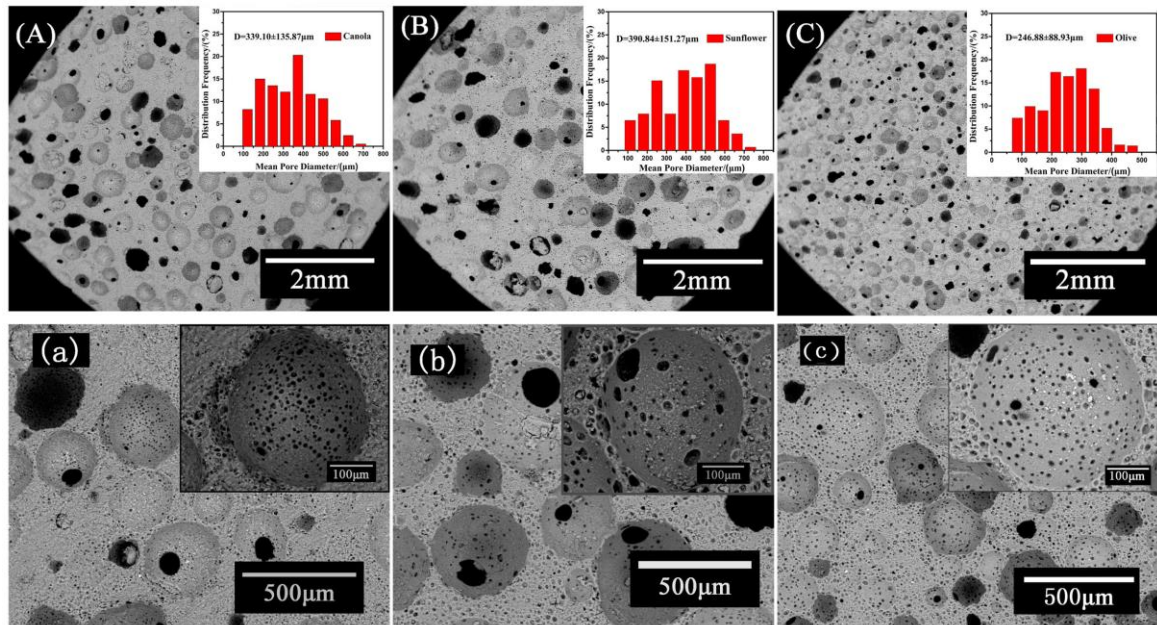


Fig. 3-19 SEM images of MPGs using (A-a) canola oil; (B-b) sunflower oil; (C-c) olive oil. The insets of (A~C) are cell size analysis and the insets of (a ~c) are magnified view.

Since strength and porosity are two important parameters for porous materials, a preliminary study was conducted to investigate the influence of different kinds of cooking oil. The compressive strength and the porosity of the MPGs with different kinds of oil are illustrated in Fig. 3-18.

Considering the saponification value of the three oils is about 190 [16-17], the ratio of K_2O/SiO_2 in geopolymer slurry before and after different edible oils addition is 0.36 and 0.29. The XRD results exhibit similar patterns (not shown for brevity), which can further illustrate that different oils do not change the composition but the pore character. To perform the SEM analysis, The MPG samples were cut into slices for get a better understanding of the pore size distribution. Clearly, a cellular structure, with a large number of “closed” cells (surrounded by relatively thick walls) having a size distribution ranging from $150\mu m$ to $450\mu m$ was observed in Fig. 3-19. The types of plant oil were found to have a significant effect on both the strength and the pore structure. The average cell pore size of the foams computed by image analysis for each sample are as follows: $339.10\pm 135.87\mu m$ (canola, Fig. 3-19A), $390.84\pm 151.27\mu m$ (sunflower, Fig. 3-19B), and $246.88\pm 88.93\mu m$ (olive, Fig. 3-19C). The specimens foamed via canola and sunflower oil presented similar porosity but lower mechanical strength than foamed via olive oil.

It is well-known that the viscosity of the geopolymer slurry also influences the pore size produced by the decomposition route [15,18], a program was edited to measure the viscosity with time (per 30s for 1h). And the viscosity-time curve prior to gel hardening results showed that viscosity (V) increases with time, simultaneously, the cure of type of oils following this order: $V_{Olive} > V_{Canola} > V_{Sunflower}$; the order of viscosity is accordance with the pore size using different oil, i.e., the low viscosity of the flowable slurry is beneficial to rising pores collapsing.

As the sample foamed by olive oil showed that a total porosity of $\sim 81.39\%$, open porosity as high as $\sim 79.45\%$, and possessing a compressive strength of $\sim 3.11\text{MPa}$, the optimum foaming agent in the foaming was found to be olive oil. Previous work [19] also showed that at a similar porosity for given materials, the compression strength drops sharply with the rise of the average cell pore size.

Also, many small pores (existed on the cell wall and struts) were observed in Fig. 3-19

(a-c). To explain this phenomenon, a higher magnification is showed in the inset of Fig. 3-19 (a-c). These small pores were attributed to the extraction of water-soluble soap and glycerol molecules [12-13]. The influence on average strut and cell wall pore also was tested, adding different cooking oils shows similar window and wall window pore size ($15.05\pm 4.50\mu\text{m}$ (canola Fig. 3-19a), $22.79\pm 8.27\mu\text{m}$ (sunflower Fig. 3-19b), and $17.27\pm 5.26\mu\text{m}$ (olive Fig. 3-19c)). Additionally, the both window pores and wall window pores lead to the “closed” cells to be open; and the existence of connected and open mesopores in the geopolymer matrix further confirm the solvent and other molecules to freely flow [12].

Simultaneously, the thick struts are beneficial to excellent mechanical strength. Previous work also showed that oil type, alkali contents and [12], and oil contents [13] could affect the pore size (mesopore) and mechanical strength, so in the following experiments in order to investigate the following properties: (i) the effects of addition of olive oil (alkali contents) and hydrogen peroxide and (ii) the relationship between open porosity and compressive strength.

3.2.2.2 Effect of addition of olive oil

Figs. 3-20 (a-c) show the microstructures of MPGs with different amounts of olive oil content, and Table 3-7 report the values of the porosity (total and open), the relative density, the average cell size, and compressive strength depending on the kinds and amounts of pore foaming agent. It is obvious that different content of olive oils have a significant effect on the pore characteristic. The compressive strength and porosity show different extent decrease. When the olive oil content increased from 20 to 70wt%, the total porosity fell sharply from ~81% to ~67%. However, the corresponding compressive strength dropped slightly from 3.11 to 2.19MPa. Cantarel’ work [13] also showed similar downtrend about mechanical strength when the oil content increases. Both of the average strut and the cell wall size for samples SO (1-4) were compared. All of the cells and channels between cells and the wall widows growing here had typical teardrop-shape morphology. The cell size ($246.88\pm 88.93\mu\text{m}$ Fig. 3-19c, $209.72\pm 73.12\mu\text{m}$ Fig. 3-20a, $169.15\pm 50.87\mu\text{m}$ Fig. 3-20b, and $130.17\pm 51.72\mu\text{m}$ Fig. 3-20c, respectively) showed a gradually upward trend, but the strut and the cell wall size ($17.27\pm 5.26\mu\text{m}$, $20.88\pm 6.04\mu\text{m}$, $28.29\pm 9.58\mu\text{m}$ and $37.85\pm 13.64\mu\text{m}$, respectively)

demonstrate a slightly descending tendency. The decrease of average of cell diameter is due to the fall of viscosity [13,14]. The trend of the strut and the cell wall size is in accordance with the result of porosity. When 20wt% hydrogen peroxide added, the average window size increases with the content of olive oils.

In the absence of peroxide, Table 3-7 showed the channel size generated by olive oil is $39.80 \pm 14.60 \mu\text{m}$ and the compressive strength is $25.96 \pm 5.12 \text{MPa}$; The channel size using canola oils as a reactive emulsion template was about $22 \mu\text{m}$ by Medpelli et al. [12]; Formulation with 20 vol% of liquid oil waste in a geopolymer showed that the cell widow size is about $17.26 \mu\text{m}$ and corresponding compressive strength is $22 \pm 1 \text{MPa}$ [13]; And Table 3-7 also exhibited the result by Cilla et al.[15]. The value for the porosity (total and open), the relative density, the average cell size, and compressive strength of the foams obtained by our investigation were consistent with the results obtained in previous works for porous geopolymers fabricated through the saponification reaction process.

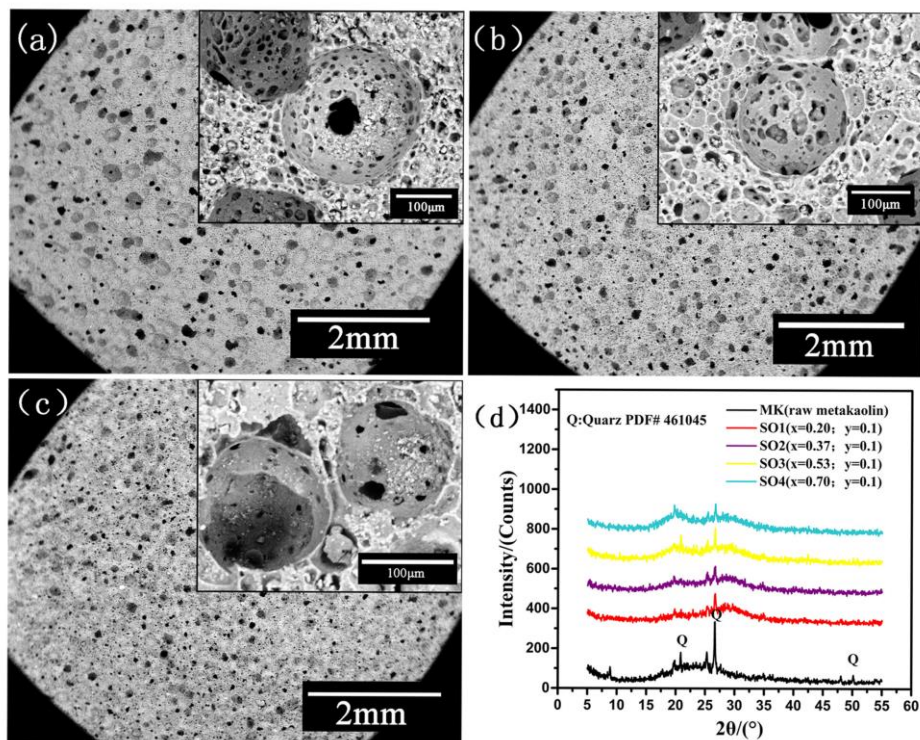


Fig.3-20 (a-c) show the microstructures of MPGs with various amounts of olive oil content and the insets of (A)-(C) are magnified -view of SEM images; (d) is XRD patterns of MK and sample SO (1-4).

Since KOH would be consumed by the saponification reaction, the value of K_2O/SiO_2 in geopolymer decreases from 0.28 to 0.12. An XRD diffraction analysis has been performed to compare the different composition. Figure 3-20d displayed the XRD patterns of the original metakaolin and the different K_2O/SiO_2 ratio. A typical amorphous peak characteristic of MK centered at 15° – $35^\circ 2\theta$ was detected [8,11], another distinguishable “hump” of geopolymer materials centered at around 27° – $29^\circ 2\theta$ was displayed [11]. Further, a small amount of quartz peaks were observed on both the raw MK and subsequent MPGs in the XRD diffractogram, and Williams’ work [20] showed that the sawtooth-like hump at approximately $20^\circ 2\theta$ is related to disordered kaolin; MK is partially dissolved in geopolymer, the fraction of MK dissolution (the geopolymerization process) depends strongly on react $[OH^-]$. The degree of dissolution of the metakaolin have strong positive correlation with OH^- concentration (mol/L) of the alkali activating solution (the ration of K_2O/SiO_2) and the mechanical property. Apart from the foaming process, the geopolymer matrix chemistry contributed to the development of all the above-mentioned properties.

Table 3-7 Data of the relative density, the average cell size, the porosity, and compressive strength depending on the kinds and amounts of pore forming agent.

Sample	x	y	K ₂ O/SiO ₂	Bulk density (g/cm ³)	Average size (μm)		Open porosity (vol%)	Total porosity (vol%)	Compression strength (MPa)
					Cell	Strut and cell wall pores			
SO1	0.20	0.1	0.29	0.40±0.01	247±89	17.3±5.3	79.5±0.1	81.4±0.5	3.11±0.82
SO2	0.37	0.1	0.23	0.42±0.01	210±73	20.9±6.0	75.2±0.3	75.4±0.6	2.57±0.52
SO3	0.53	0.1	0.17	0.48±0.02	169±51	28.3±9.6	68.4±0.3	70.3±1.3	2.38±0.47
SO4	0.70	0.1	0.12	0.51±0.02	130±52	37.8±13.6	62.9±0.2	67.4±1.3	2.19±0.21
SH0	0.20	0	0.29	0.84±0.01	40±15	-	-	62.0±0.5	25.96±5.12
[15]	0.25	0	0.24	0.81±0.01	98±12	-	59.8	66.4	-
[15]	0.25	0.06	0.24	0.34±0.01	318±18	-	69.2	83.5	0.45 ±0.08
SH2	0.20	0.05	0.29	0.59±0.02	125±46	16.5±5.4	67.0±0.1	72.6±0.9	8.83±2.38
SH6	0.20	0.15	0.29	0.30±0.01	383±265	17.2±5.9	84.0±0.1	86.3±0.5	0.78±0.12
SH8	0.20	0.20	0.29	0.26±0.01	490±335	20.9±8.6	85.8±0.3	89.2±0.4	0.38±0.08

3.2.2.2.3. Effects of hydrogen peroxide content and pore size distribution

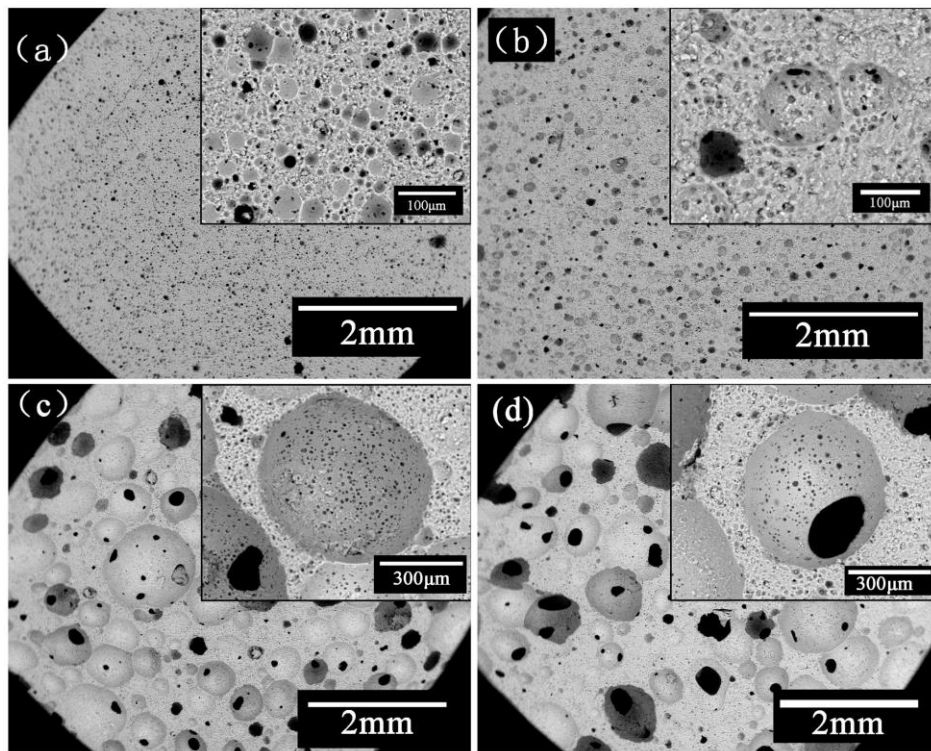


Fig. 3-21 SEM images of MPGs with different amounts of hydrogen peroxide content and the insets of (a)-(d) are magnified-view.

Table 3-7 shows the porosity and strength of the MPG specimens prepared with various H_2O_2 loadings (SO1, SH(0-8)). As can be seen, the increase of H_2O_2 amount declines the relative density and compressive strength when adding the same amount of olive oil. However, the corresponding average of cell size and pore volume fraction increase. Besides, the relationship between total porosity and the corresponding compressive strength was explored. According to the minimum solid area models by Rice [21-23], when the other factors of porous materials, such as synthesis temperature and the pore character that may affect the mechanical strength of cellular ceramics, are not dominant, the strength-porosity dependence can be approximated closely via an exponential function: $\sigma = \sigma_0 \exp(-bp)$

Where σ is the strength at total porosity p , σ_0 is the value when $p=0$ at the same composition, and b is an empirical constant determined by pore characteristics.

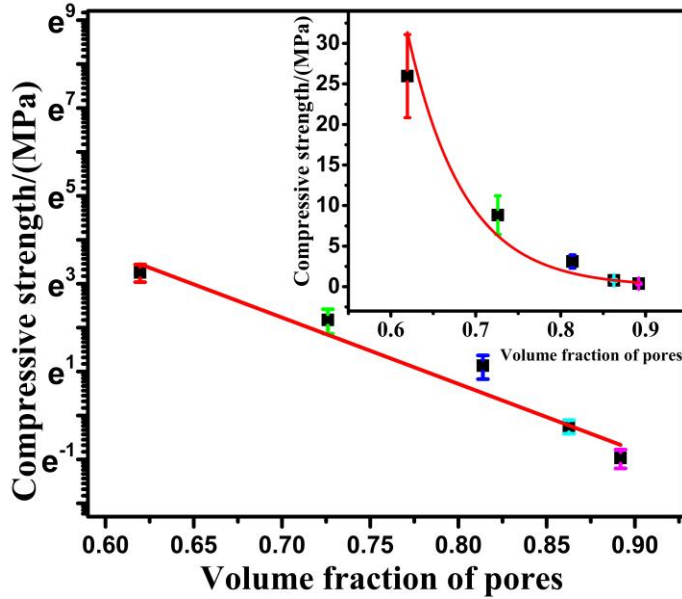


Fig.3-22 Plot of compressive strength vs. total porosity for the MPGs where different content of H₂O₂ and fixed olive oil were used as a pore forming agents.

The relations between the pore volume fraction and the strength in Table 3-7 were fitted directly by the equation, as shown in Fig. 3-22. In this study, the strength-porosity behavior of the MPG specimens can be estimated by the following equation (Eq. (F)): $\sigma = 364404.58 \exp(-15.11p)$ With a correlation factor $R^2 = 0.957$, it showed that the compressive strength was mainly determined by the minimum solid cross-sectional area, i.e., When the p value from 67.41 to 89.19, the compressive strength can be approximated by the Eq. (F). Previous study [24] showed that the values of σ_0 and b depend on the processing conditions and/or other parameters.

When considering the factor of the different addition of H₂O₂ on the morphology of the MPGs, firstly, we can observe (see Fig. 3-21) that when increasing the content of H₂O₂, from 5% to 20%, the average cell size increase by 291% (from 125.25±46.23 to 489.55±334.76μm), but the average strut and cell wall size is almost no changing (from 16.55±5.45 to 20.88±8.56μm). The most likely explanation is that the average of cell diameter fabricated by a direct foaming process strongly depends on the viscosity of the geopolymer slurry [14]. And in particular, the adding of H₂O₂ results in the reducing of viscosity. Lower viscosity of slurry, affected by its composition, was beneficial to forming MPGs with larger cell size. It is more

obvious to compare the cell size between samples with different H₂O₂ content. Another elucidation [18] about this phenomenon is due to the pore amalgamation, which can also be used to explain the increase of pore volume. Combined with the SEM results (Figs. 3-(19-21)), this morphology confirms that both the decomposition reaction (big pore) and the saponification reaction (small pore) were well proceed. Moreover, The MGPs with hierarchical pore architectures, with controlled mechanical porosity, and with monomodal pore size distribution, with respect to the cell size, are considered to be a promising porous media.

3.2.2.3 Conclusions

High strength and high porosity MPGs with controlled hierarchically macroporous structure were fabricated by direct foaming combined with reactive emulsion templating using H_2O_2 plus three edible oils (canola oil, sunflower oil, olive oil) as foaming agent, and the effect of the types and the addition of oils and H_2O_2 on the phase composition, microstructure, and mechanical properties of MPGs were evaluated.

As a foaming agent, the types of oil and the content of oil and H_2O_2 have a significant effect on the pore cell size distribution and mechanical performance. The open and total porosity decreased with addition of olive oil; however, it increased with increasing peroxide content. Adding more oils to the slurry changes the chemistry composition of MPGs, which has a negative effect on mechanical strength; and the increasing of the peroxide content, the minimum solid cross-sectional areas are obvious reduced. Because of the enhancement of walls (necks) between the cells and the existence of channels in the cell wall, a compressive strength of 3.11MPa was achieved for the geopolymer at a total porosity of 81.39%, containing 20wt% olive oil and 10wt% H_2O_2 , and the strength-porosity relationship could be elaborated by the minimum solid area model.

These results demonstrate that the property of MPGs as promising filtering materials with hierarchical pore structure could be tailored for particular filtering applications by adjusting their synthesis process (different types of oil and different content of oils and H_2O_2), thereby controlling their compressive strength, pore volume fraction, pore cell and window pore sizes and distribution.

This work is published in Journal of the European Ceramic Society

Bai C, Franchin G, Elsayed H, et al. High strength metakaolin-based geopolymer foams with variable macroporous structure[J]. Journal of the European Ceramic Society, 2016, 36(16): 4243-4249.

References:

- ¹ Feng J., Zhang R., Gong L., Li Y., Cao W. & Cheng X. Development of porous fly ash-based geopolymer with low thermal conductivity. *Mater Des*, 2015, 65, 529-33.
- ² Cilla M. S., Colombo P. & Morelli M. R. Geopolymer foams by gelcasting. *Ceram. Int.*, 2014, 40, 5723-30.
- ³ Böke N., Birch G. D., Nyale S. M. & Petrik L. F. New synthesis method for the production of coal fly ash-based foamed geopolymers. *Constr. Build. Mater.*, 2015, 75, 189-99.
- ⁴ Davidovits J. *Geopolymers – chemistry & applications*. 3th ed. Saint-Quentin: Institute Géopolymère; 2011.6.
- ⁵ Zhang Y. J., Liu L. C., Xu Y. & Wang Y. C. A new alkali-activated steel slag-based cementitious material for photocatalytic degradation of organic pollutant from waste water. *J. Hazard. Mater.*, 2012, 209, 146-50.
- ⁶ Zhang J., He Y., Wang Y., Mao J. & Cui X. Synthesis of a self-supporting faujasite zeolite membrane using geopolymer gel for separation of alcohol/water mixture. *Mater Lett*, 2014, 116, 167-70.
- ⁷ El-Eswed B., Yousef R. I., Alshaaer M., Hamadneh I. & Khalili F. Adsorption of Cu (II), Ni (II), Zn (II), Cd (II) and Pb (II) onto kaolin/zeolite based-geopolymers. *Advances in Materials Physics and Chemistry*, 2013, 2, 119.
- ⁸ Rasouli H. R., Golestani-fard F., Mirhabibi A. R., Nasab G. M., Mackenzie K. J. D. & Shahraki M. H. Fabrication and properties of microporous metakaolin-based geopolymer bodies with polylactic acid (PLA) fibers as pore generators. *Ceram. Int.*, 2015, 41, 7872-80.
- ⁹ Sharma S., Medpelli D., Chen S. & Seo D. Calcium-modified hierarchically porous aluminosilicate geopolymer as a highly efficient regenerable catalyst for biodiesel production. *RSC Advances*, 2015, 5, 65454-61.
- ¹⁰ Hlaváček P., Šmilauer V., Škvára F., Kopecký L. & Šulc R. Inorganic foams made from alkali-activated fly ash: Mechanical, chemical and physical properties. *Journal of the European Ceramic Society*, 2015, 35, 703-9.
- ¹¹ Prud'homme E., Michaud P., Joussein E., et al. Silica fume as porogen agent in geopolymer materials at low temperature. *Journal of the European Ceramic Society*, 2010, 30, 1641-8.

-
- ¹² Medpelli D., Seo J. & Seo D. Geopolymer with Hierarchically Meso - /Macroporous Structures from Reactive Emulsion Templating. *J Am Ceram Soc*, 2014, 97, 70-3.
- ¹³ Cantarel V., Nouaille F., Rooses A., Lambertin D., Poulesquen A. & Frizon F. Solidification/stabilisation of liquid oil waste in metakaolin-based geopolymer. *J. Nucl. Mater.*, 2015, 464, 16-9.
- ¹⁴ Papa E., Medri V., Benito P., et al. Synthesis of porous hierarchical geopolymer monoliths by ice-templating. *Microporous and Mesoporous Materials*, 2015, 215, 206-14.
- ¹⁵ Cilla M. S., Morelli M. R. & Colombo P. Open cell geopolymer foams by a novel saponification/peroxide/gelcasting combined route. *Journal of the European Ceramic Society*, 2014, 34, 3133-7.
- ¹⁶ Stavarache C., Vinatoru M. & Maeda Y. Aspects of ultrasonically assisted transesterification of various vegetable oils with methanol. *Ultrason. Sonochem.*, 2007, 14, 380-6.
- ¹⁷ Hoq M. M., Yamane T., Shimizu S., Funada T. & Ishida S. Continuous hydrolysis of olive oil by lipase in microporous hydrophobic membrane bioreactor. *Journal of the American Oil Chemists Society*, 1985, 62, 1016-21.
- ¹⁸ Masi G., Rickard W. D., Vickers L., Bignozzi M. C. & Van Riessen A. A comparison between different foaming methods for the synthesis of light weight geopolymers. *Ceram. Int.*, 2014, 40, 13891-902.
- ¹⁹ Liu D. Influence of porosity and pore size on the compressive strength of porous hydroxyapatite ceramic. *Ceram. Int.*, 1997, 23, 135-9.
- ²⁰ Williams R. P., Hart R. D. & Van Riessen A. Quantification of the Extent of Reaction of Metakaolin - Based Geopolymers Using X - Ray Diffraction, Scanning Electron Microscopy, and Energy - Dispersive Spectroscopy. *J Am Ceram Soc*, 2011, 94, 2663-70.
- ²¹ Rice R. Comparison of stress concentration versus minimum solid area based mechanical property-porosity relations. *J. Mater. Sci.*, 1993, 28, 2187-90.
- ²² Rice R. Evaluating porosity parameters for porosity–property relations. *J Am Ceram Soc*, 2002, 76, 1801–08.
- ²³ Rice R. Comparison of physical property-porosity behaviour with minimum solid area models. *J. Mater. Sci.*, 1996, 31, 1509-28.
- ²⁴ Bai C., Deng X., Li J., Jing Y. & Jiang W. Preparation and properties of mullite-bonded porous SiC ceramics using porous alumina as oxide. *Mater Charact*, 2014, 90, 81-7.

3.2.3 SiC-geopolymer foam composites

3.2.3.1 Experimental procedure

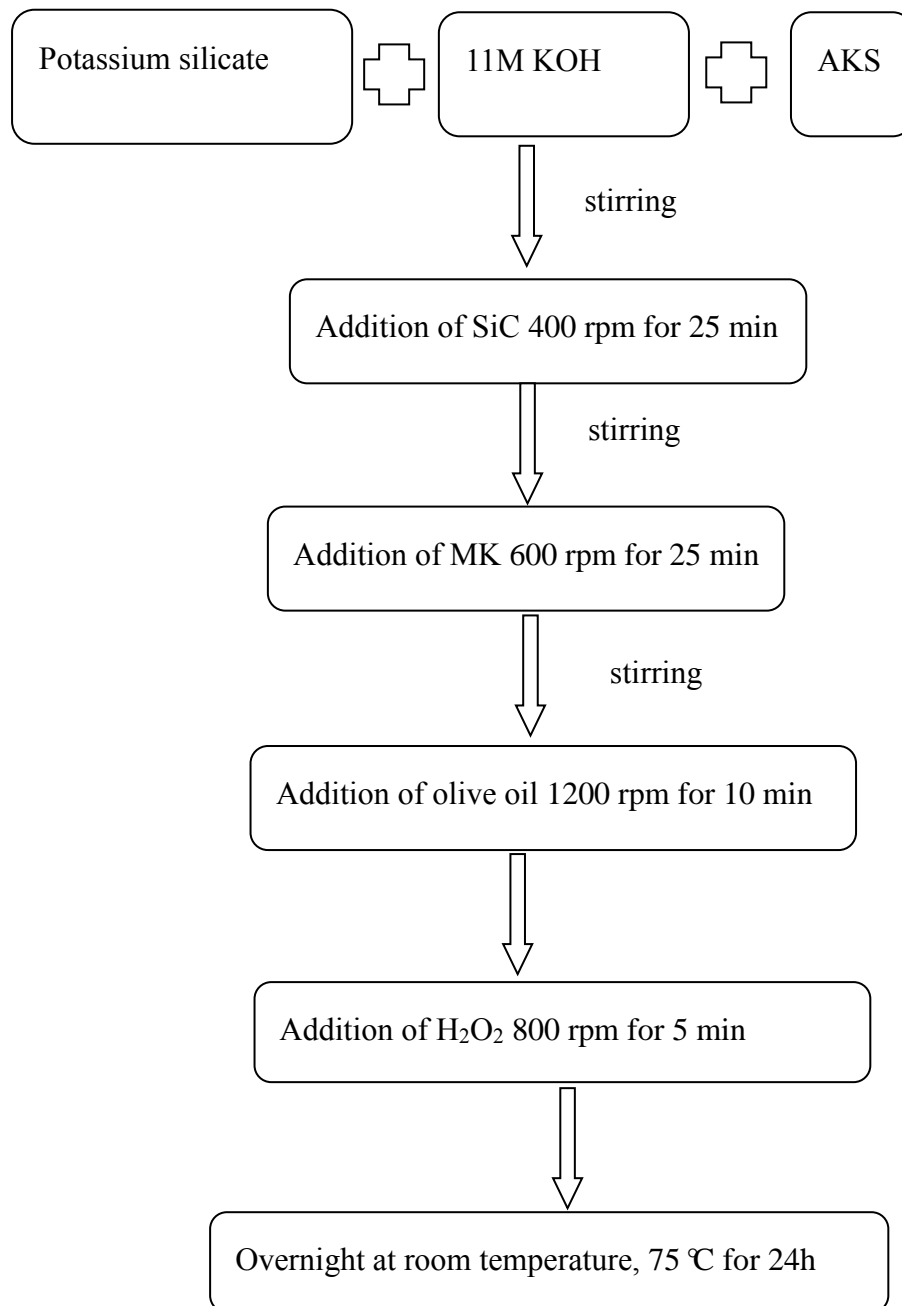


Fig. 3-23 Synthesis protocol of the SiC-geopolymer foam composites

Commercial SiC particles and metakaolin (MK) were used to produce the SiC-geopolymer foam composites (SFCs). A 11M KOH solution was prepared by dissolving laboratory grade potassium hydroxide pellets into distilled water. After that, the alkali-reagents were obtained by mechanical mixing the KOH solution and a potassium silicate solution. Previous work showed that the alkali-reagents needed to be prepared more than 24h in advance, to ensure that the silicate would dissolve completely [1]. Edible olive oil and a 3wt% of H₂O₂ solution [2] (diluted by 30wt%) were used as chemical foaming agents.

The synthesis protocol of the SiC-geopolymer foam composites is showed in Fig. 3-23. We added to the geopolymer slurry an additional amount of 11M KOH solution (AKS), in order to consume completely the oil, based on its saponification index [3]. The SiC and MK were added successively to the alkali medium solution using laboratory mixer, to obtain the original suspension (OS). Thereafter, the olive oil was added, followed by the addition of the hydrogen peroxide. The weight fraction of olive oil in OS was defined as x, the weight fraction of H₂O₂ in OS as y, and the weight fraction of SiC in OS was fixed at 0.33 (excluding the weight of AKS when calculating the weight ratios). It should be noted that this excess KOH does not modify the final composition of the geopolymer because it is completely consumed by the saponification reaction with the oil, generating glycerol and soap molecules that are then washed away (see below). Separate experiments showed that the reaction between the oil and the KOH solution was very fast, being completed in about 5 minutes after mixing, therefore well within the timeframe for the fabrication of the geopolymer foams. So, assuming that the saponification reaction goes to completion, the molar ratios of SiC/geopolymer slurry are as follows: SiO₂/Al₂O₃= 3.53, K₂O/SiO₂= 0.29, SiC/SiO₂=2.5, and H₂O/K₂O = 15.1. (excluding the content of water in the H₂O₂ solution and AKS). The SiC/geopolymer foams were produced by casting the wet foam into a sealed plastic mold and pre-curing overnight at ambient temperature [2,3], followed by 24 h at 75 °C in a drying oven.

To obtain the final SiC/geopolymer foam composites (SFCs), an additional extraction step [3] was needed to eliminate the water-soluble soap and glycerol generated by the saponification reaction. The composite samples were put into hot water (~80 °C) in a covered beaker (water renewed every 50 min until it remained clear). This step can also serve as a simple way to test

the degree of the geopolymerization reaction, since non-fully condensed geopolymer structures would disaggregate (undergo swelling or complete destruction) in water [3]. Prior to characterization, the SFCs were dried at 40 °C for one week.

The porosity (open and total), phase composition, pore morphology, and mechanical properties were investigated. Furthermore, measurements were conducted on samples cured at 75 °C and after firing for 2h at 600 °C, 800 °C, and 1000 °C. The high temperature performance and phase transformation characteristics of the samples were evaluated, respectively, by TG/DTA and by dilatometer. The crystalline phase assemblage was identified on ground samples using an X-ray diffractometer. The porosity (open and total), mechanical properties, macrostructure, cell size distribution was investigated. Thermal conductivity (λ) of selected sample with the size $\sim 12 \times \sim 50 \times \sim 50 \text{ mm}^3$ was tested using a hot-disc thermal analyzer based on the transient plane source technique [4].

To evaluate the electrochemical properties, electrochemical impedance spectroscopy (EIS) data were recorded on samples without SiC (sample R16-SO1, $\text{K}_2\text{O}/\text{SiO}_2 = 0.29$, average cell size = $247 \pm 89 \mu\text{m}$, open porosity = 79.5 vol%, bulk density = 0.4 g/cm^3) [3] and with SiC (Sample SO₂, $\text{K}_2\text{O}/\text{SiO}_2 = 0.29$, average cell size = $233 \pm 72 \mu\text{m}$, open porosity=82.7 vol%, bulk density= 0.4 g/cm^3).

3.2.3.2 Results and discussion

3.2.3.2.1 Effect of the content of olive oil

A preliminary study was carried out to investigate the influence on pore, porosity, microstructure, and mechanical properties of different contents of oils. Table 3-8 reports the relative density (ρ_b), porosity (total and open), average cell size (ACS), and compression strength(σ) data for the different specimens of SiC/geopolymer foam composites(SFCs). The SEM images (the axial cross-sections, Figs. 3-24(a–d); radial cross-section of sample SO₂r, Fig. 3-24e) of SFCs produced using different contents of olive oil ($x=0.22-0.46$) and fixed amount of H_2O_2 ($y = 0.1$). And the particle morphology and the XRD pattern of the SiC powder

is showed in Fig. 3-24f. The particle morphology was relatively regular and the average particle size was about 6.5 μm , which is accordant with the supplier; no presence of carbon (C) and silicon (Si) impurities was observed in the XRD patterns.

Table 3-8. Values of relative density (ρ_b), average cell size (ACS), total porosity (TP), and compression strength (σ) as a function of different contents of olive oil and hydrogen peroxide (x = weight fraction of olive oil in OS; y = weight fraction of H_2O_2 in OS)

Sample label	x	y	ρ_b (g/cm^3)	ACS (μm)	TP (vol%)	OP (vol%)	σ (MPa)
SO1	0.22	0.1	0.43 \pm 0.01	241 \pm 98	82.5 \pm 0.4	81.7 \pm 0.2	1.43 \pm 0.54
SO2	0.30	0.1	0.40 \pm 0.01	233 \pm 72	83.7 \pm 0.4	82.7 \pm 0.2	1.07 \pm 0.26
SO2r	0.30	0.1	0.40 \pm 0.01	223 \pm 88	83.7 \pm 0.4	82.7 \pm 0.2	1.19 \pm 0.30
SO3	0.38	0.1	0.38 \pm 0.01	206 \pm 71	84.5 \pm 0.4	84.2 \pm 0.2	0.83 \pm 0.50
SO4	0.46	0.1	0.37 \pm 0.01	181 \pm 50	84.9 \pm 0.4	84.6 \pm 0.3	0.74 \pm 0.12
SH1	0.30	0.05	0.61 \pm 0.02	122 \pm 32	75.1 \pm 1.3	70.7 \pm 0.8	3.87 \pm 0.65
SH2	0.30	0.07	0.49 \pm 0.01	n.d.	80.0 \pm 0.9	79.7 \pm 0.4	2.01 \pm 0.50
SH3	0.30	0.08	0.42 \pm 0.01	226 \pm 50	82.9 \pm 0.6	82.2 \pm 0.2	1.42 \pm 0.26
SH4	0.30	0.1	0.40 \pm 0.01	233 \pm 72	83.7 \pm 0.4	82.7 \pm 0.2	1.07 \pm 0.26
SH5	0.30	0.12	0.35 \pm 0.01	298 \pm 81	85.7 \pm 1.0	84.6 \pm 0.1	0.47 \pm 0.15
SH6	0.30	0.13	0.34 \pm 0.01	n.d.	86.1 \pm 0.6	85.5 \pm 0.2	0.29 \pm 0.09
SH7	0.30	0.15	0.32 \pm 0.01	324 \pm 16	86.9 \pm 1.1	86.2 \pm 0.3	0.21 \pm 0.06

n.d. = not determined

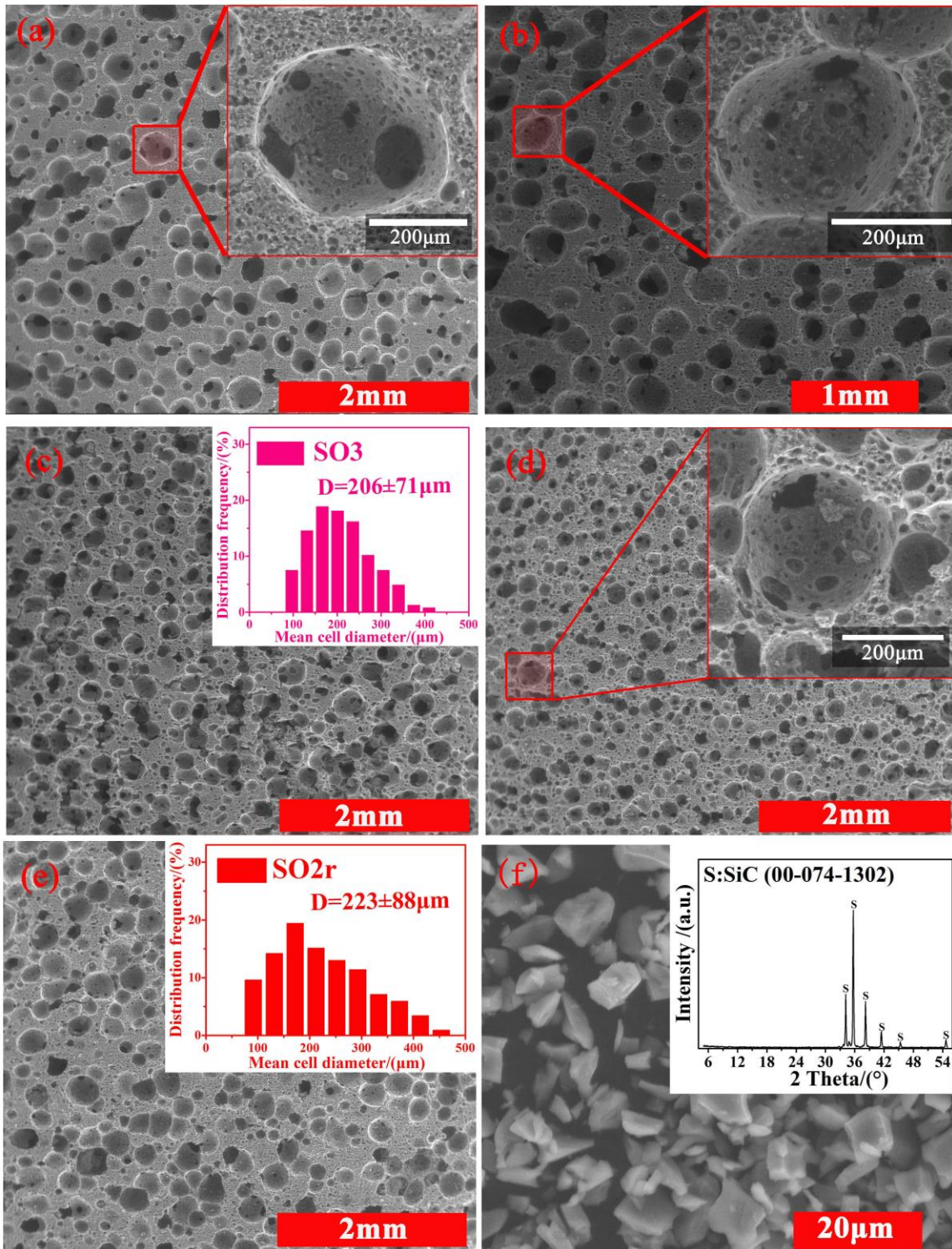


Fig. 3-24. SEM images of SFC specimens produced using different amounts of olive oil: (a) $x = 0.22$, inset is a magnified view; (b) $x = 0.30$, inset is a magnified view; (c) $x = 0.38$ inset is cell size distribution; (d) $x = 0.46$, inset is a magnified view; (e) $x = 0.30$ radial direction view, inset is cell size distribution, (f) SiC particle morphology, inset is XRD pattern.

Also, a cellular-like structure, with large amounts of cells (randomly distributed on the cross-section), was observed in Figs. 3-24(a-e). As can be seen in the SEM micrographs, varying the addition of olive oil with fixed peroxide content, while maintaining the alkali and Si/Al ratio of geopolymer, had an effect on the porous characteristics. Most the cells show interconnecting cell windows with spherical shape, and the homogeneity of the cellular structure was reduced with increasing olive oil content, furthermore, there are lots of small pores less than (100 μ m) in the struts and cells (both cell wall and cell windows) ((Fig.3-24). This behavior is due to the trapped oil droplets or/and glycerin and is likely to increase the permeability of the structure [3].

The results (Figs. 3-24(b, e) and Table 3-8) show that similar values for the morphological feature, bulk density, pore size distribution, porosity, and mechanical property were obtained for the specimen produced with $x=0.3$ and $y=0.1$ and measured along the axial (sample SO2) and radial (sample SO2r) direction, respectively, indicating that the porosity in the composite foams was homogeneously distributed throughout the volume, namely, it is less effective with the foaming direction by the combined route.

When the olive oil content in the OS increased from 22 to 46 wt%, the TP increased slightly from ~83 to ~85vol%. However, the corresponding compressive strength fell from 1.4 to 0.7MPa. As the extra 11M KOH solution were added in the alkali-reagents to consume completely the oil based on the saponification index, i.e., the composition of the geopolymer composites is constant. And the relationship between total porosity and the corresponding compressive strength can be well explained by the minimum solid area (MSA) models[5,6]. The increase in total porosity decreased the strength of SFCs because it reduced the minimum solid area of the fracture surface, and the strength-total porosity relationship could be well approximated by the simple equation proposed by Rice [5,6]: $\sigma = \sigma_0 \exp(-bp)$ The total porosity affected the strength of SFCs by changing the minimum solid area of fracture surface. The results of the strengths for the SFCs are plotted versus porosity in Fig. 3-25. It indicates that the increases in the porosity with decreasing the strength for SFC specimens could be approximated by the simple equation proposed by Rice. where p is the total porosity, σ is the corresponding compression strength at porosity p , σ_0 is the extrapolated strength at $p = 0$, and

b is an empirical constant. The value of the R^2 fitting parameter was 0.99. The relationships between the pore volume fraction and the strength in Table 3-8 were fitted directly by the equation, as shown in Fig. 3-25.

As an overview, the goodness of fit R^2 , obtained from the curve fitting of compressive strength–porosity data of SFCs with various content of olive oils and fixed H_2O_2 content (Fig. 3-25), exhibited high value (0.99). Such a high value indicates that the MSA model had an excellent predictive power to the strength in the total porosity (p) range from ~83 to ~85 vol%, i.e., the relationship of compressive strength and total porosity can be elaborated by the MSA model.

The pore morphologies of the samples were observed by scanning electron microscopy were slightly different considering the varying content of olive oil. And the pore size distribution, based on the SEM image, also showed in (Fig. 3-24 (c, e); table 3-8). Clearly, the wide distribution of the pore size is typical of foams produced using a direct foaming technique. The total amount of cells increased, while the average of cell diameters decreased from 241 to 181 μ m with increasing olive oil content. The decrease of the average cell diameter could be explained by the higher amount of surfactant molecules formed, which is helpful in stabilizing more gas bubbles in the slurry [3]. Simultaneously, the ratio between the open porosity and the total porosity remained constant (nearly 100%), i.e., almost none of the pores were closed pores but rather open pores. The probably explanation is that the boiled water can be penetrated into intrinsic interconnected meso/macro-pores in the geopolymer matrix, and the presence of SiC particles improve the permeability.

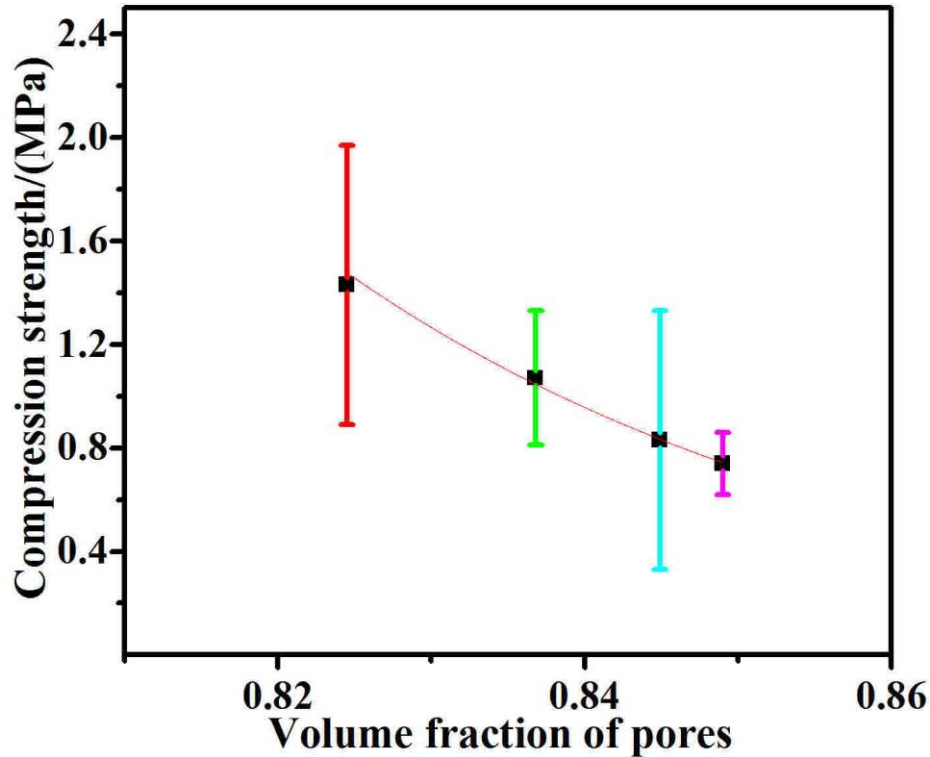


Fig. 3-25. Plot of compressive strength vs. total porosity for SFCs with various content of olive oils and fixed H_2O_2 content.

3.2.3.2.2 Effect of the content of hydrogen peroxide

Foam expansion and increase of pore dimension are favored by increasing the amounts of hydrogen peroxide as shown in Figs. 3-26(a-d), and Table 3-8. Table 3-8 reports the values of the ρ_b , the ACS, the porosity (total and open), and σ as a function of H_2O_2 content ($x = 0.3$). When the H_2O_2 content increased from 4.9 to 15.1wt%, the TP and ACS increased from ~ 75 to ~ 87 vol%, and from ~ 122 to $\sim 324\mu m$, respectively, while the amount of OP remained stable at around 98%. The corresponding σ and ρ_b fell from ~ 3.9 to ~ 0.2 MPa and ~ 0.61 ~ 0.32 g/cm³, respectively.

Also, as the composition of the geopolymer composites is constant with the different amounts of H_2O_2 addition. And the relationship between porosity and the corresponding strength can be explained by the MSA models, i.e., the strength–porosity dependence can be approximated by the equation. The values of goodness of fit R^2 are low 0.84(SH1-SH7) and

0.86(SH2-SH7) respectively. However, the R^2 of the liner fits of logarithmic strength versus porosity is 0.99 for the samples (SH3-SH7). It indicates that the model could be employed to elaborate the relation between the strength and the porosity (from ~83 to ~87vol%).

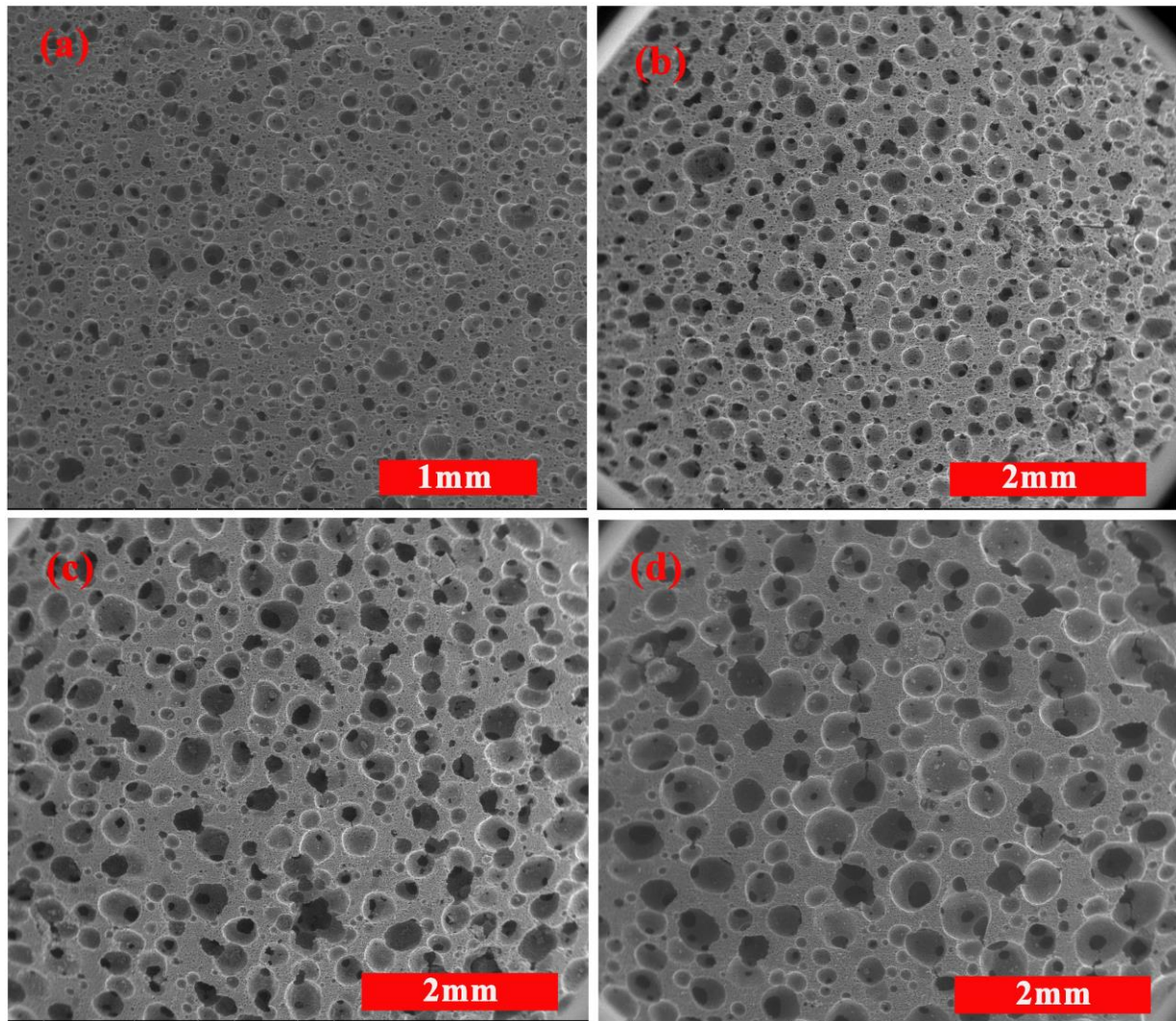


Fig. 3-26. SEM images of SFCs produced using different amounts of hydrogen peroxide with fixed olive oil content: (a) $y = 0.05$; (b) $y = 0.08$; (c) $y = 0.12$; (d) $y = 0.15$.

3.2.3.2.3 Effect of high temperature heat treatment

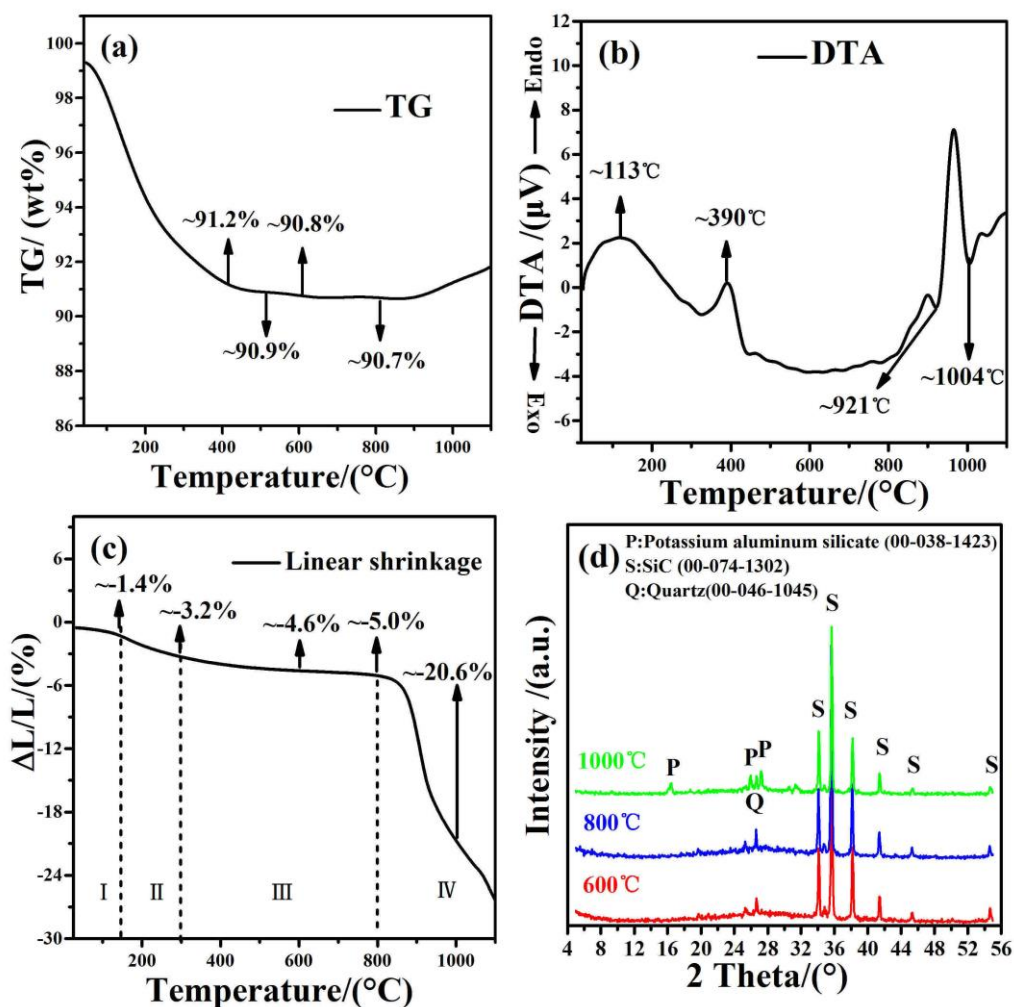


Fig. 3-27. SFCs sample: (a) TG analysis; (b) DT analysis; (c) linear shrinkage; (d) XRD patterns for samples heat-treated at different temperatures.

The thermal analysis of a representative geopolymer-SiC composite sample ($x=0.3$; $y=0.1$) is reported in Figs. 3-27(a-b), showing two endothermic peaks at ~113 °C and ~390 °C associated to a weight loss of ~8.8wt% at 400 °C. The initial weight decrease is due to the evaporation of free water and condensation/polymerization of hydroxyl [7,8]. The total weight loss was ~9.1 wt % at 500 °C, and no further mass change was observable at higher temperatures. The exothermic peak located at ~921 °C was associated to the crystallization of a potassium alumino-silicate phase (see also Fig. 3-27(d)), while the one at ~1004 °C can be attributed to

the oxidation of SiC.

A concurrent thermal shrinkage was observed during the heat treatment (see Fig. 3-27(c)) that can be divided into 4 different stages, according to published literature [9-10]. We can observe that both the total weight loss and the linear shrinkage at 1000 °C were lower than those of a pure geopolymer of the same composition, without SiC powders added, obviously due to the fact that SiC does not undergo obvious physical changes up to that temperature.

Also, after thermal treatments, X-ray diffractograms were compared (Fig. 3-27(d)). Unlike previous works [3] displayed the typical amorphous peak characteristic of geopolymer samples centered at around 27° – 29° 2θ , but only small amorphous peak were observed due to effect of the strong peaks of SiC. However, after firing at 1000 °C, while the impurities remained in the material, traces of the formation of new crystalline phase (KAlSi_2O_6) appeared, in accordance with the observed exothermic peak at $\sim 921^{\circ}\text{C}$ (see Fig. 3-27(b)).

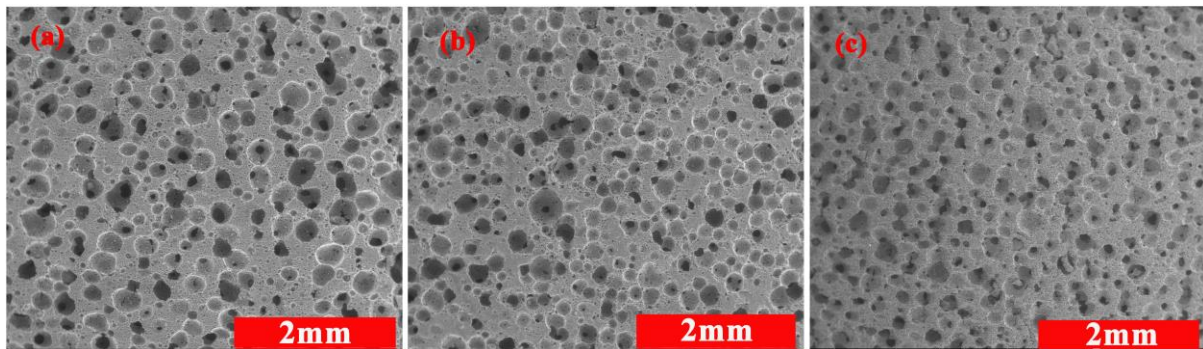


Fig. 3-28. SEM images of SFCs sintered at different temperatures: (a) 600, (b) 800, (c) 1000°C for 2h.

Table 3-9. Values of relative density (ρ_b), average cell size (ACS), total porosity (TP), open porosity (OP), compression strength (σ), and thermal conductivity (λ) as a function of heat treatment temperature, and comparison with literature data (sample made with $x=0.3$; $y=0.1$)

Sample label	Composition	Synthesis T	ρ_b (g/cm ³)	ACS (μm)	TP (vol%)	OP (vol%)	σ (MPa)	λ (W/mK)
RT	GP-SiC	75	0.40±0.01	233±72	83.7±0.4	82.7±0.2	1.1±0.3	0.147
T600	GP-SiC	600	0.41±0.02	225±99	84.3±0.8	83.6±0.5	1.5±0.5	-
T800	GP-SiC	800	0.44±0.02	212±74	83.4±0.7	82.2±0.6	2.0±0.7	-
T1000	GP-SiC	1000	0.65±0.02	215±67	76.1±0.7	74.3±0.6	5.4±2.1	-
Ref[11]	GP	80	0.34±0.01	318±18	83.5	69.2	0.45±0.1	-
Ref[12]	GP-SiC	25	0.63±0.02		78	-	1.7±1.1	-
Ref[4]	GP	75	0.33±0.01	260±190	85.1±0.4	82.4±0.9	0.6±0.1	0.099
Ref[13]	SiC	1200	0.35		87	-	0.75	0.120
Ref[14]	SiC	900	0.4	52	~86	-	1.5	-
Ref[14]	SiC	900	0.324	66	~86	-	1.6	-
Ref[15]	SiC	1100	0.002	-	~99.1	-	0.4-0.6	0.060-0.210
Ref[16]	C-SiC	1500	0.166	-	~93	-	1.9	-
Ref[17]	Al ₂ O ₃ -SiC	1200	-	-	~87	-	0.2	-
Ref[18]	C-SiC	1400	0.1-0.3	-	~78-84	-		-

The SFCs maintained the open-celled morphology with the high temperature heat treatment (Fig. 3-28), and the mechanical properties showed an increase trend (from 1.1 to

5.4MPa) with increasing firing temperature from without heat-treatment (RM, room temperature) to 1000 °C (Table 3-9). The average cell size decreased associated with the linear shrinkage and weight loss, and the porosity and pore structure can maintain at $T \leq 800^\circ\text{C}$. However, when $T \geq 800^\circ\text{C}$, a small part of the pores was filled by viscous flow and the fusion and the oxidation of SiC particles as can be seen in Fig. 3-28(c). Both the open (~74vol%) and total porosity (~76vol%) decreased and the strength increased to ~5.4MPa.

The compression strength (~1 MPa), total porosity (~84 vol%), bulk density (~0.4 g/cm³) and thermal conductivity (~0.15 W/mK) of the SiC-based composite foam (SCF) produced by the combined route was consistent with the data obtained in previous investigations for SiC foams [13-15] or SiC-based composite foams [16-18]. However, geopolymer foams with similar composition without SiC addition [4], and produced also using a similar foaming route [11], had a similar total porosity (~83vol%) but lower TC (~0.10W/mK) and compression strength (~0.5MPa). At the same time, the ratio between the open porosity and the total porosity remained constant (at around 99%), i.e., virtually all of the porosity was interconnected. It should be stressed that geopolymer foams with a very similar composition and produced using the same approach, but without the presence of SiC particles, possessed a lower amount of open porosity [4].

3.2.3.2.4 Electrochemical Impedance Spectroscopy tests

In Fig. 3-29 are reported the results from the EIS tests. The obtained Z values (Modulus in Figure 3-29) in the range ~0.1-1 Hz show that the resistance of sample R16-SO1 (without SiC addition) was ~10⁷ Ω, which is more than 10³ times that of sample SO2 (~10⁴ Ω). According to the phase plots, the values of phases at high frequency (10⁴~10⁵ Hz) of sample R16-SO1 were about 90 degrees while those of sample SO2 were about 20 degrees, suggesting also that sample R16-SO1 was an insulator while sample SO2 behaved as a semiconductor. Both spectra could be fitted with the same model, consisting of a constant phase element, Q₁, modelling the low frequency part, and a constant phase element Q₂ in parallel with a resistance R to reproduce the high frequency domain [19]. Q₁ is modelling the double layer adsorbed on

sample surfaces, while Q_2 corresponds to the diffusion of the electrolyte into the pores of the samples; R corresponds to the resistance of the sample. The fitted value of Q_1 for sample SO2 was 10 times that of sample A, indicating that sample SO2 was characterized by a higher surface area. The fitted value of Q_2 for sample R16-SO1 was 10^{-6} times than the one of sample SO2, and this result also indicates that the sample SO2 contained more open pores than sample R16-SO1. These results are in agreement with the morphological data from SEM images. Finally, the R value for sample R16-SO1 was, as expected, about 10^3 times higher that of sample SO2.

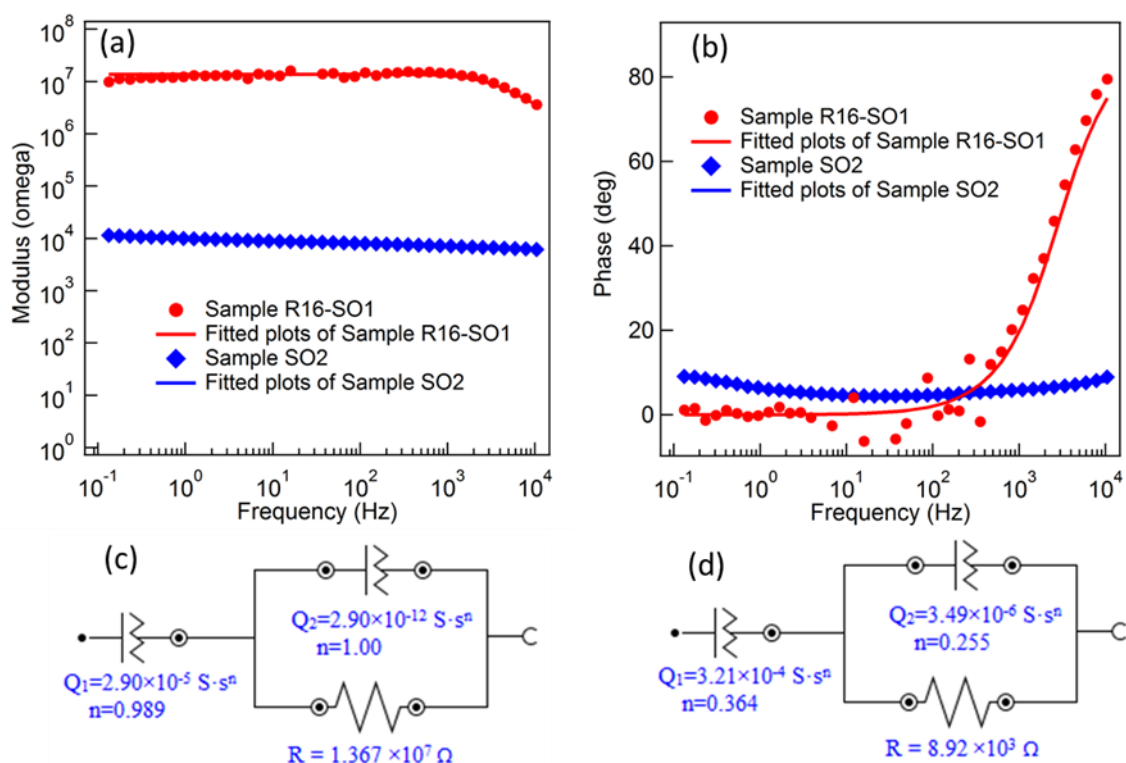


Fig. 3-29. Bode plots for sample R16-SO1 and sample SO2. The corresponding equivalent circuits and the fitted values are shown in the lower part of the figure. Plots of modulus and phase are shown in figure (a) and (b), respectively. The equivalent circuits together with the fitted values are shown in figure (c) for sample R16-SO1 and (d) for sample SO2. Q_1 models the double layer, Q_2 and R correspond to the capacity of open pores in the sample and the resistance of the sample.

The SFCs using combined route developed here have several advantages. First, the high temperature treatment process [13-17] was replaced by the geopolymerization (alkalination, depolymerization of silicates, gel formation, polycondensation, geopolymer solidification), the processing temperature was very low (75 °C) and the curing atmosphere was air[13-16]. Second, the preparation process is simple, and both the starting SiC and the bonder are inexpensive and easily available. Third, it is founded that the resulting SFCs have good thermal stability, resistance oxidation [20], and semi-conducting properties. They have similar strength (~1MPa at 84vol% porosity) and λ to other SCFs, And the SFCs could be used as macro-porous semiconductors [21-23], high temperature components, and thermal insulation materials.

3.2.3.3 Conclusions

A cost effective and simple process to obtain SiC-based composite foams with high porosity and strength were presented. The combined saponification/peroxide route using olive oil and H₂O₂ solution as pore forming agents. When the composition was fixed, increasing the amount of olive oil and H₂O₂ increased the porosity, and the corresponding strength decreased. And the relationship between the strength and porosity could be explained by the MSA models. Compressive strength of ~1.1 MPa and thermal conductivity of ~0.15W/Mk at a total porosity of 84vol% were achieved for the SFCs, and the SFC samples showed chemical and physical stability up to 800 °C.

The experimental findings (morphology, mechanical properties, thermal resistance, etc..) displayed the versatility and tailor of the open-celled SiC-based foams that could be appropriately designed according to the possible industrial application. These foams with hierarchically interconnected macro structure have potential applications such as high temperature separation and filtration components, catalyst and membrane supports, semiconductor devices, thermal insulators, and refractory materials.

This work is published in Composites Part B

Bai C, Zheng J, Rizzi G A, et al. Low-temperature fabrication of SiC/geopolymer cellular composites[J]. *Composites Part B: Engineering*, 2018, 137: 23-30.

References

- ¹ Franchin G, Colombo P. Porous Geopolymer Components Through Inverse Replica of 3D Printed Sacrificial Templates. *J.Ceram.Sci.Technol* 2015;6(2):105-112
- ² Feng J, Zhang R, Gong L, Li Y, Cao W, Cheng X. Development of porous fly ash-based geopolymer with low thermal conductivity. *Mater Des* 2015;65:529-533
- ³ Bai C, Franchin G, Elsayed H, Conte A, Colombo P. High strength metakaolin-based geopolymer foams with variable macroporous structure. *J Eur Ceram Soc* 2016; 36:4243–4249.
- ⁴ Bai C, Franchin G Elsayed, H Zaggia, A, Conte L, Li H, Colombo, P. High-porosity geopolymer foams with tailored porosity for thermal insulation and wastewater treatment. *J Mater Res* 2017;1-9.
- ⁵ Rice R. Comparison of physical property-porosity behaviour with minimum solid area models. *J Mater Sci* 1996;31(6):1509-1528
- ⁶ Rice R. Comparison of stress concentration versus minimum solid area based mechanical property-porosity relations. *J Mater Sci* 1993;28(8):2187-2190
- ⁷ He P, Jia D, Wang M, Zhou Y. Thermal evolution and crystallization kinetics of potassium-based geopolymer. *Ceram Int* 2011;37(1):59-63
- ⁸ Prud'homme E, Michaud P, Joussein E, Peyratout C, Smith A, Arrii-Clacens S, Clacens JM, Rossignol S. Silica fume as porogent agent in geo-materials at low temperature. *J Eur Ceram Soc* 2010; 30:1641–8.
- ⁹ Kuenzel C, Vandeperre LJ, Donatello S, Boccaccini AR, Cheeseman C. Ambient Temperature Drying Shrinkage and Cracking in Metakaolin-Based Geopolymers. *J Am Ceram Soc* 2012;95(10):3270-3277
- ¹⁰ Bell JL, Driemeyer PE, Kriven WM. Formation of Ceramics from Metakaolin-Based Geopolymers. Part II: K-Based Geopolymer. *J Am Ceram Soc* 2009;92(3):607-615
- ¹¹ Cilla MS, Morelli MR, Colombo P. Open cell geopolymer foams by a novel saponification/peroxide/gelcasting combined route. *J Eur Ceram Soc* 2014;34:3133–3137.
- ¹² Medri V, Ruffini A. The influence of process parameters on in situ inorganic foaming of alkali-bonded SiC based foams. *Ceram Int* 2012;38(4):3351-3359
- ¹³ Jana P, Zera E, Sorarù GD. Processing of preceramic polymer to low density silicon carbide foam. *Mater Des* 2017; 116:278–86.

-
- ¹⁴ Mary Q, Road ME, London E. Porosity and Strength of Silicon Carbide Foams Prepared Using Pre-ceramic Polymers. *J Porous Mater* 2002;131–40.
- ¹⁵ Wang Y, Chen Z, Yu S, Saeed M, Xu T, Wang W, et al. A novel ultra-light reticulated SiC foam with hollow skeleton. *J Eur Ceram Soc* 2017; 37:53–59.
- ¹⁶ Zera BE, Campostrini R, Aravind PR, Blum Y, Soraru GD. Novel SiC/C Aerogels Through Pyrolysis of Polycarbosilane Precursors. *Adv Eng Mater* 2014; 16:814–19.
- ¹⁷ Altinkok N, Demir A, Ozsert I, Findik F. Compressive Behavior of Al₂O₃-SiC Ceramic Composite Foams Fabricated by Decomposition of Aluminum Sulfate Aqueous Solution. *J Compos Mater* 2007; 41(11): 1361-1373.
- ¹⁸ Vignoles L, Lorrette C, Birot M, Ungureanu BS, Sigaud G. First Biosourced Monolithic Macroporous SiC/C Composite Foams (Bio-SiC/C (HIPE)) Bearing Unprecedented Heat Transport Properties. *Adv Eng Mater* 2013; 15:893–902.
- ¹⁹ Melar J, Renaudin G, Leroux F, Hardy-dessources A, Nedelec J, Taviot-gueho C, et al. The Porous Network and its Interface inside Geopolymers as a Function of Alkali Cation and Aging. *J Phys Chem C* 2015; 119(31): 17619-17632.
- ²⁰ Medri V, Ruffini A. Alkali-bonded SiC based foams. *J Eur Ceram Soc* 2012;32(9):1907-1913.
- ²¹ Hao D, Yang Z, Jiang C, Zhang J. Synergistic photocatalytic effect of TiO₂ coatings and p-type semiconductive SiC foam supports for degradation of organic contaminant. *Appl. Catal. B-Environ.* 2014; 144:196–202.
- ²² Yang X, Jiang C, Yang Z, Zhang J. Hydrochlorination of Acetylene Using SiC Foam Supported Structured C/Au Catalysts. *J Mater Sci Technol* 2014; 30:434–40.
- ²³ Natalie A, Masson R, Robert D, Keller N, Keller V. β-SiC foams as a promising structured photocatalytic support for water and air detoxification. *Catal Today* 2013; 209:13–20.

4. Phosphate-based porous geopolymers

4.1. Introduction

Porous geopolymers (PGs) or geopolymer foams (GFs), green alternative to conventional foams based on ordinary Portland cement, have attracted more and more attention from the porous materials fields due to their excellent mechanical and thermal properties [1-5], promising chemical and high temperature stability [6-8], and high internal surface area [9-10]. The porous components have a wide potential applications in different industry such as membranes and catalyst supports [11-12], coatings [7], adsorbents and filters [13-15], and insulating materials [16-17].

Inorganic polymers having $[\text{PO}_4]^{3-}$ in place of $[\text{SiO}_4]^{4-}$ could also be considered as a new class of geopolymers. Only few researches [1-2] exist in the previous literature referring to phosphorus-based geopolymer foams (PGFs). Le-Ping et al. [1] fabricated phosphoric acid-based geopolymers with tailored porosity (40-83%) and high compressive strength (6-14MPa), which showed an excellent thermal stability and superior mechanical property, with a linear shrinkage of only 5.3% at 1450°C, the porous specimens were synthesized from metakaolin, Al_2O_3 , Al powder and phosphoric acid at 80 for 5h. The porosity and the related properties were controlled by the Al content (pore-forming agent), the water content, and heat-treatment temperature. Porous phosphorus-based geopolymer foams with low bulk densities ($0.58 < \rho_b < 0.73 \text{ g/cm}^3$), low thermal conductivities ($0.07 < \lambda < 0.09 \text{ W/(m.K)}$), and high porosity ($69 < p < 76 \text{ vol\%}$) were successfully fabricated using natural limestone (CaCO_3) as pore forming agent by Gualtieri and co-workers [2]. Previous work [9] showed that the pores produced by only the in situ generation of gas (for instance from the decomposition of peroxide) were typically closed, which limited the range of applications such as catalysis and membrane supports, adsorption, and separation, while combined routes or the use of surfactants enabled the production of open cell foams [9,18]. In comparison with alkali-based geopolymers, phosphoric acid-based geopolymers exhibit much better thermal stability [19], and mechanical strength [20], and low dielectric properties [16-17].

Limited work has been aimed investigated the pore properties of phosphorus-based geopolymers. More researches are required to fabricate porous PGFs, especially in reference to the amount of open porosity and mechanical property of the components. In this study, we explore for the first time the fabrication of highly porous open cell PGFs via a direct foaming approach using Triton X-100 as physical blowing agent.

4.2. Experimental procedure

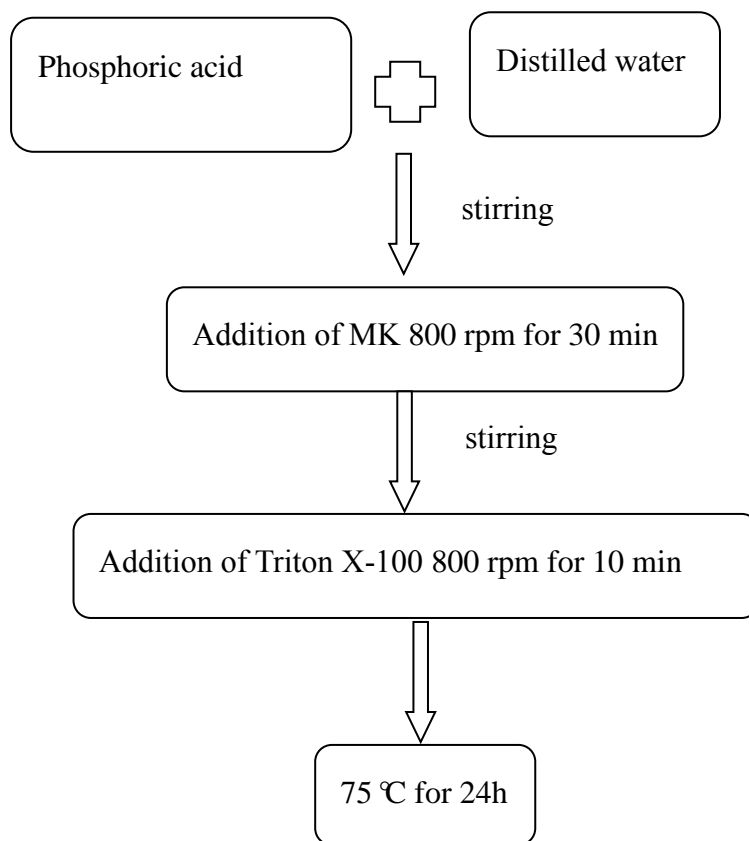


Fig. 4-1 Synthesis protocol of the phosphorus-based geopolymer foams.

Fig. 4-1 showed the synthesis protocol of the phosphorus-based geopolymer foams. As can be seen in Fig. 4-1, phosphoric acid and distilled water were mechanically mixed in a mass ratio of 1.12. A homogeneous aqueous slurry was obtained by mechanically mixing

commercially available metakaolin (MK) with the liquid acid solution mentioned above at room temperature. The geopolymer slurry had the following theoretical molar ratios: $\text{SiO}_2/\text{Al}_2\text{O}_3=2.4$, $\text{H}_3\text{PO}_4/\text{Al}_2\text{O}_3=1.8$ and $\text{H}_2\text{O}/\text{H}_3\text{PO}_4=6.7$. In this study, Triton X-100 (4-(1,1,3,3-Tetramethylbutyl)phenyl-polyethylene glycol – $(\text{C}_2\text{H}_4\text{O})_n\text{C}_{14}\text{H}_{22}\text{O}$) was selected as physical blowing agent. Triton X-100 added to the slurry in an amount of 15.7 wt% by continuous mixing to generate wet foams through the entrapment and stabilization of air bubbles. The high amount of physical blowing agent existed in the wet foams ensure the balance with the gas pressure, thereby preventing the sandwich-like or lamellar structure. Finally, PGFs were obtained by casting the wet foams into a sealed plastic mold and curing for 24 h at 75 °C in an oven.

Prior to the characterization of bulk density, porosity, pore morphology, pore size distribution, and mechanical strength, the specimens were cut into a parallelepiped with $\sim 11 \times 11 \times 13 \text{ mm}^3$ dimension; then a hot water extraction step should be carried out till the water clear, as so much Triton X-100 were added in the slurry. The extraction step is also a simple way to verify the completion of the geopolymerization reaction, as a non-fully condensed geopolymer structure would disaggregate (undergo dehydroxylation and expansion) in hot water [8-9]. Then, the PGFs were dried at 40 °C for one week. Measurements were conducted on samples cured at 75 °C and after firing for 2h at 600 °C, 800 °C, and 1000 °C with 3 °C/min in a resistance muffle furnace and static air atmosphere.

The porosity (open and total) [9,21], phase composition, pore morphology [21-22], and mechanical properties were investigated. Furthermore, measurements were conducted on samples cured at 75 °C and after firing for 2h at 600 °C, 800 °C, and 1000 °C. The high temperature performance and phase transformation characteristics of the samples were evaluated, respectively, by TG/DTA and by dilatometer up to 1100 °C in air. The crystalline phase assemblage was identified on ground samples using an X-ray diffractometer.

4.3. Results and discussion

The open porosity (OP), total porosity (TP), average cell size (ACS), relative density (ρ_b) and compressive strength (σ) of the PGFs are reported in Table. 4-1. Geopolymer foams with a TP of $\sim 78.3\text{vol}\%$, OP as high as $\sim 76.8\text{ vol}\%$, and possessing an average σ of $\sim 0.60\text{ MPa}$ after curing at 75°C were successfully fabricated by direct foaming. Fig. 4-2(a-b) shows the microstructure of the axial (i.e. along the foaming direction) and the radial (i.e. perpendicular to the foaming direction) cross-sections of porous sample. A cellular structure with a large amount of open cells, surrounded by relatively thick walls, having a size distribution ranging from ~ 100 to $\sim 800\mu\text{m}$. To better illustrate the pore size distribution, an image analysis was carried out. The results of the SEM analysis (Table 4-1) showed that the average pore size are $287.7 \pm 134.2\mu\text{m}$ (axial) and $274.8 \pm 135.4\mu\text{m}$ (radial) in different section, respectively. Furthermore, Fig. 4-2(c) shows the detail about the pore diameter distribution histogram, which is obtained by the image analysis software (Nano Measurer 1.2). The cell size distribution for the axial (see inset of Fig. 4-2(a)) and radial section (see Fig. 4-2(c)) is not very narrow, but this is typical of cellular structures obtained from direct foaming. Moreover, the sample appears to possess a very good homogeneity, and a large number of interconnections (cell windows) exist between adjacent cells which are surrounded by relatively thick struts, having a size distribution ranging from ~ 10 to $\sim 200\mu\text{m}$ (Fig. 4-2(b)). Their presence significantly increase the permeability of the structure. It should be noted that such a uniform, open cellular morphology was never reported in previous literature works dealing with porous acid-based geopolymers, suggesting that the proposed fabrication procedure offers significant advantages in terms of the porous architecture achievable in the components.

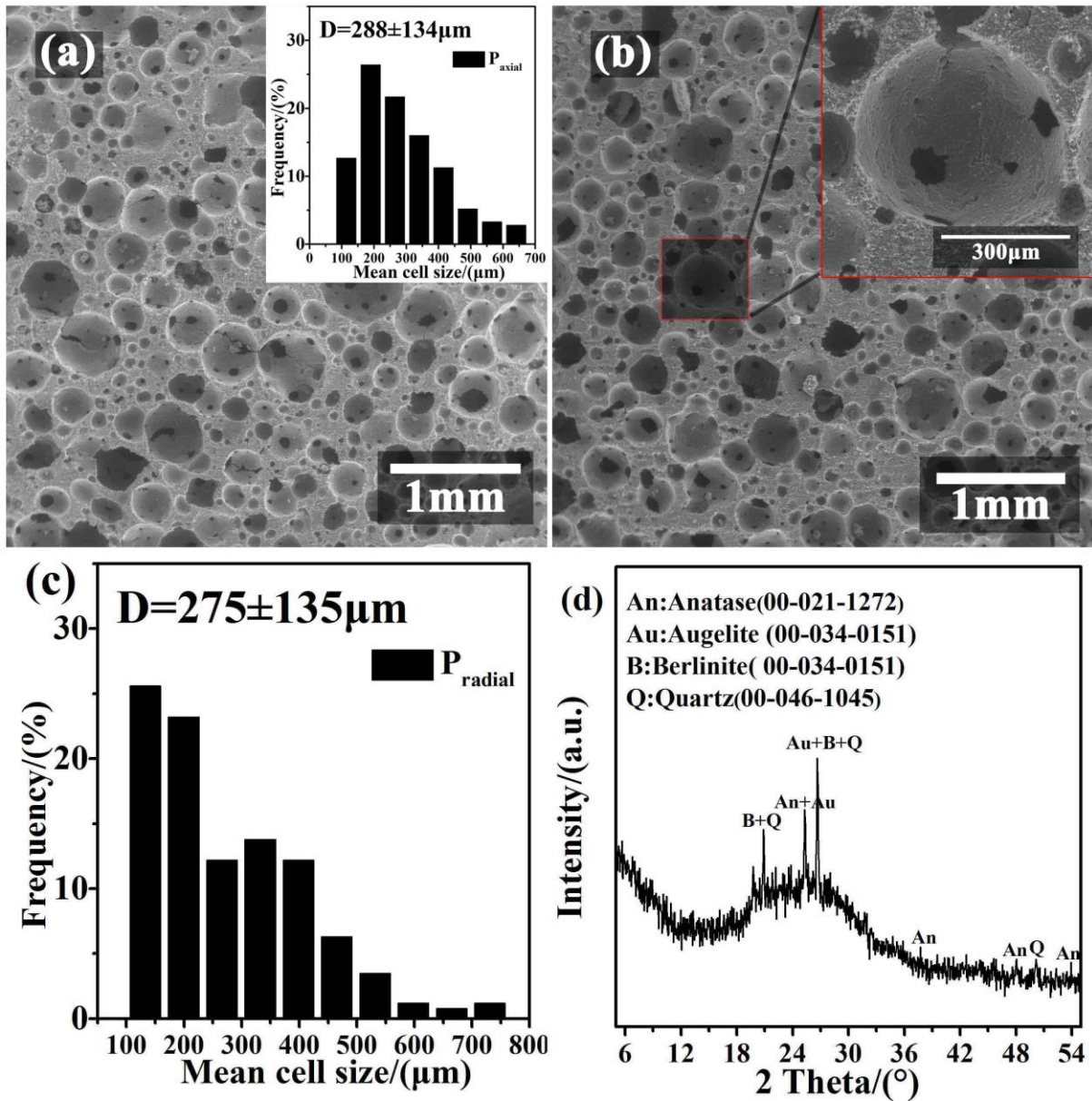


Fig. 4-2. Microstructure of a PGF sample after curing at 70°C: (a) axial direction, inset is the cell size distribution histogram; (b) radial direction, inset is a magnified view of a cell and surrounding struts; (c) cell size distribution histogram for radial direction; (d) XRD pattern.

Table 4-1. The data of the relative density (ρ_b), the average cell size (ACS), the open porosity (OP), total porosity (TP), and compressive strength (σ) depending on different heat treatment temperature.

Sample label	ρ_b (g/cm ³)	ACS (μm)	OP (vol%)	TP (vol%)	σ (MPa)
P _{axial}	0.43±0.02	287.7±134.2	76.8±1.2	78.3±0.8	0.64±0.11
P _{radial}	0.43±0.02	274.8±135.4	76.8±1.2	78.3±0.8	0.57±0.10
600	0.41±0.01	257.2±140.4	79.8±0.6	81.4±0.5	0.68±0.09
800	0.40±0.01	247.1±133.1	81.9±0.4	82.5±0.4	0.78±0.05
1000	0.40±0.01	235.2±124.0	82.1±0.6	82.6±0.4	0.81±0.08

The sample possessed a mainly amorphous nature (hump located at $\sim 24^\circ$, see Fig. 4-2(d)), similarly to what is observed for alkali-based geopolymers [11,21]. Three dimensional polymeric Si–O–Al–O–P units were formed by the recombination of dissolved metakaolin species in phosphoric acid solution [1]. In phosphoric acid-based geopolymers, the positive charges on of the [PO₄] tetrahedra are balanced by the negative charges of the [AlO₄] tetrahedra, so that neutrality is maintained in the structure. The presence of quartz (SiO₂) and anatase (TiO₂) impurities, which not participate in the geopolymerization reaction [1,21] is visible, together with a peak attributable to augelite and aluminum phosphate [1,16]. It is interesting to note that it is rather unusual that stable crystalline phases form in materials obtained by low temperature reaction, and this is not observed for alkali-based geopolymers.

The thermal analysis of the porous geopolymer sample after curing at 75 °C is reported in Figs. 4-3(a-b), showing an endothermic peak at about 130 °C, and a corresponding marked weight loss which reached 12.7wt% at 200 °C and 17.5wt% at 400 °C. Previous work [1-2] indicated that the initial weight decrease is due to dehydration of absorbed water. The TG curve (Fig. 4-3(a)) was sharply drop from room temperature to $\sim 400^\circ\text{C}$, the mass loss ($\sim 17.5\text{wt}\%$) was quite higher than geopolymer analogs reported in literature [1-2], which attribute to the vast foaming agents addition. In fact, the exothermic peak at $\sim 285^\circ\text{C}$ can be assigned to the

burn out of Triton X-100 [23]. Another exothermic located at $\sim 962\text{ }^{\circ}\text{C}$ were observed in the DTA curve (Fig. 2(b)), and considering the XRD results (see Fig. 4-3 (d)), it can be attributed to the structural reorganization of the unreacted MK [16]. No further weight change was detected in the temperature ranging from 500 to 1100 $^{\circ}\text{C}$, similarly to what reported for other phosphoric acid-based geopolymers in the literature[1-2], and alkali-based geopolymers [24]. A concurrent shrinkage occurred with the weight loss, which was more pronounced when water was eliminated from the structure. And a further shrinkage occurring above $\sim 500\text{ }^{\circ}\text{C}$ was observable, probably due to the decrease in meso-porosity and concurrent densification, as the total shrinkage was limited ($\sim 6.4\%$) up to 1000 $^{\circ}\text{C}$, and it showed that the shrinkage of the samples mostly attributable to the dehydration (see Fig. 4-3 (c)). In contrast with the alkali-based geopolymers, the further shrinkage of phosphoric acid-based specimens occurring above $\sim 500\text{ }^{\circ}\text{C}$ was fairly lower [19,25-26]. The results of TG (Fig. 4-3 (a)), DT (Fig. 4-3 (b)), and XRD analysis (Fig. 4-3 (d)) are consistent with the results reported by Douiri and co-workers [16-17]. Heating of the cellular specimens at higher temperatures resulted in a much stronger crystallization of aluminum phosphate (see Fig. 4-3 (d)), while the impurities remained in the material. We can also posit that some cristobalite formed at the highest heating temperature, although a clear identification from the diffraction patterns is difficult because its main peaks overlap with those of aluminum phosphate.

With the increasing of firing temperature, the PGFs maintained the porous structure (see Fig. 4-4), and the mechanical properties displayed a slight increase (see Table 4-1). Data published by other researchers indicate that firing at higher temperature will increase the strength of the produced ceramic components [1]. Although the ACS (axial cross-section) showed a decreasing trend from 287.7 ± 134.2 to $235.2\pm 124.0\mu\text{m}$, in accordance with the observed linear shrinkage, both the OP and TP increased due to the elimination of Triton X-100 from the structure.

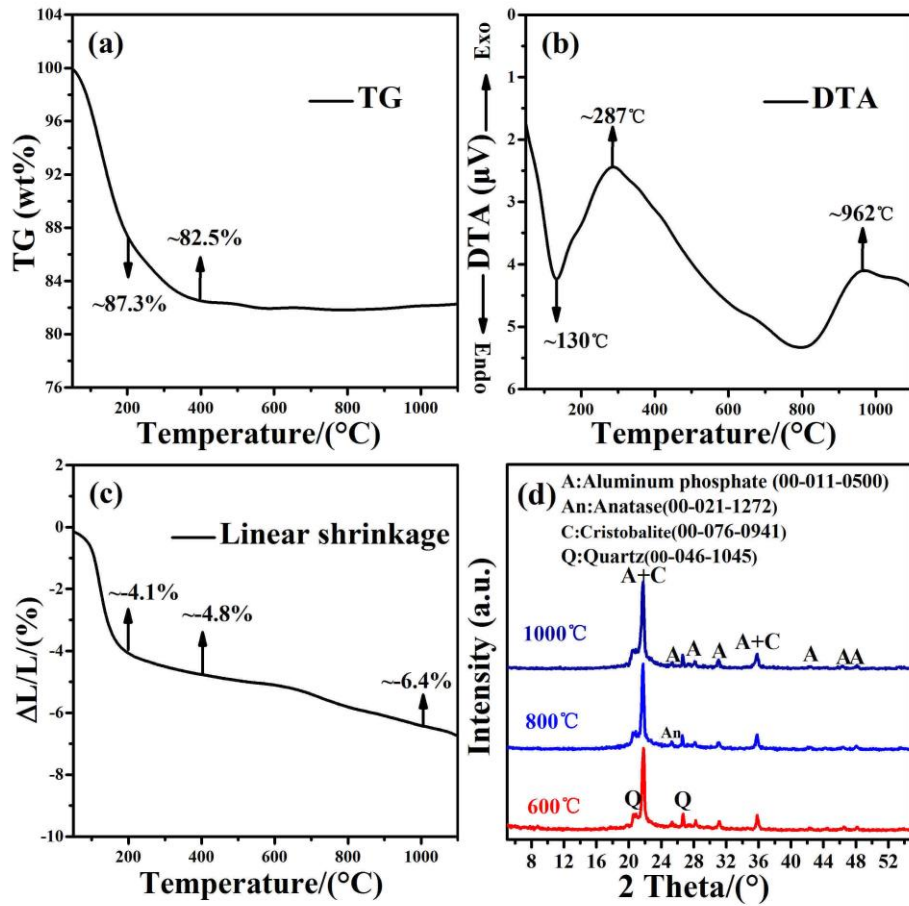


Fig. 4-3. PGF sample after curing at 70°C: (a) TG analysis; (b) DT analysis; (c) linear shrinkage; (d) XRD patterns for samples heat-treated at different temperatures.

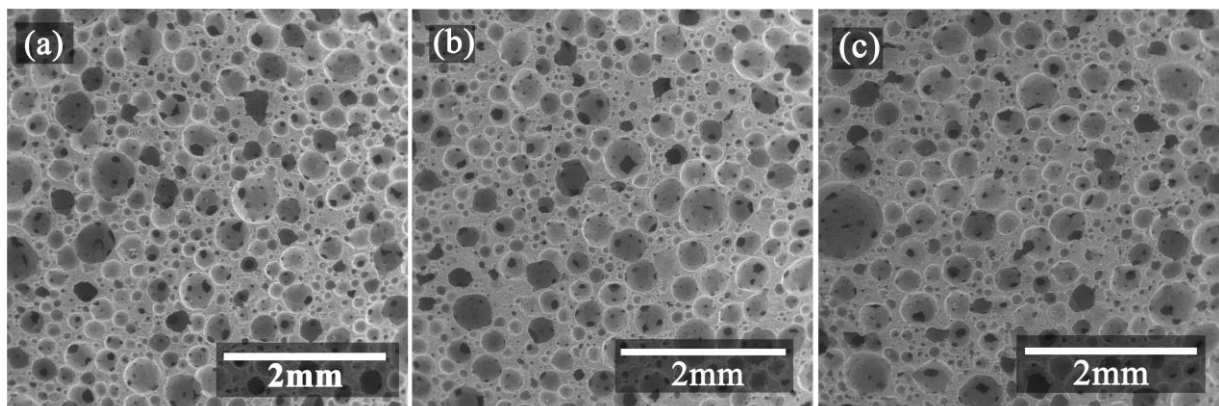


Fig. 4-4. SEM images of PGFs (axial cross-section) heat-treated at different temperature: (a) 600 °C, (b) 800 °C, (c) 1000 °C

Finally, it should be noted that acid-based GPs have a different surface chemistry with respect to alkali-based GPs and, after being immersed in an aqueous solution, they do not increase its pH to the level observed for alkali-based geopolymers. In particular, water in contact with an acid-based geopolymer powder reaches a pH of ~ 5.7 after 1 day at room temperature, while the same experiment carried out with a potassium-based geopolymer gives a pH of ~ 10.1 .

4.4. Conclusions

Open cell phosphate-based geopolymers with a homogeneous macroporous structure (average cell size $\sim 280\mu\text{m}$) were produced by gelcasting using Triton X-100 as physical blowing agent, and the effect of firing temperature on the phase composition, microstructure, and mechanical properties of MPGs were investigated. The open and total porosity and corresponding compression strength increased with the firing temperature; however, the average of cell size decreased with temperature.

These results (porosity, morphology, mechanical properties, and thermal resistance) of the phosphate-based geopolymer foams demonstrate that they could be employed as promising eco-friendly substitutes for highly porous materials in applications such as catalysis and membrane supports, high temperature separation and filtration and refractory components.

This work is published in materials letters

Bai C, Conte A, Colombo P. Open-cell phosphate-based geopolymer foams by frothing[J]. *Materials Letters*, 2017, 188: 379-382.

References

- [1] Le-Ping L., Xue-Min C., Shu-Heng Q., Jun-Li Y. & Lin Z. Preparation of phosphoric acid-based porous geopolymers. *Appl. Clay. Sci.*, 2010, 50, 600-3.
- [2] Gualtieri M. L., Romagnoli M. & Gualtieri A. F. Preparation of phosphoric acid-based geopolymer foams using limestone as pore forming agent–Thermal properties by in situ XRPD and Rietveld refinements. *Journal of the European Ceramic Society*, 2015, 35, 3167-78.
- [3] Abdollahnejad Z., Pacheco-Torgal F., Félix T., Tahri W. & Aguiar J. B. Mix design, properties and cost analysis of fly ash-based geopolymer foam. *Constr. Build. Mater.*, 2015, 80, 18-30.
- [4] Novais R. M., Buruberri L., Ascensão G., Seabra M. & Labrincha J. Porous biomass fly ash-based geopolymers with tailored thermal conductivity. *J. Clean. Prod.*, 2016, 119, 99-107.
- [5] Hlaváček P., Šmilauer V., Škvára F., Kopecký L. & Šulc R. Inorganic foams made from alkali-activated fly ash: Mechanical, chemical and physical properties. *Journal of the European Ceramic Society*, 2015, 35, 703-9.
- [6] Temuujin J., Rickard W., Lee M. & van Riessen A. Preparation and thermal properties of fire resistant metakaolin-based geopolymer-type coatings. *J. Non Cryst. Solids*, 2011, 357, 1399-404
- [7] Zhang Z., Yao X. & Zhu H. Potential application of geopolymers as protection coatings for marine concrete: I. Basic properties. *Appl. Clay. Sci.*, 2010, 49, 1-6.
- [8] Davidovits J. *Geopolymers – chemistry & applications*. 3th ed. Saint-Quentin: Institut Géopolymère; 2011.6.
- [9] Cilla M. S., Morelli M. R. & Colombo P. Open cell geopolymer foams by a novel saponification/peroxide/gelcasting combined route. *Journal of the European Ceramic Society*, 2014, 34, 3133-7.
- [10] Medpelli D., Seo J. & Seo D. Geopolymer with Hierarchically Meso-/Macroporous Structures from Reactive Emulsion Templating. *J Am Ceram Soc*, 2014, 97, 70-3.
- [11] Zhang J., He Y., Wang Y., Mao J. & Cui X. Synthesis of a self-supporting faujasite zeolite membrane using geopolymer gel for separation of alcohol/water mixture. *Mater Lett.*, 2014, 116, 167-70.

-
- [12] Candamano S, Frontera P, Macario A, Crea F, Nagy JB, Antonucci PL. Preparation and characterization of active Ni-supported catalyst for syngas production. *Chem Eng Res Design* 2015;96:78-86
- [13] Minelli M, Medri V, Papa E, et al. Geopolymers as solid adsorbent for CO₂ capture[J]. *Chemical Engineering Science*, 2016.148:267-274.
- [14] Ge Y, Yuan Y, Wang K, He Y, Cui X. Preparation of geopolymer-based inorganic membrane for removing Ni²⁺ from wastewater. *J Hazard Mater* 2015;299:711-8
- [15] Luukkonen T, Sarkkinen M, Kempainen K, Rämö J, Lassi U. Metakaolin geopolymer characterization and application for ammonium removal from model solutions and landfill leachate. *Appl Clay Sci* 2016;119, Part 2:266-76
- [16] Douiri H., Louati S., Baklouti S., Arous M. & Fakhfakh Z. Structural, thermal and dielectric properties of phosphoric acid-based geopolymers with different amounts of H₃PO₄. *Mater Lett*, 2014, 116, 9-12.
- [17] Douiri H., Louati S., Baklouti S., Arous M. & Fakhfakh Z. Enhanced dielectric performance of metakaolin-H₃PO₄ geopolymers. *Mater Lett*, 2016, 164, 299-302.
- [18] Cilla MS, Colombo P, Morelli MR. Geopolymer foams by gelcasting. *Ceram Int* 2014;40:5723-30
- [19] Liu L, Cui X, He Y, Liu S, Gong S. The phase evolution of phosphoric acid-based geopolymers at elevated temperatures. *Mater Lett* 2012;66:10-2
- [20] Perera DS, Hanna JV, Davis J, Blackford MG, Latella BA, Sasaki Y et al. Relative strengths of phosphoric acid-reacted and alkali-reacted metakaolin materials. *J Mater Sci* 2008;43:6562-6
- [21] Bai C, Franchin G, Elsayed H., High strength metakaolin-based geopolymer foams with variable macroporous structure, *Journal of the European Ceramic Society*, 2016; 36(16): 4243-4249..
- [22] Chen X, Zhang N, Sun K. Facile ammonia-induced fabrication of nanoporous NiO films with enhanced lithium-storage properties. *Electrochemistry Communications* 2012;20:137-40
- [23] Mitsuda K, Kimura H, Murahashi T. Evaporation and decomposition of Triton X-100 under various gases and temperatures. *J Mater Sci* 1989;24:413-9.

-
- [24] He P, Jia D, Wang M, Zhou Y. Thermal evolution and crystallization kinetics of potassium-based geopolymer. *Ceram Int* 2011;37:59-63
- [25] Cilla MS, Morelli MR, Colombo P. Effect of process parameters on the physical properties of porous geopolymers obtained by gelcasting. *Ceram Int* 2014;40:13585-90
- [26] Kuenzel C, Vandeperre LJ, Donatello S, Boccaccini AR, Cheeseman C. Ambient Temperature Drying Shrinkage and Cracking in Metakaolin - Based Geopolymers. *J Am Ceram Soc* 2012;95:3270-7

5. Concluding remarks and future perspectives

A series of open cell geopolymer (using different types of stabilizing agents (egg white, tween80, vegetable oils)) combined with pore forming agent (H_2O_2) were produced by direct foaming technique, and geopolymer and composites (geopolymer-SiC) with controlled porosity were fabricated using a direct foaming plus reactive emulsion templating route. And open-cell porous phosphate-based geopolymers with homogenous microstructure were synthesized by only using Triton X-100 as physical blowing agent.

This thesis was mainly devoted to the investigation of different processing methods for the fabrication of PGs, and their influence on the main characteristics of the porous bodies. The data can serve as a basis for the development of components with microstructure and properties tailored for a specific application. For instance, catalyst supports need to possess a large geometric surface, hence small pores, and a highly accessible pore surface, hence a large volume of interconnected porosity, allowing for good permeability throughout the structure. Membrane supports require having a graded porous architecture that would enable the deposition of a thin top separation layer, while minimizing the pressure drop through the support structure. Thermal insulation materials need to possess a large volume of small pores, while at the same time maintaining a suitable mechanical strength.

The developed processing routes appear to be capable of reaching at least some of these goals, but of course, further work will be required to precisely optimize the fabrication procedure to more precisely match the required properties for each potential application considered. In the future, we will focus on the potential application such as solid adsorbent for CO_2 capture or heavy metal removal. And using waste raw materials such as fly ash, slag, waste glass partly or totally replace the metakaolin. 3D printing will also be applied to geopolymer systems. Fiber reinforced geopolymer foam composites will be investigated, etc.

Curriculum vitae

Personal Data

Name: Chengying Bai

Date of Birth: 18th May 1986

Gender: Male

Place of Birth: Xing Tai, Heibei Province

Nationality: Chinese

E-mail: chengyingbai@163.com or chengyingbai@gmail.com

Education

11/2014-

PhD student of Industrial Engineering in University of Padova (CSC), Italy

Open-celled geopolymer foams produced by different methods and for various applications.

09/2011-07/2014

Master of Materials and Chemical Engineering Institute in Hainan University (211), China

Took part in the “Preparation of high temperature Silicon carbide filter tube”, fund by the Ministry of Sciences and Technology of China through 863-program under grant 2012AA03A610.

09/2006-06/2010

Bachelor of Environmental and Chemical Engineering in Tangshan College, China

Studied of process of cement and the foundation of inorganic non-metallic materials in Tangshan College.

Publications

1. **Bai C**, Ni T, Wang Q, et al. Porosity, mechanical and insulating properties of geopolymer foams using vegetable oil as the stabilizing agent[J]. Journal of the European Ceramic Society, 2017. In press.
2. **Bai C**, Franchin, G., Elsayed, H., Conte, A., & Colombo, P. (2016). High strength metakaolin-based geopolymer foams with variable macroporous structure. Journal of the European Ceramic Society, 36(16), 4243-4249.
3. **Bai, C.**, & Colombo, P. (2017). High-porosity geopolymer membrane supports by peroxide route with the addition of egg white as surfactant. Ceramics International, 43(2), 2267-2273.
4. **Bai, C.**, Conte, A., & Colombo, P. (2017). Open-cell phosphate-based geopolymer foams by frothing. Materials Letters, 188, 379-382.
5. **Bai C**, Franchin G, Elsayed H, et al. High-porosity geopolymer foams with tailored porosity for thermal insulation and wastewater treatment [J]. Journal of Materials Research, 201 32(17), 3251-32597.
6. **Chengying Bai**, Jian Zheng, Gian Andrea Rizzi, Paolo Colombo. Low-temperature Fabrication of SiC/geopolymer Cellular Composites. [J]. Composites Part B: Engineering, 2018, 137: 23-30.

International conference

15th Conference & Exhibition of the European Ceramic Society 2017 Hungary (EcerS 2017, Oral presentation)

Geopolymer camp 2016 France (Oral presentation)

6th International Congress on Ceramics 2016 Germany (ICC6, Oral presentation)

14th International Conference of the European Ceramic Society 2015 Spain (EcerS 2015, Poster)

Reviewer for peer-reviewed journals

Materials letters

Journal of Materials Science

Research Interest

Geopolymer foams, Porous ceramics, hot gas filtration, SiC ceramics, membrane supports, filter, membrane

APPENDIX- A

**Goole scholar Citation indices: Citations–119, h-index–6, i10-index–5 as on (Dated-
24/10/2017)**

<https://scholar.google.com/citations?user=LIBdEyMAAAAJ&hl=zh-CN>

Acknowledgements

Firstly, I would like to express my sincere gratitude to my advisor Prof. Paolo Colombo for the continuous support of my Ph.D study and related research, for his patience, motivation, and immense knowledge. His guidance helped me in all the time of research and writing of this thesis. I could not have imagined having a better advisor and mentor for my Ph.D study.

I would like to thank Prof. Enrico Bernardo (University of Padova), Prof. Hongqiang Li (Hunan University), Prof. Lino Conte (University of Padova), and Prof Gian Andrea Rizzi (University of Padova) for their fruitful discussion and comments.

My sincere thanks also goes to Dr. Hamada Elsayed, Dr. Giorgia Franchin, Dr. Alberto Conte, Dr Alessandro Zaggia, Dr Acacio Rincon, Dr Renata Botti Fuss, Dr Marcelo S Cilla, Dr Jian Zheng, Dr Tao Ni, and Dr Qiaoling Wang who provided me an opportunity to widen my research fields. and who gave me the chance to co-operation. Without their precious support it would not be possible to conduct this research. Thanks a lot to Mauro Gobbin(TG-DTA test), Andrea Paduano(BET test), Flavio Pendolino (BET test), Claudio Furlan(SEM test). Many thanks also to all friendly and wonderful people that I have met at University of Padova (Chengyi Tu, Chuanyu Sun, Xiaohuan Sun, Lu Liu, Yang Yang, Haitao Cao, Xiuli Mao, Yongheng Zhao, Can Lai, Bili Zhong, Bin Zhu, Sha Song, Wei Pang, Xin Jin, Yawei Wang, Jingzheng Ren, Wenjie Wang, Yan Hu, Mengmeng Zheng, Qianqian Li, Lei Chang, Yutao Chen, Ru Gao, Fan Jiang, Lu Yuanhao, et al.) (Mattia Lago, Alessio Settimi, Lisa Biasetto, Johanna Schmidt, Valentina Naglieri et al.) and at Italy (Wuhe Jike, Fangfang Sun, Weixing Li, Xuwen Zhang, Chao Lu, Haochen Wang, Chengkai Qu et al.) , it was a pleasure to work and play with them. I also want to thank to Wechat, Xiaomuchong, Baidu, Google scholar, Sciencenet, Google map, Here map, etc.

Again, I would sincerely like to thank Prof. Paolo Colombo for his supervision. I gratefully acknowledge the financial support of the China Scholarship Council (CSC) (No. 201407565009). To my family and to Xiao Li, for the love and the support during these years, despite the distance.

